POR-3000
(WT-3000)

FERRIS WHEEL SERIES

AIR VENT/FLAT TOP EVENTS

PROJECT OFFICERS REPORT

SCIENTIFIC DIRECTORS SUMMARY

M. L. Merritt, Scientific Director

Sandia Corporation
Box 5800
Albuquerque, New Mexico 87115

Issuance Date: September 27, 1968

[redacted]

Enclosure 3

Defense Nuclear Agency
6801 Telegraph Road
Alexandria, Virginia 22310-3398

IMTS 23 August 1994

MEMORANDUM FOR DEFENSE TECHNICAL INFORMATION CENTER
ATTENTION: DTIC/OCC

SUBJECT: Documents Submitted for Inclusion In the DTIC System

The Defense Nuclear Agency Information Management Technical Support Office requests the enclosed technical reports be included in the DTIC system.

Distribution statement 'A' (approved for public release) applies. Please direct all inquires to Mrs. Naomi E. Fields at (703) 325-1038.

FOR THE DIRECTOR:

JOSEPHINE B. WOOD
Chief, Technical Support

Enclosures
POR-6206 (2)
POR-3021 (2)
POR-6546 (2)
POR-2039 (2)
POR-6300 (2)
POR-2725 (2)
POR-6337 (2)
POR-3000 (2)
WT-561 (2)
WT-601 (2)

Inquiries relative to this report may be made to

Director, Defense Atomic Support Agency
Washington, D.C. 20305

DISPOSITION INSTRUCTIONS

When this report is no longer needed, Department of Defense organizations will destroy it in accordance with appropriate procedures. Contractors will destroy the report according to the requirements of the Industrial Security Manual for Safeguarding Classified Information.

DO NOT RETURN THIS DOCUMENT

POR-3000
(WT-3000)

FERRIS WHEEL SERIES

AIR VENT/FLAT TOP EVENTS

PROJECT OFFICERS REPORT

SCIENTIFIC DIRECTORS SUMMARY

M. L. Merritt, Scientific Director

Sandia Corporation
Box 5800
Albuquerque, New Mexico 87115

ABSTRACT

Air Vent and Flat Top were HE experiments studying ground shock and cratering. There were 33 shots varying in size from 64 pounds to 20 tons, all spheres and all but one in the playa of NTS Area 5. The 20-ton shots comprised one at 17-foot depth (Air Vent I) and two half-buried in playa (Flat Tops II and III), and one half-buried in limestone (Flat Top I).

Air blast measurements were made on the three Flat Top shots. Results are much as predicted preshot.

Ground motion measurements were made on the Flat Top shots and on Air Vent I. Associated calculations were made postshot; their results are in general agreement with the data but do not go out to distances where most of the data were taken. Air-blast-induced ground motions on Flat Tops II and III in playa were superseismic through the whole range of measurement. Acceleration and vertical component of velocity were dominated by air-blast-induced shock; displacements and horizontal components of velocity by direct ground shock. Flat Top I in limestone was subseismic through most of the range of measurement. Gages at similar positions had similar wave forms, but the time scale of records in limestone was much faster than of records in playa. Horizontal velocities were larger in limestone than in playa; vertical velocities higher in playa than in limestone.

Note. 5 is first page number to appear in the report.

Crater measurements were made on all shots. Radii of HE surface bursts in playa scale by a factor significantly higher than cube root of yield, depths by the cube root. Area 5 playa yielded smaller craters than Area 10 alluvium. Soil moisture was an important factor; Flat Top III, fired in the same soil 60 percent more moist than Flat Top II, gave a crater 60 percent larger in volume. Finite permanent displacements were observed even in the limestone shot.

Ejecta measurements were made on all shots, including traceable pellets or markers on the four 20-ton shots. Ejecta thicknesses do not quite scale as crater radii. Pellets went further than the native material; they indicate the initial velocity field albeit with scatter. Mass balances are consistent with past experience: for the playa shots 35 percent of the true crater became ejecta, 10 percent upthrust, 30 percent fallback. In the limestone shot 2/3 became ejecta, 1/3 fallback. In the limestone shot individual missiles went far beyond distances considered safe by the usual handbooks.

CONTENTS

TABLES

FIGURES

CHAPTER 1

INTRODUCTION

Air Vent and Flat Top were high-explosive (HE) experiments supporting the DASA Ground Shock and Cratering Program, officially nicknamed Ferris Wheel. The purpose of this program is to develop theoretical methods of predicting ground motion and cratering and to perform fundamental field experiments that may also be used to check the theoretical techniques.

As originally conceived, the Ferris Wheel experimental program was entirely nuclear. Its initial, or B-series, shots were to be very small surface shots in Area 10 of the Nevada Test Site (NTS). Air Vent was conceived after it was determined that this initial shot series had to be located in Area 5 instead. Since most previous HE and nuclear cratering shots had occurred in Area 10, Air Vent was to provide a bridge to make that previous experience more directly applicable to the initial shot series of Ferris Wheel.

This initial, B-series was never executed. In May 1963, a significant part of the instrumentation for two small nuclear and an accompanying HE detonation had been completed; in fact, the HE experiment was to be fired within 3 days. A public announcement of the series created an unfortunate reaction which made them prejudicial to the negotiations leading up to the present limited test ban treaty, and the series was called off by order of the President.

The Air Vent HE tests were nevertheless continued and were fired between December 1963 and February 1964. In December 1963 the decision was made to use the sites prepared for one nuclear shot and the HE shot of the Ferris Wheel initial series as HE shots, together with a shot in limestone. These experiments became the three-shot Flat Top series fired between February and June of 1964.

Although they were conceived, authorized, and executed separately, the Air Vent and Flat Top series have enough in common that it is useful to discuss them together in this summary report.

1.1 OBJECTIVES

The basic theme of Air Vent was the correlation of nuclear shots in the playa of Area 5 with HE shots fired elsewhere. Three questions were to be answered:

1. What is the relative cratering effectiveness of nuclear and chemical high explosives? This requires equal yield events at the same depth in the same medium. The canceled series provided for such comparison shots at the surface and at a 17-foot depth. This question was not answered by Air Vent/Flat Top because the comparative nuclear shots were not fired.

2. What is the cratering depth-of-burst curve in Area 5 playa and how does it compare with similar curves in other media, especially with that in Area 10?

3. What is the correct scaling for HE surface-burst craters? Results from nuclear shots in the Pacific and from hemispherical HE shots in Canada implied a scaling of radius as a power of charge weight greater than one-third. There were legitimate questions about the applicability of those results because the Pacific data were for various heights of burst, the craters were flooded before measurement, and the Canadian data were from hemispherical charges.

Air Vent was primarily a series of cratering shots; Flat Top was primarily a set of ground shock experiments. The basic theme of Flat Top was that of Ferris Wheel itself, to produce data to be compared with computations. The general questions at which Flat Top was directed are:

1. What are the pressures and motions induced by true surface HE bursts? In the hydrodynamic region, no such data existed at all, either for HE or nuclear explosions (NE); at larger distances, such data were very sparse.

2. What effect does the medium have on these motions?

3. What are the ground motions and how big are the craters from surface bursts in hard rock? The limestone shot was added for the interest in hard rock, of and by itself, as well as for a different medium; plans for hardened missile systems and hardened command and control centers suffer for lack of reliable information on direct ground shock and the distribution of debris from large surface bursts in rock.

4. If nuclear events are again permitted, the Flat Top shots would provide one end for HE versus NE comparisons.

5. With hindsight, an important use of Flat Top turned out to be the field proving of new instrumentation systems, especially those for measuring ground motions in the high-pressure regions.

1.2 SHOTS FIRED

There were 33 shots in all as shown in Table 1.1. Air Vent I and the three Flat Top shots each contained 1113 blocks of TNT, each block an 8-5/8-inch cube weighing 35.9 pounds. The shape formed in stacking them was only approximately a sphere. Figures 1.1, 1.2, and 1.3 show the stacks for the three Flat Top shots. All shots were center detonated.

Each Flat Top charge was stacked in a hole of about 5-foot radius. In Flat Top II the space between HE and native soil was filled with alluvium, screened to remove coarse material. In Flat Top III the original soil was tamped back around each layer of HE. In Flat Top I a Hugoniot-matching grout was used. More details are described in Section 3.4, where ground motion is discussed.

All shots but one (Flat Top I) were fired in the playa of Area 5 of NTS. Playa is the material of dry desert lake beds. It is fine silt and clay, compact, and generally quite uniform laterally and vertically. Its <u>in situ</u> density is about 1.55 gm/cm^3, of which normally

13 percent is water although the Flat Top III playa was much wetter. Chemically it is like the surrounding mountains, a little over 50-percent silica and about 35-percent calcium and magnesium carbonates (Reference 5). The playa surface is very smooth and level.

Flat Top I was fired in the Banded Mountain limestone of Area 9 of NTS. This was chosen as the best hard rock available on the surface, the local granite being too weathered and the local basalt too vesicular. The limestone was sound but heavily bedded with a dip of 40 degrees. Its density is about 2.7 gm/cm^3, and its sonic velocity about 20,000 ft/sec. Chemically it is 95-percent $CaCO_3$ (Reference 17, Tables III and IV). This limestone was covered with a thin layer of alluvial detritus. Immediately around the shot this cover was removed for better ground shock coupling. This removal left a very rough surface which was somewhat smoothed by filling the deepest holes with a concrete grout (Figure 1.4).

Air Vent I was fired on December 14, 1963, on a clear calm day. Flat Top II was fired on February 17, 1964, on a clear calm day. Flat Top III was fired on March 24, 1964 on a cold day with periodic squalls of rain and snow. There was a brisk wind. Flat Top I was fired on June 22 on a warm, clear summer day, with a moderate wind blowing down the blast line. Weather details are given in Table 1.2.

Air Vent was carried out primarily by Sandia Laboratory, with Mr. T. J. Flanagan as test director. Crater ejecta studies were carried out by the Illinois Institute

of Technology Research Institute (IITRI) under contract to Sandia and by the Boeing Company under contract to the Air Force Weapons Laboratory. The major part of the financial support was from Headquarters, Defense Atomic Support Agency. Flat Top was fielded by Weapons Test Division, DASA, with Major Marc Colvin, Jr., as test director.

Projects are listed by title, agency, and project officer in Table 1.3. The resultant reports are References 1 through 15. In addition to DASA-financed projects, the Weather Bureau, U.S. Department of Commerce, gave supplemental support to Project 9.8 (Technical Photography) for the sake of studies of cloud rise; these results are reported in Reference 16. Reference 17 is a summary of materials properties relevant to Air Vent/Flat Top as well as other Ferris Wheel activities.

TABLE 1.1 SHOTS FIRED IN AIR VENT/FLAT TOP

Designation	Date	Charge Weight	Depth of Burst Actual	Depth of Burst Scaled	Material
		lb	ft	ft/lb$^{1/3}$	
Air Vent					
Phase I	12/14/63	40,000	17.19	0.5	Playa
Phase II					
II-1	1/30/64	256	-0.865	-0.136	Playa
II-2A	1/30/64	256	0	0	Playa
II-2B	1/29/64	256	0	0	Playa
II-3	1/29/64	256	+0.865	+0.136	Playa
II-4	1/29/64	256	1.59	0.25	Playa
II-5A	1/28/64	256	3.175	0.5	Playa
II-5B	1/28/64	256	3.175	0.5	Playa
II-6	1/28/64	256	4.76	0.75	Playa
II-7A	1/27/64	256	6.35	1.0	Playa
II-7B	1/27/64	256	6.35	1.0	Playa
II-8	1/27/64	256	7.94	1.25	Playa
II-9A	1/24/64	256	9.53	1.5	Playa
II-9B	1/23/64	256	9.53	1.5	Playa
II-10A	1/24/64	256	12.7	2.0	Playa
II-10B	1/23/64	256	12.7	2.0	Playa
II-11A	1/16/64	256	15.9	2.5	Playa
II-11B	1/16/64	256	15.9	2.5	Playa
II-12	1/17/64	256	19.05	3.0	Playa
II-13	1/17/64	256	22.2	3.5	Playa
II-14	1/17/64	256	25.4	4.0	Playa
Phase III					
III-1A	1/31/64	64	0	0	Playa
III-1B	1/31/64	64	0	0	Playa
III-1C	1/31/64	64	0	0	Playa
III-1D	1/31/64	64	0	0	Playa
III-2A	1/11/64	1,000	0	0	Playa
III-2B	1/11/64	1,000	0	0	Playa
III-2C	1/13/64	1,000	0	0	Playa
III-3A	1/8/64	6,000	0	0	Playa
III-3B	1/9/64	6,000	0	0	Playa
Flat Top					
II	2/17/64	40,000	0	0	Playa
III	3/24/64	40,000	0	0	Playa
I	6/22/64	40,000	0	0	Limestone

TABLE 1.2 WEATHER CONDITIONS FOR FLAT TOP SHOTS

	Flat Top II 2/17/64	Flat Top III 3/24/64	Flat Top I 6/22/64
Moisture	None	Intermittent rain	None
Sky	Clear	Cloudy	Clear
Pressure (psi)	13.25	13.06	12.6
Temperature (°C)	3.0	9.0	20.9
Winds: Direction	340°	250°	30°
Speed (knots)	1	18	12
Blast line direction	185°	168°	152°

TABLE 1.3 LIST OF PROJECTS; AIR VENT/FLAT TOP

Project Number	Project Title	Agency	Project Officer	Results Reported in Reference
Air Vent				
A	Ground Motion	SC	D. B. List	1
B	Surface Motion Photog.	SC	S. Farrelly	2
C	Ejecta (Phase I)	IITRI	E. B. Ahlers	4
D	Ejecta (Phase II and III)	Boeing	G. D. Jones	3
E	Crater Measurements	SC	T. J. Flanagan	5
Flat Top				
1.1	Surface Air Blast	BRL	J. H. Keefer	6
1.2	Earth Motion	SRI	C. T. Vincent	7
1.3a	Close-in Pressures	SRI	C. T. Vincent	7
1.3b	Close-in Pressures	IITRI	P. Lieberman	8
1.4	Close-in Studies	SC	R. C. Bass	9
1.5a	Debris Studies (FT-II, III)	IITRI	E. B. Ahlers	10
1.5b	Ejecta Studies (FT-I)	Boeing	M. V. Anthony	11
1.9	Crater Measurements	WES	A. D. Rooke	12
1.11	Permanent Displacement	AFWL	G. V. Bulin	13
9.1	Grouting and Soil Properties Support	WES	J. M. Polatty	14
9.8	Technical Photography	EGG	L. P. Donavan	15

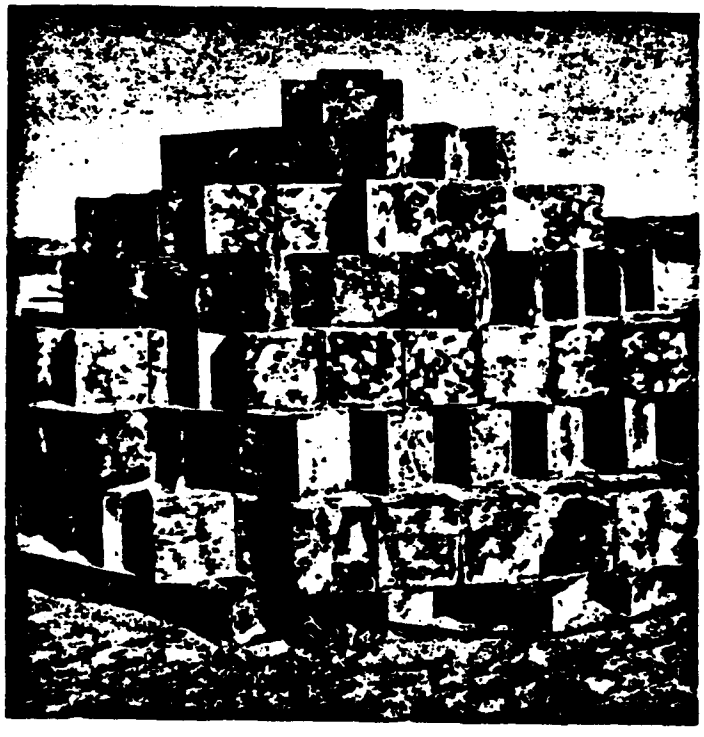

(a) (DASA-20-58-NTS-64)

(b) (DASA-20-60-NTS-64)

Figure 1.1 Flat Top II: HE stack and detonation.

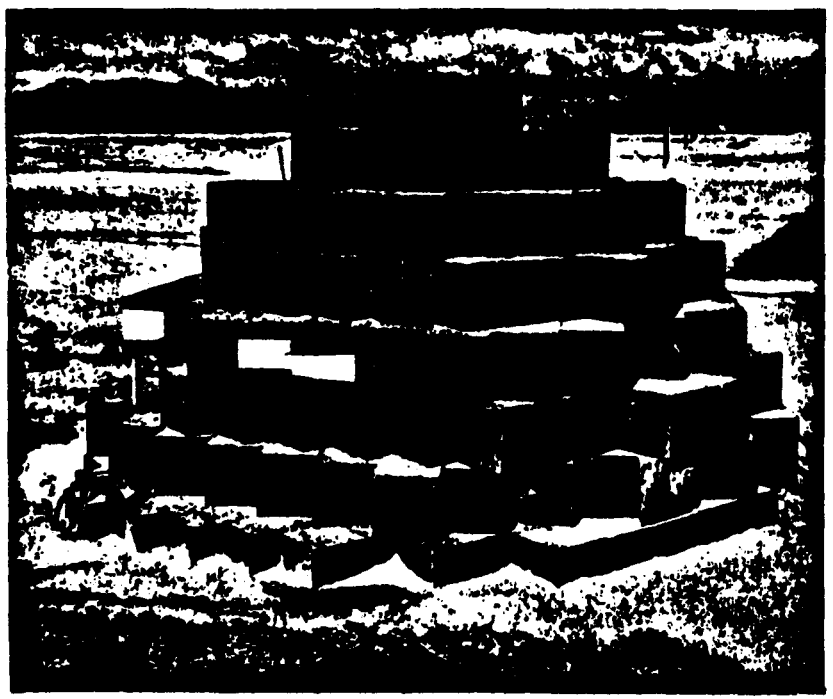

(a) (DASA-35-12-NTS-64)

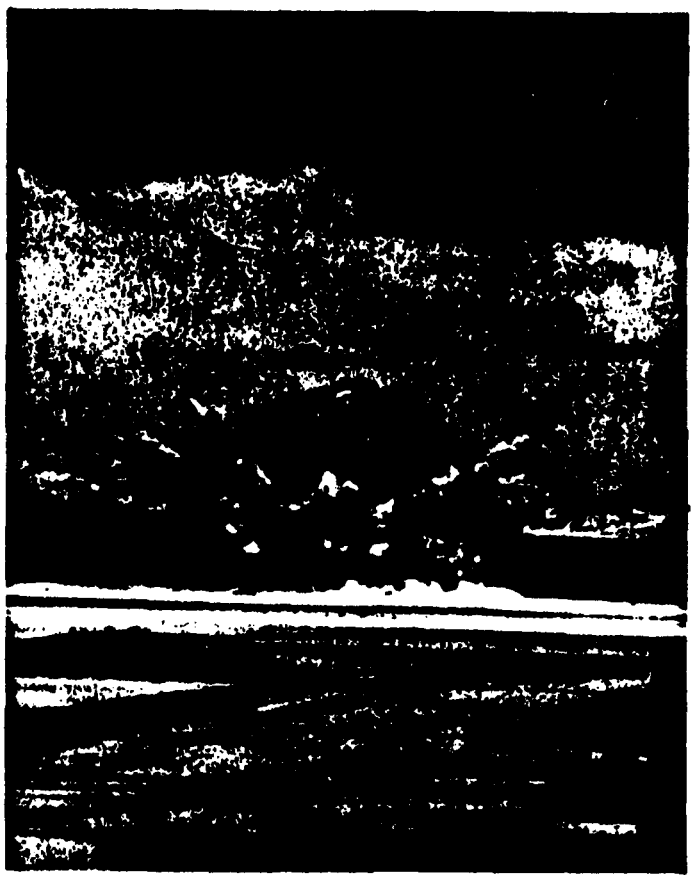

(b) (DASA-35-10-NTS-64)

Figure 1.2 Flat Top III: HE stack and detonation.

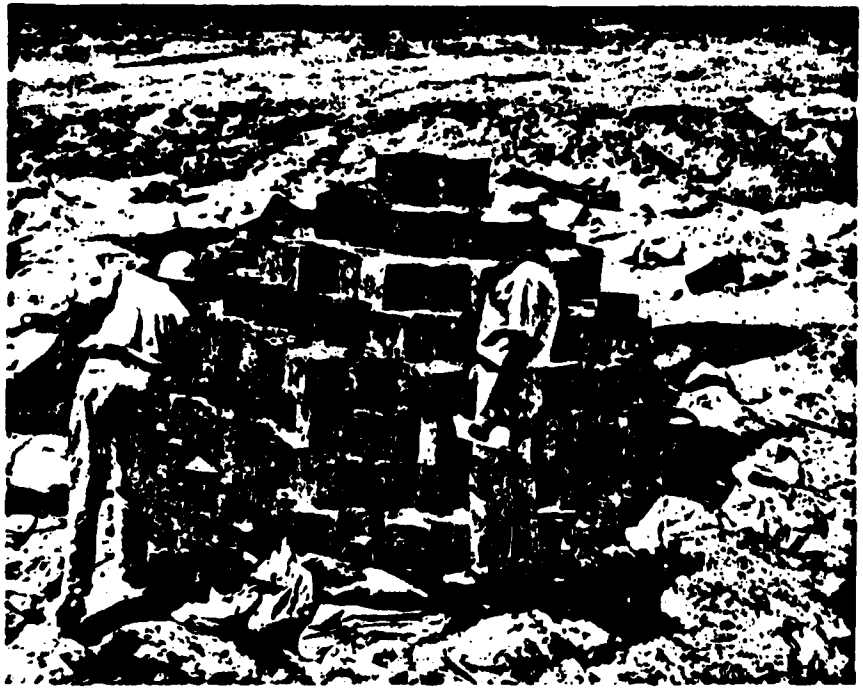

(a) (DASA-63-13-NTS-64)

(b) (DASA-64-22-NTS-64)

Figure 1.3 Flat Top I: HE stack and detonation.

Figure 1.4 Filling Flat Top I surface irregularities with grout. (DASA-58-07-NTS-64)

CHAPTER 2

AIR PRESSURE

Before Air Vent/Flat Top there had been very few air-pressure measurements from true surface bursts. Vortman and Shreve had included half-buried 250-pound spheres as part of their study of HE height-of-burst curves (Reference 18), but the principal experience had been with hemispheres resting on the ground at the Suffield Experimental Station in Canada (Reference 19). Measurements at higher pressures (> 200 psi) were also very scarce, so standard free-air pressure/distance curves to 1000 psi and above were extrapolations based more on theoretical calculations than on experiments. The various standards existing in 1963 were the Kirkwood-Brinkley curves (Reference 20), the IBM Problem M (Reference 21), the free-air pressure curves of DASA 1200 (Reference 22), and Brode's 1959 calculations (Reference 23).

The lack of experimental air pressure data and the fact that air pressure is a significant mode of coupling energy to ground shock (Reference 24) caused air-blast measurements to be planned for the initial, B-series of Ferris Wheel nuclear shots and included in the Flat Top HE shots which replaced them. No air-blast measurements were made on Air Vent.

Blast lines were conventional, extending from 20 feet (40 feet on FT-II) to more than a mile away,

covering an expected pressure range of 2000 to 0.1 psi. The principal gage used was the Ballistic Research Laboratory (BRL) mechanical self-recording gage, which uses a flexible diaphragm (of various strengths depending on expected pressure) as the sensing element and a stylus scribing a motor-driven drum as the recorder. Three kinds of electronic instruments were also used. All were diaphragm gages, but one type used bonded strain gages as the sensing element and the other two used variable reluctance pickups. Details may be found in References 6 and 7.

In Flat Top II gages extended from 40 to 9700 feet; there were 13 mechanical and 7 electronic gages measuring pressure on the ground and 2 gages measuring stagnation pressure. In Flat Top III gages were placed from 20 to 9100 feet, and there were 16 mechanical and 11 electronic gages measuring pressure on the ground and 2 gages measuring stagnation pressure. In Flat Top I gages ranged from 20 to 6545 feet; they consisted of 10 mechanical and 7 electronic gages measuring pressure on the ground and 2 gages measuring stagnation pressure.

Air pressure results taken from the original reports are given as Tables 2.1, 2.2, and 2.3. Dynamic pressure results are given in Table 2.4. These dynamic pressures were determined by point-to-point subtraction of ground-baffled pressure gage results from the stagnation pressure gage results. Therefore, maximum stagnation pressures cannot be determined simply by addition of the results reported in Table 2.4 to those in the other tables.

To scale these results to standard conditions, i.e., to sea level, 15°C, and 1 pound of TNT, the appropriate scaling factors are given in Table 2.5. The results so scaled are given in Tables 4.1 through 4.4 of Reference 6.

Dynamic pressures are consistent with ground-baffled pressures and the Rankine-Hugoniot equations. This was to be expected since the pressure/time wave shapes were clean and sharp.

Calculations of HE-generated air blast such as by Brode (Reference 23) imply that at the higher pressures there should be second pulses from reverberations within the HE gas sphere. Wave shapes from Flat Top did not show these; either the reverberant signals were small in magnitude and/or duration, and so were lost in the noise, or the assumption of spherical symmetry necessary in the calculations breaks down, most likely the latter.

In Figure 2.1 the peak pressure data are plotted together with a free-air pressure curve for 20 tons of TNT (Reference 22). At all distances, except possibly the closest, the Flat Top I data lie slightly above the data from Flat Tops II and III. The amount by which they are high is slight, hardly more than the scatter in data. Flat Top I was at a higher elevation (4840 versus 3080 feet) and hence at a lower ambient pressure, but this should lower, not raise, the pressure/distance curve. A 12-knot wind was blowing down the blast line, in the proper direction to influence peak pressure,

but examination proves that it did not have much effect. A contributing factor may have been the harder medium, limestone rather than playa silt, in which Flat Top I was fired.

Of perhaps more interest than these small differences between the Flat Top events is a comparison of the Flat Top data with free-air pressure curves and with the Suffield Experimental Station (SES) data from surface-burst hemispheres. If the surface were a perfect reflector, then a 20-ton surface burst should yield the same pressures as a 40-ton free-air detonation. In general, however, the surface of the earth is not an ideal reflector so that for near-surface bursts 1.6 or 1.7 is a more usual reflection factor. In Figure 2.1 the solid line is a standard free-air pressure curve for 20 tons at these elevations (Reference 22). It is seen that overpressures along the surface are lower than the free-air curve in the high-pressure region and higher at greater distances. The apparent reflection factor thus increases with distance, and no single factor can be ascribed to these tests. Vortman and Shreve's half-buried 250-pound spheres had yielded reflection factors of about 1.0 at all distances, but their work was done on a coarse alluvial fill (Reference 18).

Similarly, a comparison of measured overpressures with predictions based on the SES hemispheres shows good agreement at 10 psi and below, but above 10 psi the measured data were considerably lower than would have been predicted from the SES experience (Reference 6, Figure 4.3).

TABLE 2.1 AIR PRESSURE RESULTS, FLAT TOP I

Station No.	Ground Range	Gage Type	Arrival Time	Maximum Overpressure	Positive Duration	Positive Impulse	Record Quality
	ft		msec	psi	msec	psi-msec	
BRL-1	20	Elec	1.0	1280	4.6	485	Good
BRL-2	40	Elec	3.4	625	5.6	453	Good
		Mech	-	-	-	-	Questionable
BRL-3	55	Elec	6.4	354	8.0	-	Good
		Mech		348	-	-	Poor
SRI-4B	65	Elec	8.6	270	19.5	760	Fair
BRL-4	85	Mech	-	145	30	554	Good
SRI-5B	85	Elec	13.2	190	24	550	Good
BRL-5	120	Elec	23.6	75	78	691	Good
		Mech		80	75	604	Good
SRI-6B	150	Elec	34.4	65	51	470	Good
BRL-6	180	Mech	-	38	59	462	Good
BRL-7	210	Mech	-	24.5	57	353	Good
BRL-8	305	Mech	-	12.2	68	300	Good
BRL-9	900	Mech	-	2.7	-	-	Peak Only
BRL-10	1750	Mech	-	0.95	240	88	-
BRL-11	6545	Mech	-	0.18	240	18.5	-

TABLE 2.2 AIR PRESSURE RESULTS, FLAT TOP II

Station No.	Ground Range	Gage Type	Arrival Time	Maximum Overpressure	Positive Duration	Positive Impulse	Record Quality
	ft		msec	psi	msec	psi-msec	
BRL-1	40	Elec	2.8	450	6.0	583	Good
BRL-2	45	Mech	-	-	-	-	None
BRL-3	55	Elec	6.0	285	14.5	890	Good
		Mech	-	-	10.5	783	Poor
SRI-4B	65	Elec	7.2	425	-	-	Peak Only
BRL-4	85	Elec	13.2	145	24.5	709	Good
		Mech	-	140	-	685	Fair
SRI-5B	85	Elec	11.3	99	-	-	Peak Only
BRL-5	120	Elec	25.0	86	52	727	Good
		Mech	-	88	74	890	Good
SRI-6B	150	Elec	36.3	31	53	420	Good
BRL-6	160	Mech	-	41.4	56	544	Good
BRL-7	210	Mech	-	20	56	345	Good
BRL-8	305	Mech	-	10.5	80	287	Good
BRL-9	430	Mech	-	6.0	98	218	Good
BRL-10	900	Mech	-	1.9	122	103	Good
BRL-11	1250	Mech	-	1.4	131	83	Good
BRL-12	1750	Mech	-	0.66	150	50.5	Good
BRL-13	2700	Mech	-	0.43	174	34	Good
BRL-14	9700	Mech	-	0.076	227	9	Good

TABLE 2.3 AIR PRESSURE RESULTS, FLAT TOP III

Station No.	Ground Range	Gage Type	Arrival Time	Maximum Overpressure	Positive Duration	Positive Impulse	Record Quality
	ft		msec	psi	msec	psi-msec	
BRL-1	20	Elec	1.0	1700	-	-	Good Peak Only
BRL-2	40	Mech	-	-	-	-	None
BRL-3	45	Mech	-	-	-	-	None
SRI-3B	45	Elec	3.0	-	-	-	Poor Peak Only
BRL-4	50	Elec	5.0	455	8.5	647	Poor
		Elec	-	415	9.3	516	Good
		Elec	5.0	490	9.0	666	Good
		Mech	-	-	-	-	None
BRL-5	65	Elec	7.0	200	-	-	Fair
		Mech	-	184	-	-	Poor
SRI-4B	65	Elec	8.2	305	15.7	700	Good
SRI-5B	85	Elec	12.5	85	24.8	350	Good
BRL-6	90	Elec	13.0	130	27	-	Poor
		Mech	-	97	26	774	Fair
BRL-7	120	Mech	-	69	24	483	Good
		Mech	-	66	-	487	Fair
SRI-6B	150	Elec	38.0	35.5	47	490	Good
BRL-8	170	Mech	-	36	49	440	Good
SRI-7B	250	Elec	93.0	15.3	67.5	350	Poor
BRL-9	300	Mech	-	10.5	70	272	Good
BRL-10	390	Mech	-	6.7	90	231	Good
BRL-11	960	Mech	-	1.7	137	103	Good
BRL-12	1460	Mech	-	1.03	140	67	Good
BRL-13	2250	Mech	-	0.56	170	41	Good
BRL-14	4000	Mech	-	0.235	202	22	Good
BRL-15	9100	Mech	-	0.079	253	9.3	Good
		Mech	-	0.078	257	9.3	Good

TABLE 2.4 DYNAMIC PRESSURE RESULTS, FLAT TOPS I, II, AND III

Shot	Station No.	Ground Range	Maximum Dynamic Pressure	Maximum Mach No.
		ft	psi	
FT-I	BRL-3	55	326	1.12
	BRL-5	120	68.4	1.07
FT-II	BRL-3	55	603	1.70
	BRL-5	120	71.9	1.02
FT-III	BRL-5	65	791	2.25
	BRL-6	90	212	1.88

TABLE 2.5 SCALING FACTORS

	Flat Top I	Flat Top II	Flat Top III
$S_p = 14.7/P_o$	1.168	1.109	1.126
$S_d = [P_o/14.7W]^{\frac{1}{3}}$	0.0278	0.0283	0.0281
$S_t = S_d \times [(T_o + 273)/288]^{\frac{1}{3}}$	0.0281	0.0277	0.0278
$S_I = S_p \times S_t$	0.0328	0.0307	0.0313

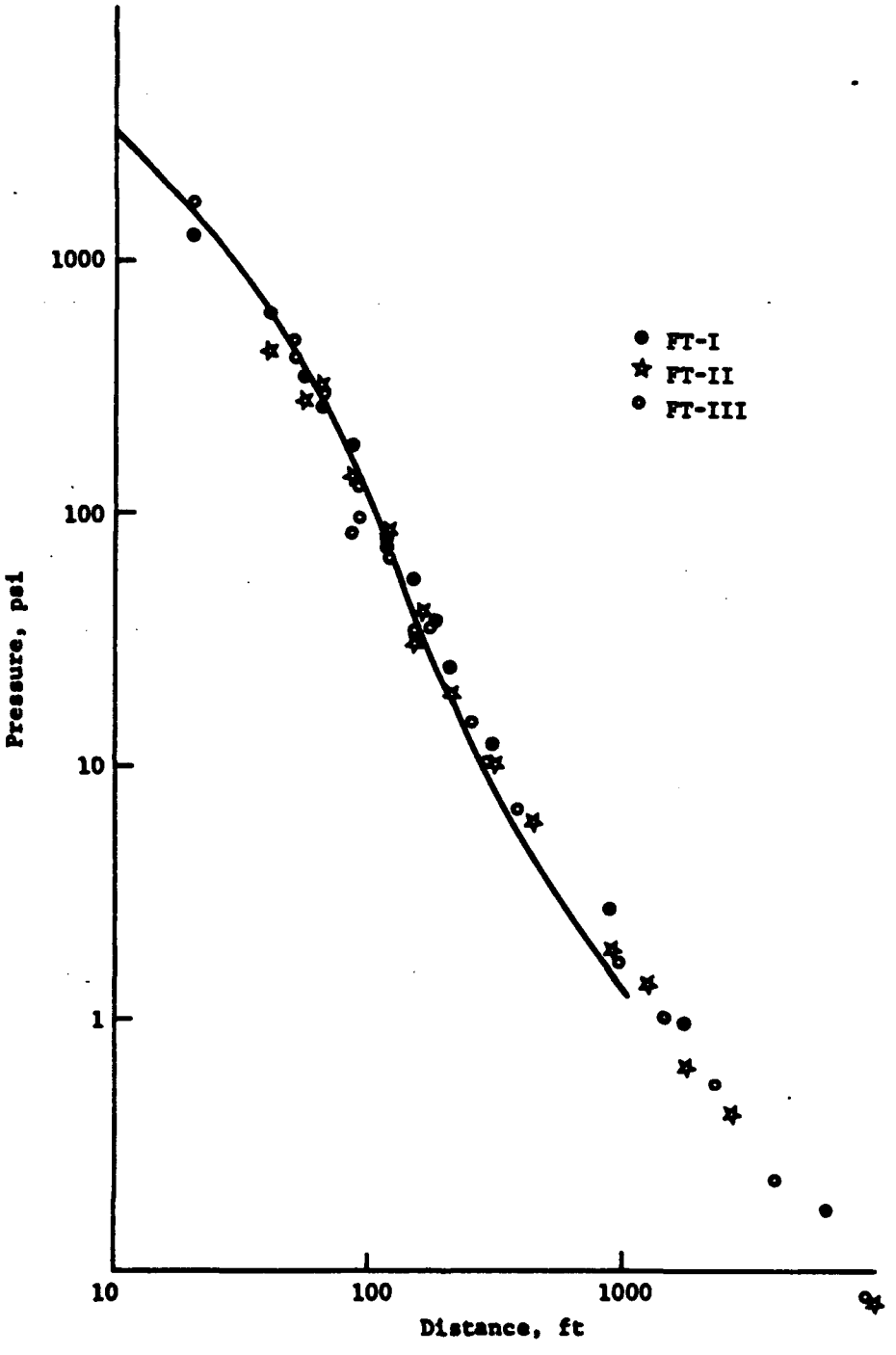

Figure 2.1 Air pressure *versus* distance, Flat Tops II, III, and I, compared with a 20-ton free airburst curve.

CHAPTER 3

GROUND SHOCK

3.1 INTRODUCTION—TYPES AND SOURCES OF GROUND SHOCK

The measurement of ground shock from near-surface bursts was pioneered by Lampson in the early forties (Reference 25). Since then there have been measurements on the Jangle, UET, Mole, Scooter, and Stagecoach HE tests and on numerous nuclear tests (References 24, 26 thru 30).

From these various sources, there has emerged a picture of ground shock produced by a combination of the direct action of the explosive on the ground and air blast (Reference 24). The directly induced ground shock is generically like the shock generated by an explosion entirely contained within the earth, although severely modified by the presence of the earth's surface. In fact, surface and contained bursts are sometimes related empirically by a coupling factor which is defined as the cube of the ratio of distances at which the same ground shock pressure (or velocity) is obtained from a surface as compared to a contained burst (Reference 31). The coupling factor is necessarily a variable, decreasing from approximate unity adjacent to the explosive to considerably lower levels at greater distances.

The air-induced ground shock varies with depth of the explosive burst in that the wave shapes of the air blast change. More important, the air-induced ground

shock also depends on the velocity of the air shock relative to the medium beneath it. Within the range of general interest, the velocity of an air shock varies markedly with the strength of the air shock, whereas the velocity of the associated ground shock varies little with its strength but is dependent on the medium it traverses. Air-induced ground shock is, therefore, commonly called superseismic, transseismic, or subseismic, as the velocity of the air shock is greater than the velocity of a compressional wave in the soil, between the soil's compressional and shear velocities, or less than either:

Superseismic	$U_{air} > C_p > C_s$
Transseismic	$C_p > U_{air} > C_s$
Subseismic	$C_p > C_s > U_{air}$

In the superseismic case, the air-induced ground shock is a wake left in the ground whose angle of progress into the ground is related to the ratio of velocities by a Snell-like law:

$$\sin \theta = C_p/U_{air}$$

In the other two cases, a ground shock gets ahead of the air shock; the two are often lumped together and called an outrunning ground shock. An outrunning shock can also be, and often is, caused by higher velocity layers not at the surface but deeper in the ground.

3.2 SCALING RULES

One other matter of general concern must be mentioned here: scaling. Scaling is the name given to rules extrapolating phenomena to yields other than those tested. Strictly speaking, scaling refers to rules governing any sort of extrapolation such as to media of different sound velocities and is closely related to the dimensional analysis of the problem. This, however, is strict beyond the common usage.

For air blast, the appropriate scaling rules were stated by Sachs 20 years ago (Reference 32) and can be summarized in the formalism

$$\frac{p}{p_o} = f\left\{r\left(\frac{p_o}{W}\right)^{1/3},\ ct\left(\frac{p_o}{W}\right)^{1/3}\right\}.$$

For totally contained explosions, the scaling rules were set forth by Lampson and can be summarized

$$\frac{u}{c} = f\left\{r\left(\frac{\rho_o c^2}{W}\right)^{1/3},\ ct\left(\frac{\rho_o c^2}{W}\right)^{1/3}\right\}.$$

For directly induced ground shock, the same formalism applies at least approximately, assuming that viscosity, gravity, and some other variables have a negligible effect. For air-induced ground shock, two media are involved and a more complex formalism is required. If the ground is isotropic and elastic, scaling rules

have been set forth by Sauer (Reference 24). There are now several dependent variables, and the formalism becomes

$$\frac{p}{p_o} = f_1\left[r\left(\frac{p_o}{W}\right)^{1/3}, at\left(\frac{p_o}{W}\right)^{1/3}\right];$$

$$\frac{u}{C_p}\left(\frac{\rho C_p^2}{p_o}\right) = f_2\left[r\left(\frac{a}{C_p}\right)\left(\frac{p_o}{W}\right)^{1/3}, z\left(\frac{a}{C_p}\right)\left(\frac{p_o}{W}\right)^{1/3}, at\left(\frac{p_o}{W}\right)^{1/3}, \frac{C_s}{C_p}, \frac{p}{p_o}\right]; \text{ and}$$

$$\frac{w}{C_p}\left(\frac{\rho C_p^2}{p_o}\right) = f_3\left[r\left(\frac{a}{C_p}\right)\left(\frac{p_o}{W}\right)^{1/3}, z\left(\frac{a}{C_p}\right)\left(\frac{p_o}{W}\right)^{1/3}, at\left(\frac{p_o}{W}\right)^{1/3}, \frac{C_s}{C_p}, \frac{p}{p_o}\right];$$

where
- p = the transient air pressure
- u = radial component of soil particle motion
- w = vertical component of soil particle motion
- r = the radial coordinate
- z = the vertical coordinate
- t = time
- a = sound velocity in air
- p_o = ambient pressure in air
- ρ = soil density
- C_p = compressional velocity in soil
- C_s = shear velocity in soil
- W = energy release

In all three instances, the distance and time scales are related to the cube root of the energy release; this is called cube-root scaling. In Sauer's scaling, the ratio of properties of air and ground are important $\left(a/C_p \text{ and } p_o/\rho C_p^2\right)$; these are equivalent to the role played by Mach numbers in scaling aerodynamic phenomena and yield the distinction between the superseismic and outrunning air-induced ground shocks already referred to. If the ground is layered, this layering too must scale by similar rules.

3.3 RELATED CALCULATIONS

The general idea of the Ferris Wheel program is of calculation tested by experiment. Ideally the calculations should precede the experiment, but organizing and running experiments is a matter in which there was experience and on which the pressure for progress was exerted. The business of organizing and running calculations is more difficult and, consequently, the desired order was reversed and calculations followed experiment.

Explicit calculations of ground motion require the use of a code capable of solving the partial differential equations for conservation of mass, momentum, and energy appropriate to the configuration of the problem. A knowledge of the constitutive relations of the ground media and of the explosives used is also required.

The classical surface-burst ground-motion problem is that of Bjork and Brode, who used a Particle-in-Cell (PIC) code to calculate a megaton surface burst on tuff,

with the tuff described by a hydrodynamic equation of state (Reference 33). At an early stage in Ferris Wheel planning, Hamada of the Air Force Weapons Laboratory used a similar code, SHELL, to calculate a 20-ton nuclear burst at a depth of 17 feet in alluvium (Reference 34). Except for source configuration, which can be quite important, this is somewhat like the Air Vent Phase I shot.

The configuration of the Flat Top shots and of Air Vent I were calculated on PIPE, Physics International's two-dimensional, Lagrangian, plastic-elastic code. This code is two-dimensional in that it simplifies such problems to two dimensions by taking advantage of their cylindrical symmetry. It is Lagrangian in that the space zones needed for the finite difference analogs to the equations of motion are constrained to move with the material whose motion they describe. It is nonhydrodynamic in that it keeps track of the tensor nature of the stresses and strains of the material, resolving, for instance, the stress tensor into pressure and deviator components. It is elastic-plastic in that the magnitude of the stress deviators is limited by a von Mises or a Mohr-Coulomb yield criterion, after which irrecoverable work is done distorting the material. The crushing of porous playa material and irreversible phase changes in limestone are also approximated.

PIPE calculations were made over a period of 2 years, first for Flat Tops II and III (Reference 35), then for Flat Top I and Air Vent I last (both Reference 36). The methods used were more sophisticated in the later calculations. This may be seen in the mate-

rial properties used, indicated in Table 3.1. The description of limestone used in the Flat Top I calculation uses a crushing-type equation-of-state to approximate phase changes. The Air Vent I problem was treated as a problem of layered media; three equations-of-state were used, each of which is a volume-weighted mixture of those for pure water and quartz sand.

In Figure 3.1 the limestone Hugoniot implied by Table 3.1 is compared with experimental data. As the code handles it, the shock front is smeared out into several zones by an artificial viscosity within which region the material compresses to a point along the Hugoniot shown. If a zone of material ever goes past the 115-kilobar stress level, it then relaxes along the second branch of the curve to a density of about 2.91, instead of the initial density of 2.66. This irreversible compression is to represent an irreversible conversion of at least part of the material from calcite into aragonite. If a stress of less than 115 kilobars is reached, the relaxation is to an intermediate density.

Another mechanism providing for dissipation of energy comes through the yield criteria used. Work is done against the stress deviators, appearing as strain distortion energy, but when the yield limits are exceeded part of the work done is irrecoverable—only the elastic strain energy is recovered.

Therefore when these problems predict decreases of stress with distance, as they do, the mechanisms provided for these decreases are geometric spreading, irreversible compaction, and irreversible increases of distortional strain energy.

The results of these calculations appear in Section 3.5.5, where they are compared with measured data. Each problem was run until zone distortion made further rezoning impractical, which was for 1.5 msec real time in Flat Tops II and III, 1.83 msec in Flat Top I, and 4.57 msec in Air Vent I. These carried the problems to distances of 17 feet for Flat Tops II and III, 30 feet for Flat Top I, and to 28 feet for Air Vent I.

3.4 DESCRIPTION OF EXPERIMENTS

Six projects yielded ground motion data. They were:

Air Vent	A	SC	Ground motion	Ref. 1
	B	SC	Surface motion photography	2
Flat Top	1.2	SRI	Ground motion	7
	1.3a	SRI	High pressure measurements	7
	1.3b	IITRI	High pressure measurements	8
	1.4	SC	High pressure measurements	9

Some of the pressure and velocity data obtained are tabulated in Tables 3.2 through 3.4; more may be found in the original reports.

Four shots in the series were instrumented for ground motion, Air Vent I and the three Flat Top shots. On the buried shots of Air Vent II there was surface motion photography.

The blocks for the large buried Air Vent I charge, 20 tons, were passed down a temporarily cased drill hole, 4 feet in diameter, and stacked in an undercut cavity. Extra space under and around each layer was filled with sand, hand-poured but not tamped. When the stack was complete, the casing was withdrawn and the entry shaft filled and loosely tamped with moistened playa to approximate the original density.

The small 256-pound Air Vent charges were placed in holes drilled to the necessary depth, bedded in sand, and the entry hole refilled as for Air Vent I.

All three Flat Top shots were stacked in hemispherical holes of about 5-foot radius. In Flat Top II, the material used to fill the spaces between each layer of HE and the playa was common alluvium, screened to remove the coarser fragments. No controls were used on it; it was simply put in where and as needed. Its thickness was about 4 inches near the Stanford Research Institute (SRI) and IITRI high-pressure gages (Projects 1.3a and b). After the firing of Flat Top II, there was concern whether alluvium might have been much less dense than the native playa and could have caused the high-pressure gages to read low. A measurement was made of the alluvial material used for filling the spaces, treating it as it had been treated in the emplacement of the Flat Top II shot, and it was found to have a density of 104 lb/ft^3, or 1.66 gm/cm^3. It therefore appears that the material was about right and caused no serious data errors.

In the emplacement of Flat Top III, the original material was carefully tamped around each layer of HE, with samples being taken periodically to monitor density and moisture content. Density was 95.4 ±2.3 lb/ft^3; water content was 15.6 ±2.44 percent by weight, with the number of samples being 27 and 4, respectively.

For the emplacement of Flat Top I, a limestone-matching grout was developed (Reference 14; Table V of Reference 17) consisting of an epoxy resin binder and a dense dolomitic sand, with kerosene as a wetting agent. Specifications for the grout were that it approximately match the Hugoniot of limestone in the 100- to 200-kilobar region, that it set slowly enough for field use, and especially that its curing temperature not rise above 150°F because, except for mylar sheeting used to avoid unwanted chemical interactions, it was in direct contact with the HE. After each layer was laid in place, grout was poured around it to the level of its upper edge and allowed to set before the next layer was laid in place. A close-up of the stack with the final top of the grout is shown in Figure 3.2.

The natural surface around Flat Tops II and III was ideally flat and required no further treatment. The limestone of Flat Top I was covered by a 6- to 18-inch layer of debris. This was removed to a radius of about 50 feet, revealing a competent but irregular surface resulting from the natural bedding planes of the rock (strike N27W, dip 40° to SW). The lowest holes of this irregularity were evened out with grout, but no further smoothing was done (Figures 1.4, 3.2).

3.4.1 Instrument Plan—Air Vent. Air Vent was primarily for cratering studies on a minimum budget, so dynamic measurements were kept to a minimum. On Air Vent I, one quartz gage, two accelerometers, and five velocity meters were installed at the shot depth of 17 feet, at ranges of 25 to 170 feet. Only radial components of motion were measured. There were no gages on any other Air Vent shot.

Photography yielded surface motion data on all shots buried sufficiently deep that explosive gases did not vent immediately. This included Air Vent I and 12 of the Air Vent II shots. For this purpose, Fastax cameras were used with framing rates of 2400 to 6500 frames per second. On Air Vent I they were at a distance of 1100 feet—closer for other shots.

Data resulting are given in Table 3.2.

3.4.2 Instrument Plan—Flat Top. The Flat Top III experiment plan was the basic plan for the series of experiments, Flat Top II being much reduced in scope. Flat Top I was not authorized until after Flat Top III was designed; if Flat Tops I and III had been designed together, both experiments could conceivably have been somewhat different. As it was, the Flat Top I instrument layout included what parallels were possible.

These experiments were primarily ground motion experiments with an emphasis on measurements underneath the shots. These required the use of a shaft and tunnel for bringing out instrument cables, as pioneered

on Small Boy (Reference 37). The shaft was at a radius of about 40 feet, the tunnels at a depth of 40 feet for Flat Tops II and III, 35 feet for Flat Top I. All shafts and tunnels were filled with uncompacted soil before firing. The region of interest for measurement of directly induced ground motion lay in the range of particle velocities of 10 to 100 ft/sec. To be sure this range was covered, the experiment was designed for a somewhat larger range that put the closest motion gage 10 feet from charge center and the farthest 57 feet from charge center. In Flat Top I, these distances became 17 to 100 feet.

On Flat Tops II and III, a hole (Station 0) was drilled at ground zero to a depth of 57 feet under the charge; on Flat Top I it was to a depth of 100 feet. On Flat Top III a second hole (Station 1) was drilled at a radius of 20 feet, intersecting the instrument cable tunnel. In Flat Top I there was a hole drilled at an angle of 45 degrees for 80 feet from ground zero, intersecting its instrument cable tunnel.

Gages for measurement of air-induced ground motion were installed in 17-foot holes at distances of 30, 45, 65, 85, and 150 feet; in Flat Top III, at 250 feet also. In each hole gages were placed at nominal depths of 1 and 17 feet, except for Flat Top II, where the deeper gages were omitted.

The primary instrument used on Flat Top was the SRI Mark II velocity gage. On Air Vent I it was the Sandia-modified DX version. Accelerometers backed up some of the positions, as did a few strain gages. Generally speaking,

holes were instrumented for both vertical and radial components with a few obvious exceptions such as the zero hole, where only vertical components were expected, and the Flat Top I 45-degree hole, which was instrumented for slant components.

Flat Top I posed severe problems because the high impedance of the limestone implied large accelerations which would require a very fast time response for the then state-of-the-art. New gage systems were tried, but, it must be admitted, the return of data from Flat Top I was far from what was desired.

3.4.3 Gages for High-Pressure Measurement—Flat Top. Air Vent/Flat Top was to supply experimental data on which to test and normalize theoretical calculations. These calculations necessarily start with the source itself and therefore with the 200-kilobar Chapman-Jouget pressure of a TNT detonation wave and the somewhat lower pressure induced into playa or limestone. To check the initial coupling requires measurements of high-pressure shock waves. At the time Flat Top was undertaken, DASA had been subsidizing the development of the necessary gages for several years.

Two kinds of gages were ready for field trial and use. Both were piezoresistive gages. The one developed by IITRI and fielded in Project 1.3b (Reference 8) relies on the decrease of resistivity of water and paraffin with increase in pressure. The gage is made of a cylindrical capsule containing the piezoresistive material. Two platinum probes are maintained at a voltage

difference, and any change in resistivity of the piezoresistive material between the probes establishes a measurable change in electric current.

The gage developed at SRI and fielded in Project 1.3a (Reference 7) relies on the increase in resistance of manganin with pressure. The gage consists of a short length of fine piezoresistive manganin wire connected across appropriate electrodes, the whole imbedded in a short cylinder of Armstrong C-7 epoxy with the wire parallel and close to one flat face, which is placed transverse to the direction of shock propagation. With a constant current applied to the wire, increases in ambient pressure cause increases in voltage across the wire.

For both gages there was concern about the shock impedance of the gage material compared to the surrounding playa or limestone. The C-7 epoxy of the SRI gage was by itself a relatively good match to the playa in which Flat Tops II and III were fired (Reference 7, Figure 5.2) but a poor match to the limestone of Flat Top I. At that time the technique of mounting the manganin wire in natural materials had not yet been developed, so that the data had to be interpreted through analysis of the mismatch between the Hugoniots of limestone, grout, and gage. Similarly, the water of the IITRI gage was a fair match to the playa of Flat Tops II and III. For Flat Top I the piezoresistive material of the IITRI gage was paraffin loaded with WO_3 to get a better match to the limestone and to the epoxy grout immediately around the gage, but the match was by no means perfect.

In addition to these gages, on Flat Top III a Sandia plexiglas peak-shock pressure gage was installed by SRI next to one of their gages for a comparison of peak strengths. This gage operates by measuring shock velocity through a material whose equation of state is well known.

On Flat Top I, quartz gages were installed by Sandia as Project 1.4 (Reference 9). These gages operate by the well-known response of X-cut quartz to X-axis stresses. Charge release was integrated by accumulation on an appropriate capacitor, whose voltage versus time was monitored.

3.4.4 Gage Layout—Flat Top. On Flat Top II, two gages, one IITRI and one SRI type, were installed in a trench intersecting the hemispherical excavation for the charge. Both gages were very close to the stack (5-3/8 and 8-1/4 inches, respectively) and about 69 inches from the center of the stack (Reference 7, Figure 5.11).

The excavation for Flat Top III was hand carved in the region next to the high-pressure gages so that the TNT blocks could be fitted very close to undisturbed playa. The SRI gages were put into a hole specially dug and cut so that their front faces could also fit snugly against undisturbed surfaces. Four of them and the Sandia plexiglas gage were installed at ranges of 53 to 95 inches from charge center. Three IITRI gages were installed in a hole drilled into the bottom of the excavation for the HE at distances of 65, 71, and 77 inches from the charge center (Reference 7, Figure 5.14).

Four SRI, five IITRI, and four Sandia quartz gages were installed on Flat Top I. Two 10-inch diameter holes and one 8-inch hole were drilled for this installation, the 10-inch holes being normal to the surface and at 45 degrees to the normal, and the 8-inch hole at 30 degrees to the normal. In an effort to make the nearest measurement in as undisturbed a situation as possible, the first gages in the vertical and 45-degree holes were fastened to marble cylinders of the same diameter as the hole, but none of these four gages yielded data. One SRI gage was taped directly on a TNT block of the stack. Altogether in the 0-degree hole there were five gages, one SRI and four IITRI, at distances from 6 to 10 feet. In the 30-degree hole were one SRI gage at 8.5 feet and the four Sandia quartz gages at distances of 8.5, 10, 13, and 17 feet. In the 45-degree hole were two gages, an IITRI and an SRI, both at 6.9 feet (Reference 7, Figure 5.15). These gages were grouted in place with a cement grout loaded with magnetite to bring its density up to that of the limestone.

The data resulting from these gages are summarized in Table 3.3.

3.5 RESULTS

3.5.1 Arrival Times. In Figure 3.3 are plotted arrival time data from the three playa shots in the holes under the shots and at the 17-foot depth in the 30-foot radius hole. These positions are those away from the surface, with travel paths most apt to be representative of body waves that these shots afford. The scatter of the data is great because here are

lumped data from accelerometers, velocity gages, strain gages, and one quartz gage. It has long been believed that accelerometers give more precise and earlier arrival times, so data from accelerometers are encircled. A body-wave velocity of about 2300 ft/sec is indicated, much as expected.

Similar data from Flat Top I are shown in Figure 3.4. In this case, the data within a range of 35 feet imply a body-wave velocity of 18,000 ft/sec, consistent with preshot small sample determinations of 20,000 ft/sec (Reference 17, Table IV). Beyond that range, the apparent velocity is 100,000 ft/sec. Such a velocity is clearly impossible, and it must be presumed these are spurious signals caused by the collapse of the 35-foot deep cable tunnel and pinching of the cable. Wave shapes of a few of the gages so affected show another signal at expected arrival times (Reference 7, Gages OVV7, OVV8, OVV9, in Figures 7.12 and 7.13).

In Figure 3.5 are shown arrival time data from near-surface gages on all three Flat Top shots. On Flat Tops II and III there are many accelerometer data

from 1-foot depth and only their arrival times are plotted; on Flat Tops II and III at 17 feet and on Flat Top I at both depths there were only velocity gages, and it is their data that are plotted. Also on Figure 3.5 are curves of surface-level air pressure times of arrival, as obtained by Project 1.1 (Reference 6, Figure 4.1), and body-wave times of arrival as shown in Figures 3.3 and 3.4.

It is clear that all near-surface gages on Flat Tops II and III are responding first to air pressure; the air-induced ground wave is indeed superseismic, as defined in Section 3.1. The residual lag, running 2 msec or more, implies a compressional wave velocity over the first foot of depth of less than 500 ft/sec. A velocity of 500 ft/sec is quite low; as we shall see later, it is inconsistent with that required to account for the magnitude of coupling of air shock to ground shock. The ground motion at 17-foot depth arrives substantially later. The time differentials between 1 and 17 feet are consistent with compressional wave velocities of 1100 to 1500 ft/sec if this signal is indeed primarily air induced. It is, however, little in advance of the body wave.

On Flat Top I, arrivals are at a velocity of about 13,000 ft/sec, well in advance of the air wave. Moreover, arrivals at the 17-foot depth are substantially simultaneous with those at the surface. Clearly, the first arrival is a body wave; the air blast is transseismic or subseismic. That the radially horizontal velocity is much less than the vertical velocity must be an effect of the layering of the rock.

It is therefore to be concluded that the air-blast-induced ground motion of Flat Tops II and III was superseismic and that of Flat Top I was subseismic. This was to have been expected. The playa velocity of 2300 ft/sec corresponds, at this altitude, to a pressure of 50 psi observed at a distance of 170 feet, the limestone velocity of 13,000 ft/sec to a pressure of 2000 psi at 15 feet. Strictly speaking, Flat Top I was transseismic out to 40 feet and only subseismic farther out. These statements are summarized in Table 3.5.

3.5.2 Measurements of Close-in High Pressures. The numerical calculations made by Physics International have been described in section 3.3. They included both stresses and particle velocity both near the surface and at deeper positions. These calculations were carried out to distances of 17 feet for Flat Tops II and III, to 30 feet for Flat Top I, and to 28 feet for Air Vent I, thereby covering the region of high-pressure measurements but stopping short of the velocity measurements.

Stresses computed for Flat Tops II and III are reported differently in Physics International's final report (Reference 35) than in the preliminary results (Reference 38) that Sauer used to prepare Figure 8.4 of Reference 7. Both sets of predictions are shown in Figure 3.6. The reason for the change from preliminary to final reports is not known.

Out of ten gages, six gave some sort of data on Flat Tops II and III. At first this appeared to be a

good return on a project which was more than half field prove-in for a new kind of instrumentation; however, the data are confusing since a number of the records show multiple steps. Precursors are not to be expected in playa; its elastic limit, if any, is well below a kilobar. Perhaps the multiple steps are a result of the fact that the surface of the TNT charge was not a smooth sphere but a series of 8.5-inch steps (Figure 1.1) and, of the gages that gave data, none was more than 20 inches from the TNT.

Peak stress data are plotted in Figure 3.6. Where there are steps in the record, each level is plotted. All that can safely be said about these results is that there is for each gage one step in the record that agrees with the predictions. There may be a tendency for the measurements to be higher than the predictions.

Flat Top I is more clean-cut. Three piezoresistive gages survived out of nine installed and three quartz gages out of four. All are plotted against the computed results in Figure 3.7. The two piezoresistive gages in free-field positions agree remarkably well with the computations. Sauer, Lieberman, and Godfrey all comment on the perturbations to be expected because the gage necessarily was mounted in a grout-filled hole (References 7, 8, and 36). Sauer explains the coincidence of the agreement being so good, in spite of mismatches, by the fortunate circumstance of reflection at the axis making up for a drop on the shocks entering the lower impedance grout (Reference 7, p 171). The mismatch of a gage in grout deserves more study.

The piezoresistive gage at 4.5 feet was not free-field but was taped on an exposed surface of HE; its reading is inexplicably low. The quartz gages are low, as they were later in Tiny Tot; they were, however, much influenced by the electromagnetic pulse from the TNT.

There is indication of a two-wave shock structure in the limestone of Flat Top I from the wave-shape piezoresistive gage record, the precursor being almost 10 kilobars in strength, as expected (Reference 7, Figure 7.60).

The calculated predictions for the Flat Top shots inherently include the effects of the surface, both as its presence affects wave shapes and as it produces nadir angle variation of peak stresses. As to wave shapes, there are no useful comparisons with the data since the gages lived only very short times, none longer than 80 μsec, whereas the zoning of the calculation smeared out detail that fine. Angular dependences calculated are shown in Figures 3.8a and 3.8b. Gage positions are plotted, with peak stresses indicated next to the positions. These again show that on Flat Tops II and III there is in each case among the steps of the record one that agrees with calculation, and that on Flat Top I two of three piezoresistive gages agree nicely with calculations, but the quartz gages are low.

3.5.3 Velocity Measurements on Flat Tops II and III and Air Vent I. At larger distances on the playa shots there was a variety of measurements, plotted together in

Figure 3.9. These include velocities measured directly on Flat Tops II and III and Air Vent I, one quartz gage pressure measurement on Air Vent I converted to velocity, using as inputs to the acoustic impedance a density of 1.5 and a velocity of 2300 ft/sec, and eight velocities inferred from surface motion photography on the buried 256-pound charges of Air Vent II. The accompanying calculational results are two. That for Flat Tops II and III has two branches, one being what the calculation would have predicted had they been contained bursts and the other, below it, including the effect of the presence of a free surface. The prediction for Air Vent I is for a horizontal line at gage depth.

Setting aside for the moment the surface-motion data, velocities measured on Air Vent I can easily be construed to lie on or slightly below the implied (dashed) extension of the Air Vent I calculations; velocities measured on Flat Tops II and III are on or slightly above an implied extension of the Flat Top predictions, and below the Air Vent I data. The Air Vent II surface-motion data, on the other hand, are high by roughly a factor of two compared to direct measurements of velocity. These surface-motion data are free-surface velocities and for plotting have been divided by two in the usual fashion. Such a comparison of surface motions with contained motions had been satisfactory before, (e.g., Reference 30, p 105), so this discrepancy came as a surprise in Air Vent.

At first sight a possible explanation would be surface layers of lower acoustic impedance for then, if there is normal incidence on a single soft layer, the surface

would spall off at a velocity of $4Z_o/(Z_o + Z_s)$ as fast as the particle velocity of the body wave (where $Z = \rho c$, and subscript s refers to the surface). This multiplication factor has a maximum value of 4 for a very soft surface layer, or twice as large as the factor used to plot the data in Figure 3.9. Moreover, if the surface layer is multiple or continuous, the factor becomes larger yet: $2(Z_{initial}/Z_{final})^{1/2}$ for an impedance decreasing exponentially as one nears the surface.

Yet this explanation is not satisfying. By the latter expression above, a reduction of impedance by a factor of 4 is required at the surface. Area 5 playa is hard and unyielding and, when cut into for a trench or hole, there is no indication of such a surface layer. It is true that arrival times at accelerometers buried 11 inches deep were 2.3 msec later than air pressures at the surface, implying a sonic velocity of less than 500 ft/sec; and this is indeed about the appropriate small fraction of the body-wave velocity of about 2300 ft/sec. What is not satisfying is that no such factor had to be called into account in the alluvium of Area 10, and that on Priscilla, also in Area 5 playa, a surface velocity of 1000 ft/sec was right to account for the coupling in the other direction of air pressure into the ground (Reference 39). Again, 1000 ft/sec is about the right velocity to account for the relationship between Flat Tops II and III air pressures and vertical particle velocities near the surface. Therefore, the discrepancy of the Air Vent II surface motion measurements must be left unexplained although the free-field or body motions are about as calculated for playa.

Figure 3.9 includes only measurements that should have been relatively little affected by the presence of the surface and specifically excludes records which show signs of having been influenced by air-blast-induced ground shock. The Flat Tops II and III playa shots, however, were expected to be superseismic at all ranges beyond the immediate crater area. To study this effect, vertical and radially horizontal velocity gages were installed at the surface and at 17-foot depth, at ranges out to 250 feet.

Over this whole range, acceleration peaks were dominated by the air-induced signal and displacement by the direct or body-wave signal. As to velocities, both sources were of comparable magnitude, with air-induced motions dominating peak vertical velocities, and direct ground-transmitted motion dominating peak horizontal velocities, the latter coming at a later time.

Figure 3.10 repeats Figure 3.9 but with the addition of horizontally radial components of velocity from the 1- and 17-foot gage stations. These data really do appear to be a continuation of the data closer in. They also lie under the Air Vent I data, demonstrating the expected result that a surface shot generates a ground wave less strong than that of a buried shot.

That the maximum vertical velocities follow the air blast above has already been shown by coincidence of arrival times (Figure 3.5). It also follows from the wave shapes themselves and from the apparent coupling factor.

It will be remembered that the expected relation between air pressure and the vertical component of velocity is

$$P = \rho c u \ .$$

The coupling factor is the seismic impedance $Z = \rho c$, the product of soil density and sonic velocity. Using a density of 1.5 gm/cm^3, and a surface velocity of less than 500 ft/sec would give a surface impedance of less than 10 psi/ft/sec. Table 3.6 shows overpressures measured in Project 1.1 and vertical velocities measured in Project 1.2, together with the impedance or coupling factors to be inferred from these data. It is quite clear that the effective impedance is a good deal larger than 10 psi/ft/sec. Sauer attributes this kind of discrepancy to non-elastic dissipation.

In Figure 3.11, vertical velocities near the surfaces (circles and white stars) are compared with measured air pressures divided by 20. An impedance of 20 psi/ft/sec corresponds to a seismic velocity of 1000 ft/sec, as at Priscilla (Reference 39). Also in Figure 3.11, vertical velocities at 17 feet are shown as black stars. The attenuation with depth averages a factor of 6. (Interestingly enough, the horizontal component also decreases with depth, as can be seen in Figure 3.10, by an average factor of 2.) Finally, at the closer ranges, vertical velocities are slightly less than horizontal velocities at both depths, while at greater ranges the vertical is four times the horizontal near the surface and two times the horizontal at the 17-foot depth.

3.5.4 Velocity Measurements in Flat Top I. In Flat Top I there were fewer distant measurements that were successful. Figure 3.12 shows the lot. The final Physics International calculations (Reference 36) differ only at the lower end from the preliminary results (Reference 40) used by Sauer in Reference 7, eliminating an upturn at the end, which Sauer attributed to the onset of a two-wave structure but including the start of the expected nadir angle dependence. Of the data shown, the closest two are the velocity equivalents of pressures measured by the two piezoresistive gages, and the next three of pressures implied by quartz gages. All points plotted at 25 feet or more are of velocities measured as such, those at 66 and 86 feet being from gages 4VR2 and 5VR2, for horizontal radial components at 17-foot depth. All data are approximately in line with the predictions.

Flat Top I was expected to be subseismic or transseismic at all gage ranges, and the data bear this out. Arrivals are earlier than air blast; horizontal components are five to six times as large as vertical; there is no attenuation with depth. In short, the records and wave shapes are dominated by the direct wave.

The precursor noted in one high-pressure gage could not be expected in the velocity records since its 6-kilobar strength is equivalent to a velocity of 200 ft/sec, larger than any velocity measurement.

3.5.5 The Symmetry Experiment. On Flat Top III, seven gages were placed in a circle 65 feet in radius, all at 17-foot depth. The data are listed in Table

3.4D. Vertical velocities agree within a σ of 16 percent, radial to within a σ of 40 percent (1.29 ±0.21 and 3.03 ±1.21 ft/sec, respectively). Tangential velocities were not zero, being first clockwise then counterclockwise, as viewed from above, with magnitudes of about 1/2 ft/sec. The gage most out-of-line was the one in the direction of the main blast line; with its data left out, the deviations reduce to 13 and 28 percent (1.34 ±0.18 and 3.35 ±0.94 ft/sec).

That the gage in the direction of the main blast line was the one most out-of-line is dismaying, but it was probably because of flooding the winter before. The Flat Top III instrumentation had originally been that for Ferris Wheel B-1,and when the Ferris Wheel B-series was canceled the orders were to close down with a minimal additional expenditure of money. The zero area, shaft, and tunnel were not filled up but were surrounded by a berm, or dam, which broke in a flood. The shaft and tunnel sat full of water for several weeks until they could be pumped out again. It was evidently an error in judgment, and false economy, not to have filled up the shaft.

No such flooding problem afflicted Flat Top II. Its site had originally been for the HE Shot B-3 which was almost ready to fire at the time of cancellation, so all holes had already been refilled. Despite the flooding, the data from these two shots are in fair overall agreement in wave shape and in magnitude. Comparison of wave shapes shows that in the symmetry experiment it was the first peak itself that was principally affected, not the wave form as a whole.

3.5.6 Comparisons of Flat Top I and Flat Top III Media. It is of interest to compare similarly located gages in Flat Top I and Flat Tops II or III. Because of the low gage survival in Flat Top I, the most extensive set of comparisons that can be made is of the gages for vertical component of velocity at 17-foot depth. Their readings are shown in Figure 3.13 to common time and amplitude scales,and relevant data from them and a few others is tabulated in Table 3.7.

While the wave forms are similar, the magnitudes of the first peaks are less and the frequency contents higher for Flat Top I than for Flat Top III. One might expect the ratio of magnitudes to be as the ratio of impedances or roughly 9:1, but the ratio is less, varying from 1.3 to 6.6:1, and the ratio of impedances really should not apply because the one shot was superseismic and the other transseismic. One might also expect the ratio of frequency contents, i.e., the ratio of time scales, to be by the ratio of sonic velocities or 5.5:1. Actually, the ratio of arrival times is 4.5:1, the ratio of times of first negative peaks about 4:1, and the ratios of times of maximum positive peaks vary widely from 3:1 to over 10:1.

There are a few other comparisons possible between Flat Tops III and I. Two near-surface gages in similar positions, 3VV1 and 4VV1, gave data on both. Their ratios of peaks were 15 and 19:1, rather more than the ratio of impedances. Considering that the basic phenomena governing vertical components were quite different in the two shots, it might be apropos to compare horizontal radial components, both being body-wave signals.

At the 17-foot depth, two such comparisons are possible, at 65 and 85 feet. In this comparison (Table 3.7), wave forms are again similar, frequency content is again higher in Flat Top I than in Flat Top III, but magnitude of the first outward-velocity peak is now twice as high in Flat Top I than Flat Top III instead of the other way around.

3.5.7 Gage Performance. A purpose of these experiments was field testing the new high-stress piezoresistive gages; these systems needed to be tried against each other under the rigors of conditions on a real test. As indicated in Table 3.8, both gages installed on the first or Flat Top II shot appeared to work, except that the resulting wave forms were far different from those expected. This brought about a change in the backfill around the charge stack, elimination of a four-block first layer, and moving some gages to a more favorable location relative to the stack.

In Flat Top III, the second shot on which they were used, three piezoresistive gages out of the seven installed gave some data. Wave forms were again quite different than had been anticipated, having numerous steps in their rises. There were malfunctions for a variety of causes—early triggering of scopes and the like. Because of these troubles, both triggering and recording systems were redesigned and made multiply redundant. Triggers had been required for turning on gage power supplies, which had to be done at the last moment to be sure the gages did not burn out and for triggering the single-sweep oscilloscopes which were

the primary data recorders. Wherever possible, triggering was by a zero-time-pulse coincident with the firing signal.

Recording for Flat Top I was done three ways for each gage: by a single-sweep oscilloscope, by a raster scope, and on tape. The raster scope and tape did not require triggers, but the price paid was a more confusing signal to untangle and a degraded frequency response, respectively. For all of these precautions, the percentage return was no better in Flat Top I, but the data were of distinctly better quality.

To summarize, while the performance of the piezoresistive gages was less than satisfactory, this Flat Top experience with them helped to produce their high rate of return on later underground nuclear tests.

In contrast to the piezoresistive gages, the more conventional accelerometers and velocity gages worked very well indeed on Flat Top III. It was known before starting on Flat Top I that its higher velocity, higher impedance medium would impose severe requirements for frequency response on gages and recording systems and for acceleration sensitivity of velocity gages. These problems were in fact worse than anticipated, and the return of data on Flat Top I was disappointingly low.

3.6 SUMMARY OF GROUND SHOCK RESULTS

Calculated predictions are in general agreement with the data, but unfortunately they do not extend out to distances where the majority of the data were taken.

High-stress gages in the few records obtained seemed to be in general agreement with the predictions, but this conclusion is obscured by odd step-like rises in wave shapes on the playa shots for which the only plausible explanation is the irregularity of the surface of the charge. Not enough data were taken to affirm or deny the predicted nadir angle dependence of stress strength.

The playa shots—Flat Tops II and III— were clearly superseismic throughout the whole range of measurement. Accelerations were dominated by the air-induced shock, displacements by the directly transmitted shock wave. As to velocities, vertical components were dominated by the air-induced shock, horizontal components by the direct shock, and the vertical were roughly four times horizontal.

The limestone shot, Flat Top I, was subseismic through most of the range of measurement. Horizontal components of velocity were five or six times vertical components, and no attenuation was observed in the first 17 feet of depth.

Comparing the two media, gages at geometrically similar positions had similar wave forms although of different time and magnitude scales. The whole time scale of records in limestone was very much faster than of records in playa, almost but not quite by the ratio of seismic velocities. Radial velocities, according to two gages, were twice as large in limestone as in playa; but vertical velocities were considerably higher in playa than in limestone, in part because the very phenomenon was different, subseismic versus superseismic.

TABLE 3.1 EQUATIONS OF STATE USED IN FLAT TOP CALCULATIONS

	Flat Top II, III (Playa)	Flat Top I (Limestone)	Air Vent I		
			Layer 1	Layer 2	Layer 3
Water content, %	Dry	NA	22	19	13
Void, %	35	0	28	36	27
ρ_o	1.73	2.66	1.552	1.384	1.725
ρ_{ref}	2.66	NA	2.15	2.17	2.36
a_o	0	-0.0468	0	0	0
$a_1 = k$	0.05	0.5195	0.0638	0.0657	0.0984
a_2	-	0.262	0.940	0.974	1.48
b_o	-	0.002	0.00403	0.00846	0.00966
b_1	-	0.2546	0.0145	0.00234	0.0358
b_2	-	0.296	0	0	0
Y_o	0.0015	1	0.0175	0.0175	0.0175
Y_1	0	0.0001	0	0	0
Y_2	0	1.064	0.727	0.727	0.727
G	0.055	0.389	-	-	-
γ	0.10	0.20	-	-	-
c_o	-	0.578	0.1	0.04	0.15
c_p	-	0.625	-	-	-
c_s	-	0.121	-	-	-
Γ	0	0	0	0	0

During crushing, $P_H = b_o + b_1\mu + b_2\mu^2$

After crushing, $P_H = a_o + a_1\mu + a_2\mu^2$

Yield criteria: $\sum - P \leq \frac{2}{3}(Y_1 + Y_2P)$

$$\sum - P \leq Y_o$$

Units (gm, cm, μsec) so that P's in megabars.

k = bulk modulus $\quad c_o^2 = \left(1 + \frac{2}{3}Y_2\right)k/\rho$

G = shear modulus $\quad c_p^2 = \left(k + \frac{4}{3}G\right)/\rho$

γ = Poisson's ratio $\quad c_s^2 = G/\rho$

Γ = Grüneisen's parameter

TABLE 3.2 SUMMARY OF AIR VENT DATA

Project A (Ref. 1) Ground Motion Gages at Shot Level

Gage Type	R	TOA	A	U	D	P	End of Record
	ft	msec	g	ft/sec	in.	kb	msec
A	25	5.4		110		0.36	
A	60	16.3	12.6	12.2	10.1		260
U	60	19.5		11.7	9.5		260
A	70	21	7.0	7.5	6.0		
U	70	23		7.8	6.3		420
U	90	32		4.5	3.4,3.6		
U	130	50		2.2	1.9,2.0		
U	170	69		1.2	0.98,1.08		

Project B (Ref. 2) Surface Motion

Shot	Scaled DOB	U max	Shot	Scaled DOB	U max
	$ft/lb^{1/3}$	ft/sec		$ft/lb^{1/3}$	ft/sec
I	0.5	731	II-10a	2.0	61
II-5a	0.5	611	II-10b	2.0	33
II-5b	0.5	725	II-11a	2.5	28
II-7a	1.0	176	II-11b	2.5	28
II-7b	1.0	147	II-12	3.0	3.3 (6.0)
II-8	1.25	85	II-13	3.5	6.5 (11.6)
II-9b	1.5	82			

TABLE 3.3 SUMMARY, FLAT TOP HIGH PRESSURE RESULTS

Shot	Gage	Slant Range	Angle	Pressure	Reference
			deg	kb	
II	SRI	69.25 in.	73	30.4	7, p 148
	IITRI	69.5 in.	70	32, 90, (155?)	8, pp 39, 92
III	SRI, EP1	53 in.	72.5	17.6	7, p 149
	EP4	78 in.	62.5	25, 40, 56±10	7, p 150
	IITRI-1	65 in.	0	45.5, 130-160	8, pp 39, 92
	SC	78 in.	62.5	37	7, p 153
I	IITRI-2 (OEP2)	86 in.	0	55	8, p 41
	SRI (60 EP1)	102 in.	30	11, 30-37	7, p 154
	SRI (HEEP)	55 in.	(on the HE)	86	7, p 156
	SC-2	10 ft.	30	7±1	9, pp 27, 32
	SC-3	13 ft.	30	5.75±1.5	9, pp 27, 32
	SC-4	17 ft.	30	4±1	9, pp 27, 32

TABLE 3.4 FLAT TOP, VELOCITY DATA

A. Under the Shot

	Station	R	TOA	V_{down}	V_{up}
		ft	msec	ft/sec	ft/sec
II	OVV3	25	4.7	<110	
	OVV4	35	15.0	45-93	
III	OAV3-V	25	8.5	>41	
	OVV3	25	9.4	50-100	
	OVV4	35	13.1	<140	
	OAV5-V	57	22.0	5.0	4.6
I	OVV5	25	1.2	170	45
	OVV5X	25	1.1	125	
	OVV6X	35	2.0	44	3

B. Nearby, Not Directly Under the Shot

	Station	SR	x	y	TOA	$V_{out(down)}$	V_{in}
III	OVS1	25	20	15	10.5	100	
	1VS2	35	20	29	15.0	46	
	1VV3	55	20	51	27.6	7.0	2.6
	1VR3	55	20	51	26.0	>0.7	
I	1VS5X	25	17	17	1.5	71	35
	1VS6	35	24.5	24.5	1.9	11	12

TABLE 3.4 (Continued)

C. On the Air-Induced Motion Lines

Shot	Station	x	d = 1 ft					d = 17 ft				
			TOA[a]	Down	V_{up}	V_{out}	V_{in}	TOA	V_{down}	V_{up}	V_{out}	V_{in}
		ft	msec	ft/sec	ft/sec	ft/sec	ft/sec	ft/sec	ft/sec	ft/sec	ft/sec	ft/sec
II	2-1	30	3.5	41	31							
	3-1	45	6.6	10.1	7.9	8.5	2.8					
	4-1	65	9.2	10.5	4.0	3.7	1.5					
	5-1	85	13.5	16.4	3.8	4.0	2.4					
	6-1	150	38.3	1.7	0.9	0.43	0.53					
III	2-1, 2	30	4.5	23	31	35		13.3	11.9		30	
	3-1, 2	45	5.5	12	13	7.7	3.4	15.6	1.4	3.0	10.9	1.4
	4-1, 2	65	8.9	10.3	4	~3.6		25.2	0.98[b] (1.54)	1.36	>1.1	0.7
	5-1, 2	85	15.0	9.8	0.8[b] (1.2)	2.2[b] (2.5)	0.7	27.0	1.52	0.62[b] (1.18)	0.6	0.3
	6-1, 2	150	39.7	3.3	0.9	0.83	0.48	49	0.48	0.13[b] (0.25)	0.27[b] (0.47)	0.42
	7-1, 2	250	96.0	0.8	0.29	0.82	1.15	92.5	0.49	0.08[b] (0.26)	0.42	0.52
I	2-1, 2	30	1.9	130 (?)	30 (?)			2.1	8.7			
	3-1, 2	45	4.1	0.79				3.6	1.05	0.64		
	4-1, 2	65	5.1	0.52				5.1	0.44	0.61	2.7	
	5-1, 2	85					0.8	6.1	0.23	0.29	1.2	0.51
	6-1, 2	150						11.6	0.20	0.24		

[a] TOA's for FT II and FT III are of the accompanying accelerometers

[b] First number given is the peak comparable to other peaks in the table. Number in parentheses is a maximum elsewhere in the waveform.

TABLE 3.4 (Continued)

D. Symmetry Experiment, Flat Top III

Vertical	θ	TOA	V_{down}	V_{up}	D_-	D_+
	deg	msec	ft/sec	ft/sec	ft	ft
4VV2	0	25.2	0.98 (1.54)	1.36	0.017	0.125
14VV1	53	21.7	1.18	~1.5	0.018	0.007
24VV1	143	22.0	1.65	1.87	0.026	0.139
34VV1	198	22.0	1.28	1.47	0.019	0.064
44VV1	248	20.3	1.41	~1.6	0.021	0.087
54VV1	278	19.5	1.20	1.32	0.020	0.098
64VV1	338	21.0	1.34	1.16	0.032	0.068
	Average	21.7	1.29±0.21	1.54±0.24	0.022	0.093

Radial	θ	TOA	V_{out}	V_{in}	D_{out}	D_{in}
4VR2	0	29-35	~1.1	0.7	0.10	-
14VR1	53	23±1	2.65	1.01	0.14	-
24VR1	143	22.6	4.3	1.7	0.2	-
34VR1	198	23.0	4.3	1.7	0.21	-
44VR1	248	21.5	3.88	1.98	0.20	-
54VR1	278	21.0	2.90	1.36	0.14	-
64VR1	338	21.5	2.06	0.76	0.15	-
	Average	21.9[a]	3.03±1.21	1.32±0.5	0.10	-

Transverse	θ	TOA	V_{CW}	V_{CCW}	D_{CW}	D_{CCW}
	deg	msec	ft/sec	ft/sec	ft	ft
4VT2	0	27 (?)	~0.2	~0.2	-	-
14VT1	53	22.3	0.8	0.6	0.007	-
24VT1	143	22.6	1.1	0.7	-	0.036
34VT1	198	27.2	0.09	0.12	-	0.074
44VT1	248	22.0	~0.4	0.27	0.003	-
54VT1	278	23±2	0.52	0.46	-	0.021
64VT1	338	23.0	0.38	0.47	0.028	-
	Average	24.62	0.55[b]	0.44[b]	0.01	0.04

[a]Average excludes 4VR2 and 14VR1

[b]Average excludes 4VT2

TABLE 3.5 AIR-INDUCED MOTION REGIMES

Material	Ground Velocity	Air Pressure	Range	Regime
	ft/sec	psi	ft	
			0	
Playa	C_p = 2350	50	140	Superseismic
	C_s = 1570	15	250	Transseismic
	(Assuming ν = 0.1)		∞	Subseismic
			0	
Limestone (Flat Top I)	C_p = 13,000	2000	15	Superseismic
	C_s = 7000	600	40	Transseismic
	(Assuming ν = 0.3)		∞	Subseismic

TABLE 3.6 OVERPRESSURES, VELOCITIES, AND IMPEDANCES

Station	Distance	Flat Top II			Flat Top III		
		P	W	Z	P	W	Z
	ft	psi	fps	psi/fps	psi	fps	psi/fps
2	30	900	41	22	980	23	43
3	45	380	10.1	38	500	12	42
4	65	220	10.5	21	280	10.3	27
5	85	140	16.4	8.5	130	9.8	13
5	150	43	1.7	25	42	3.3	13
7	250				15	0.8	19
	Average			23			26

TABLE 3.7 COMPARISONS OF MEDIA

Gage	Flat Top III					Flat Top I				
	TOA	V_{down}	$t(V_d)$	V_{up}	$t(V_{up})$	TOA	V_{down}	$t(V_d)$	V_{up}	$t(V_{up})$
	msec	ft/sec	msec	ft/sec	msec	msec	ft/sec	msec	ft/sec	msec
3VV1	5.5	12	-	13	-	4.1	0.79	-	-	-
4VV1	8.9	10.3	-	4	-	5.1	0.52	-	-	-
2VV2	13.3	11.9	-	-	-	2.1	8.7	-	-	-
3VV2	15.6	1.4	26	3.0	150	3.6	1.05	8	0.64	25
4VV2	25.2	0.98	42	1.36	140	5.1	0.44	10	0.61	25
5VV2	27	1.52	48	(1.18)	230	6.1	0.25	12	0.29	26
6VV2	49	0.48	64	(0.25)	280	11.6	0.2	16	0.25	22
4VR2	29-35	>1.1	30	0.7	280	5.2	2.7	10	0.6	-
5VR2	29	0.6	38	0.3	-	6.6	1.2	17	0.3	50

TABLE 3.8 GAGE PERFORMANCE IN FLAT TOP[a]

	Flat Top II	Flat Top III	Flat Top I
High-stress gages:			
IITRI	1/1	1/3	1/5
SRI	1/1	2/4	2/4
Quartz	-	-	3/4
Impedance mismatch	-	1/1	-
Accelerometers:	5/7	9/9	2/6
Exp. same	-	-	0/8
Velocity gages:	11/14	44/49	10/30
Exp. same	-	-	4/9
Strain gages:	0/2	-	1/5

[a]The notation 5/7 means five gages gave data out of seven installed.

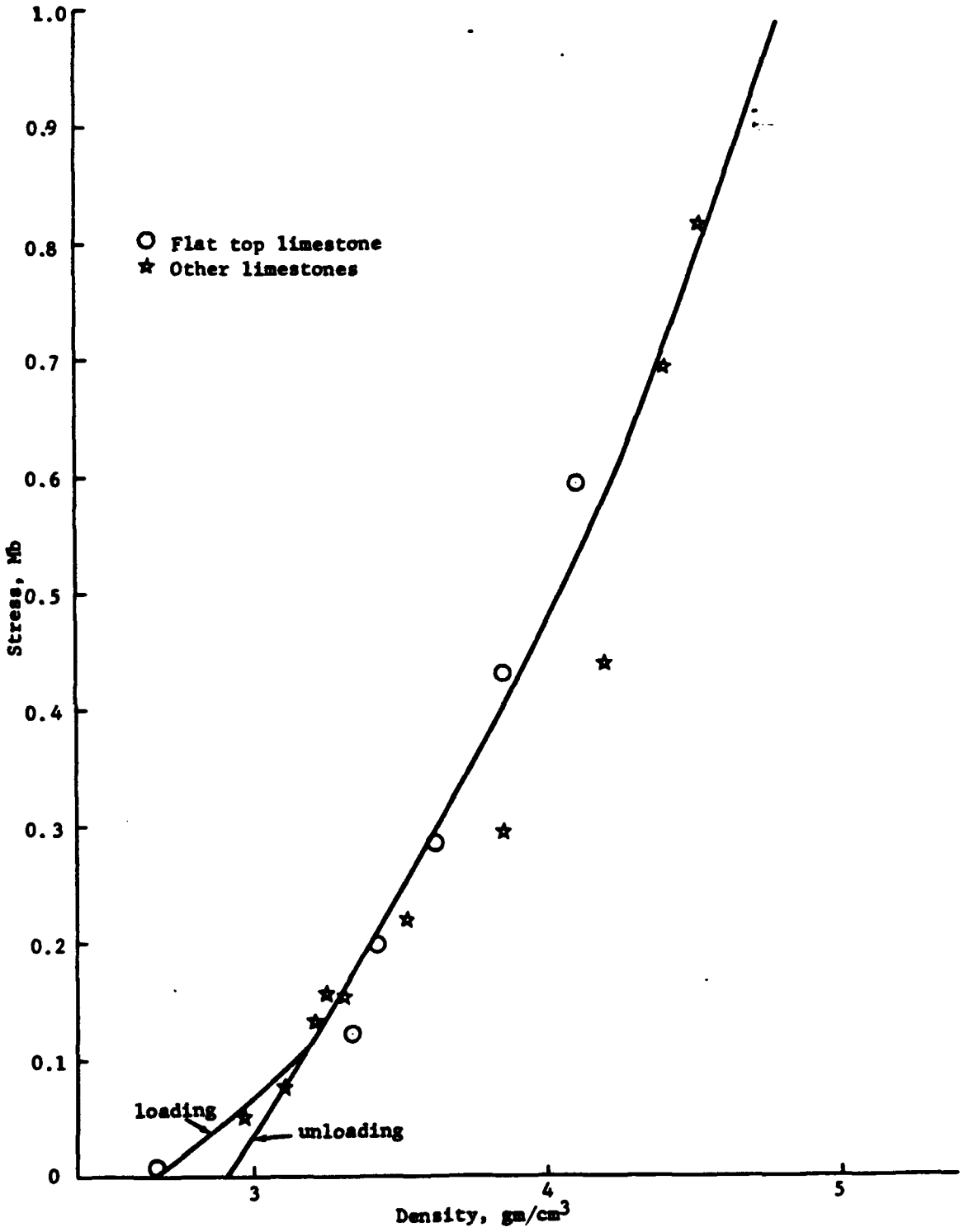

Figure 3.1 Flat Top I limestone: Experimental Hugoniot data compared with analytical description used in calculation.

(a) (64-20-NTS-64)

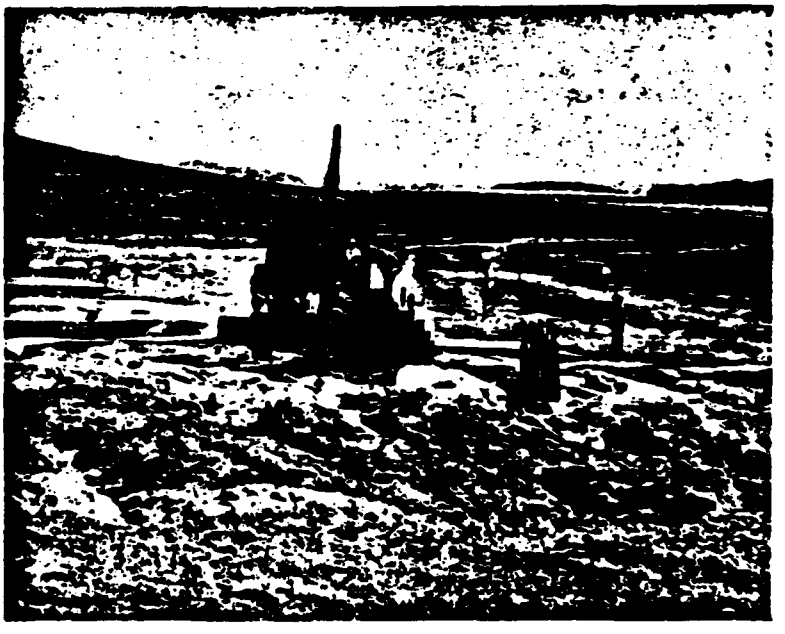

(b) (63-17-NTS-64)

Figure 3.2 Flat Top I working area, near and far views.

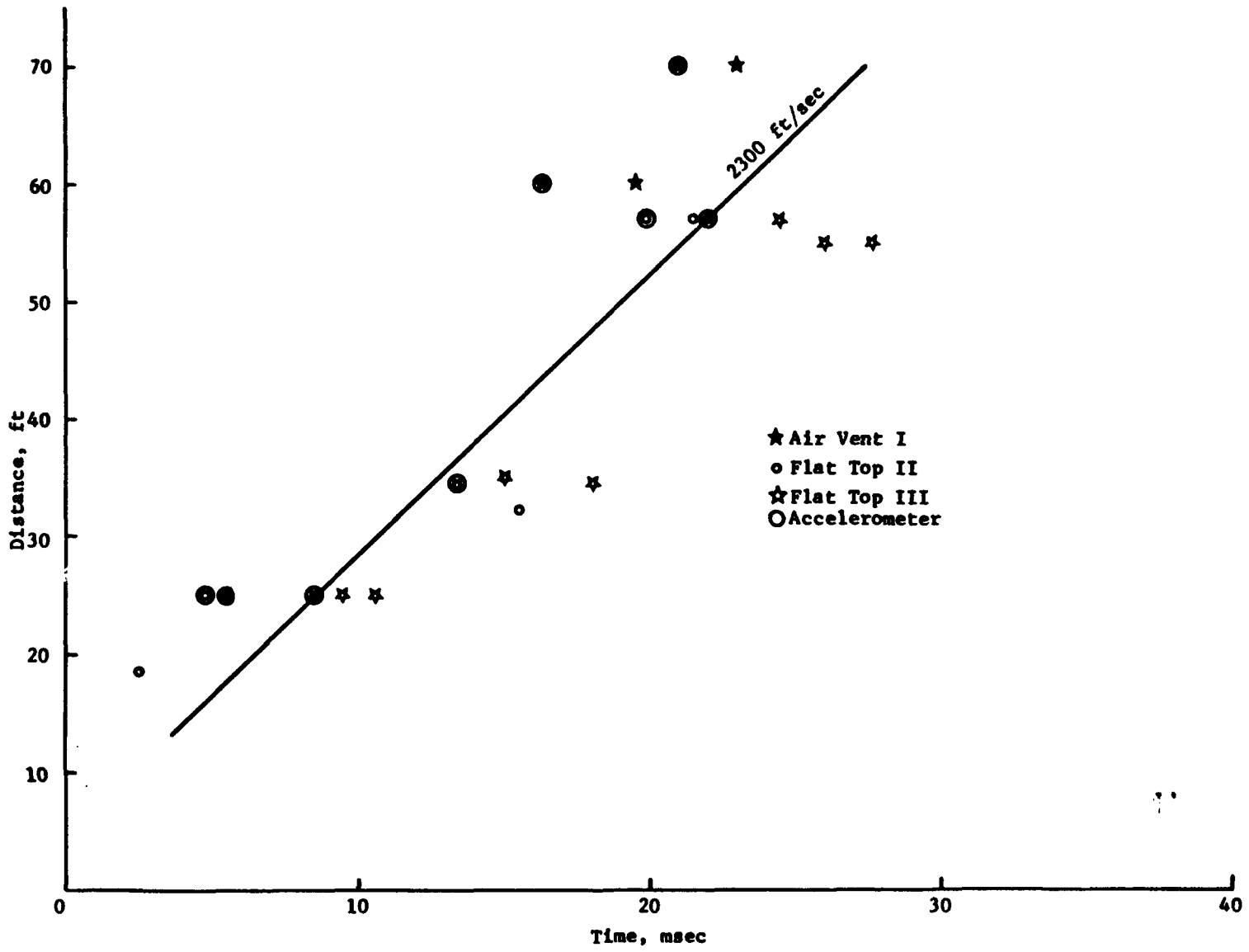

Figure 3.3 Arrival times of the body wave, Air Vent I and Flat Tops II and III.

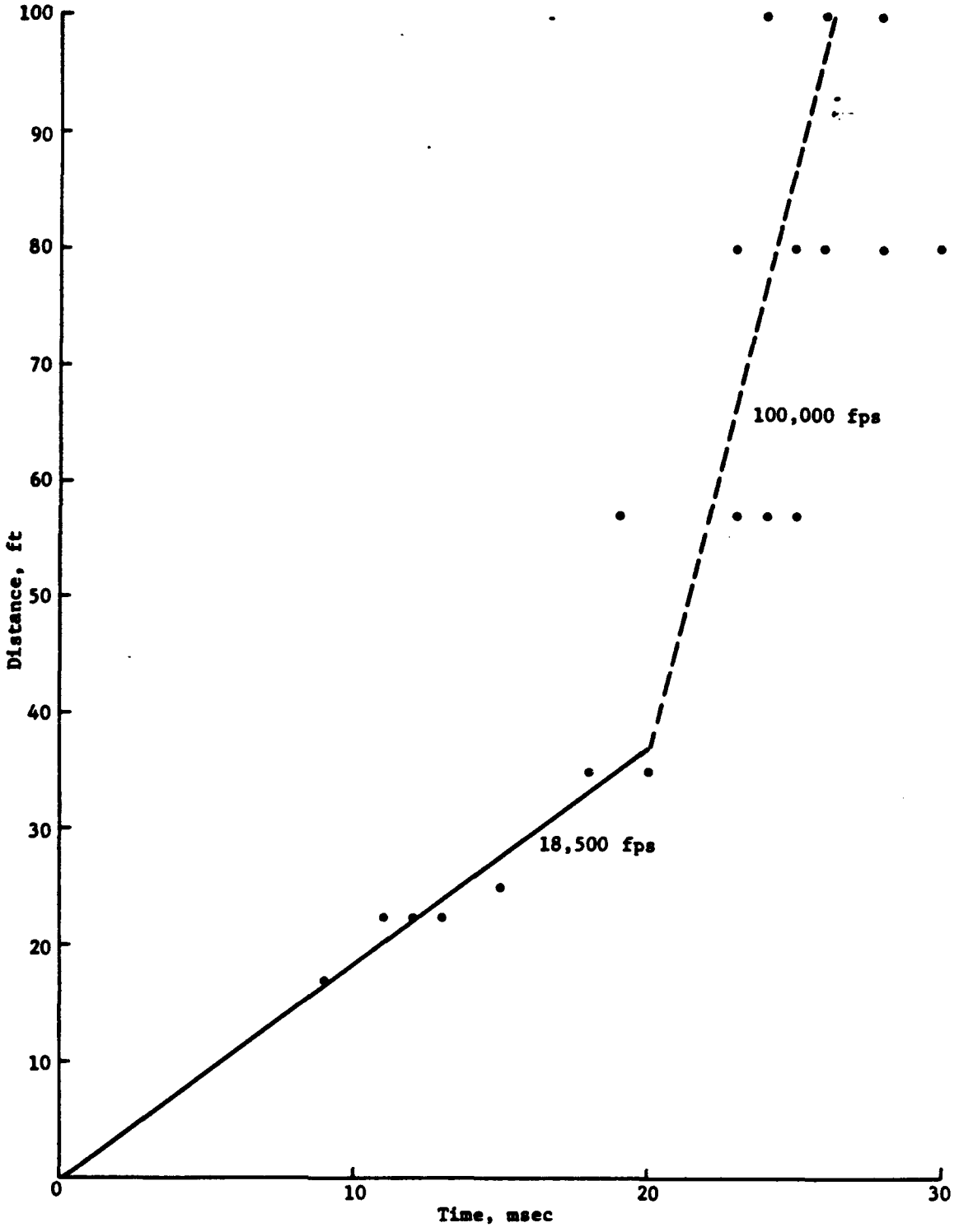

Figure 3.4 Arrival times of the body wave, Flat Top I.

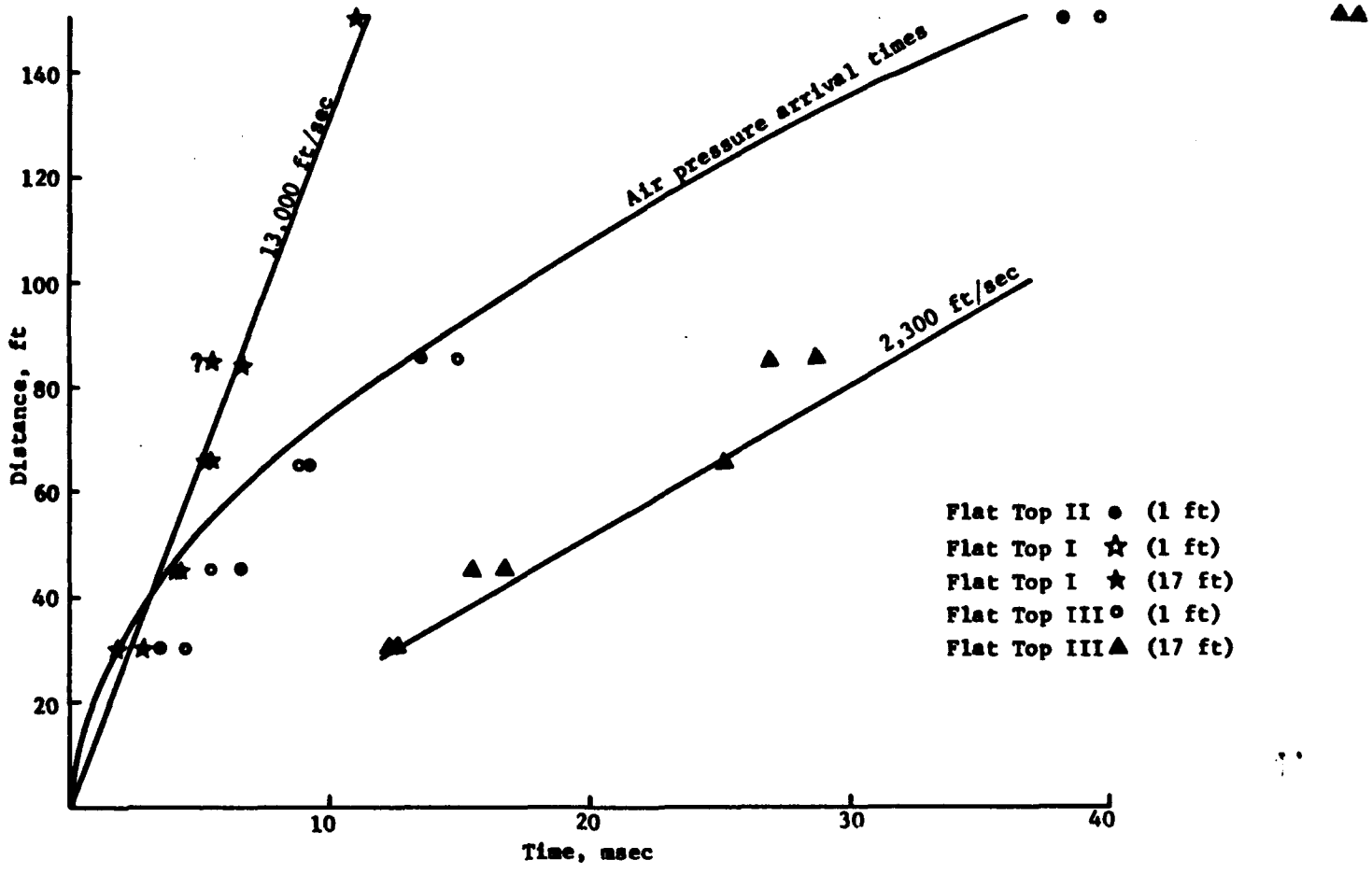

Figure 3.5 Arrival times of the surface wave, Flat Tops II, III, and I.

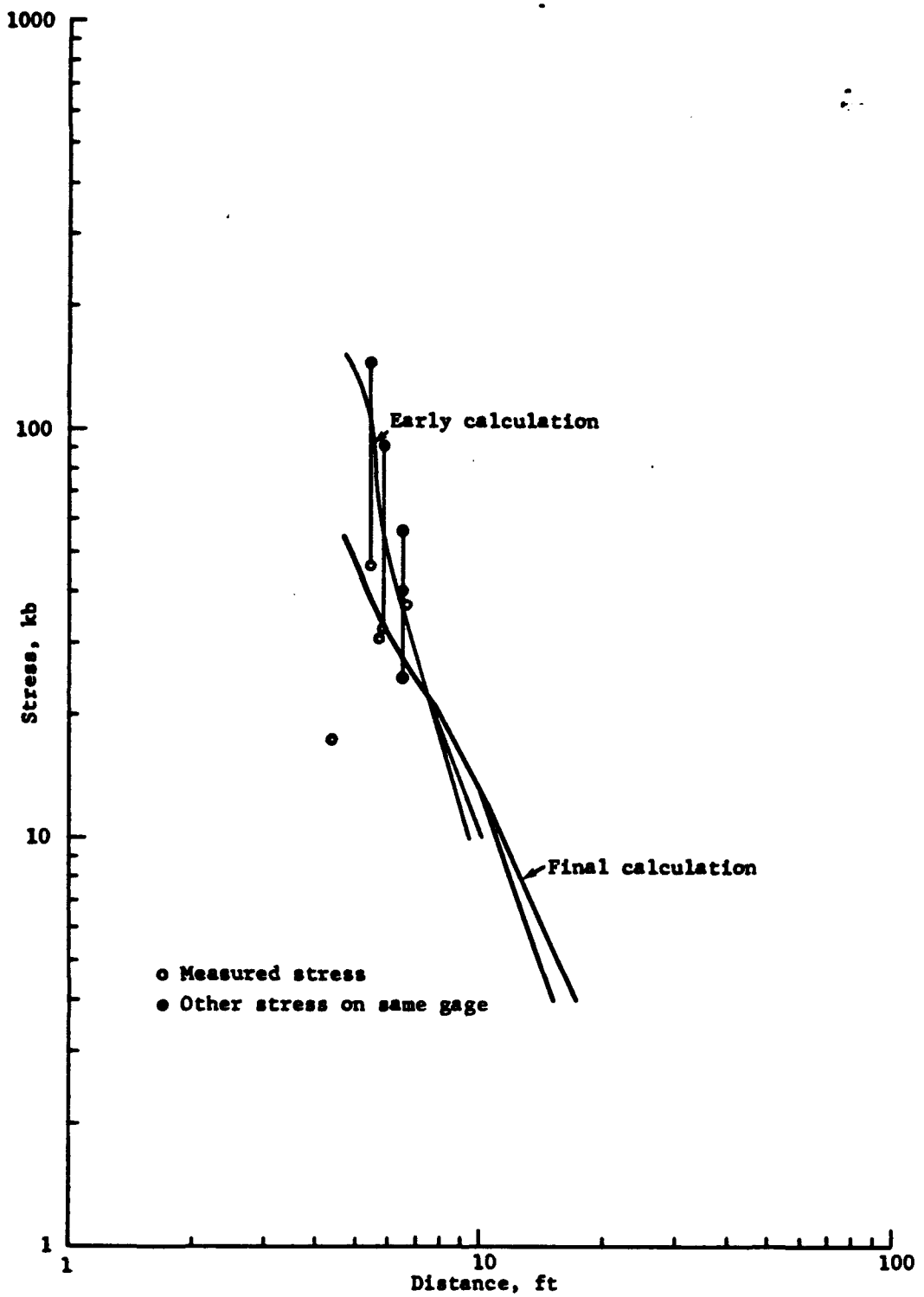

Figure 3.6 High stress data compared with calculation, Flat Tops II and III.

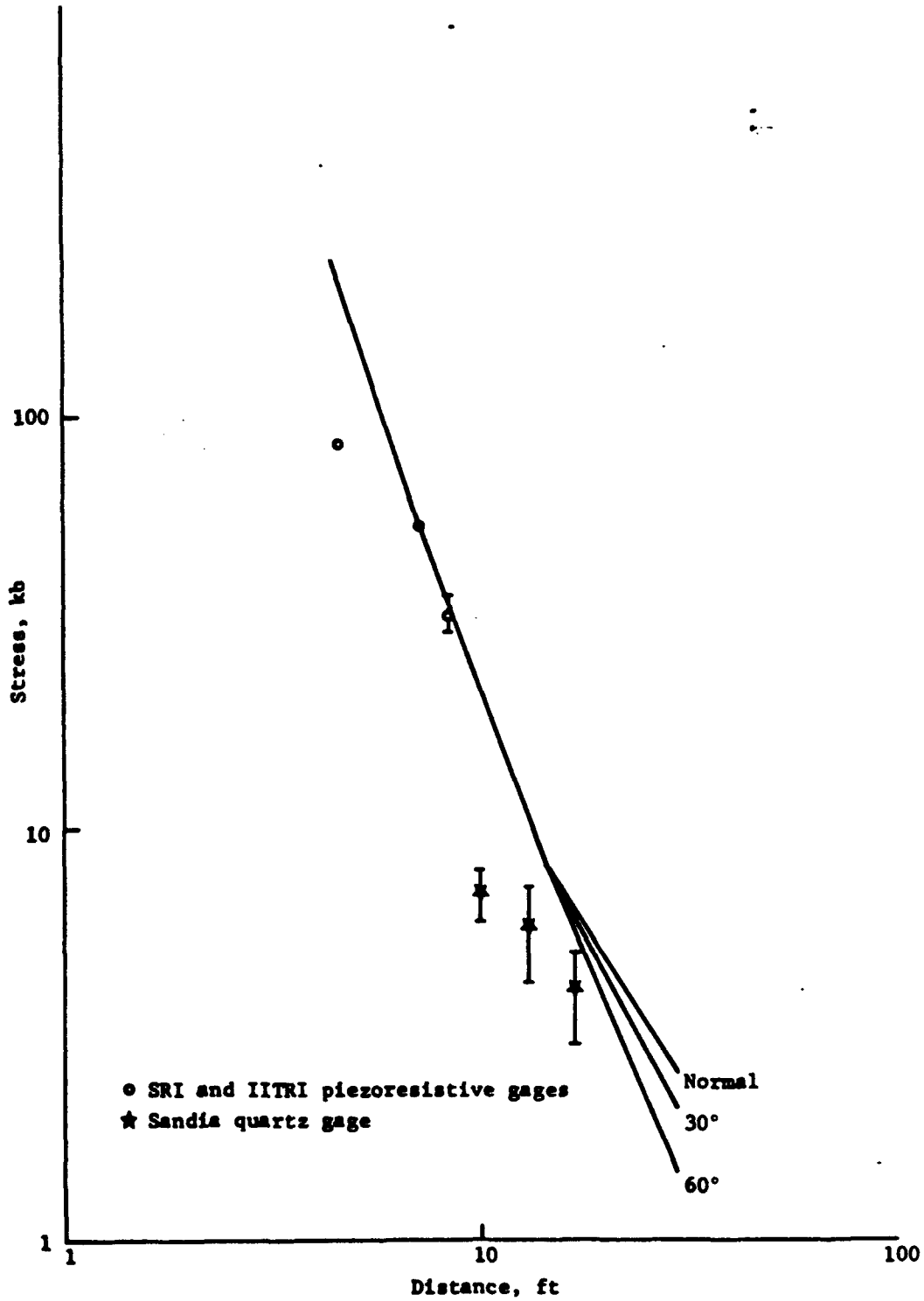

Figure 3.7 High stress data compared with calculation, Flat Top I.

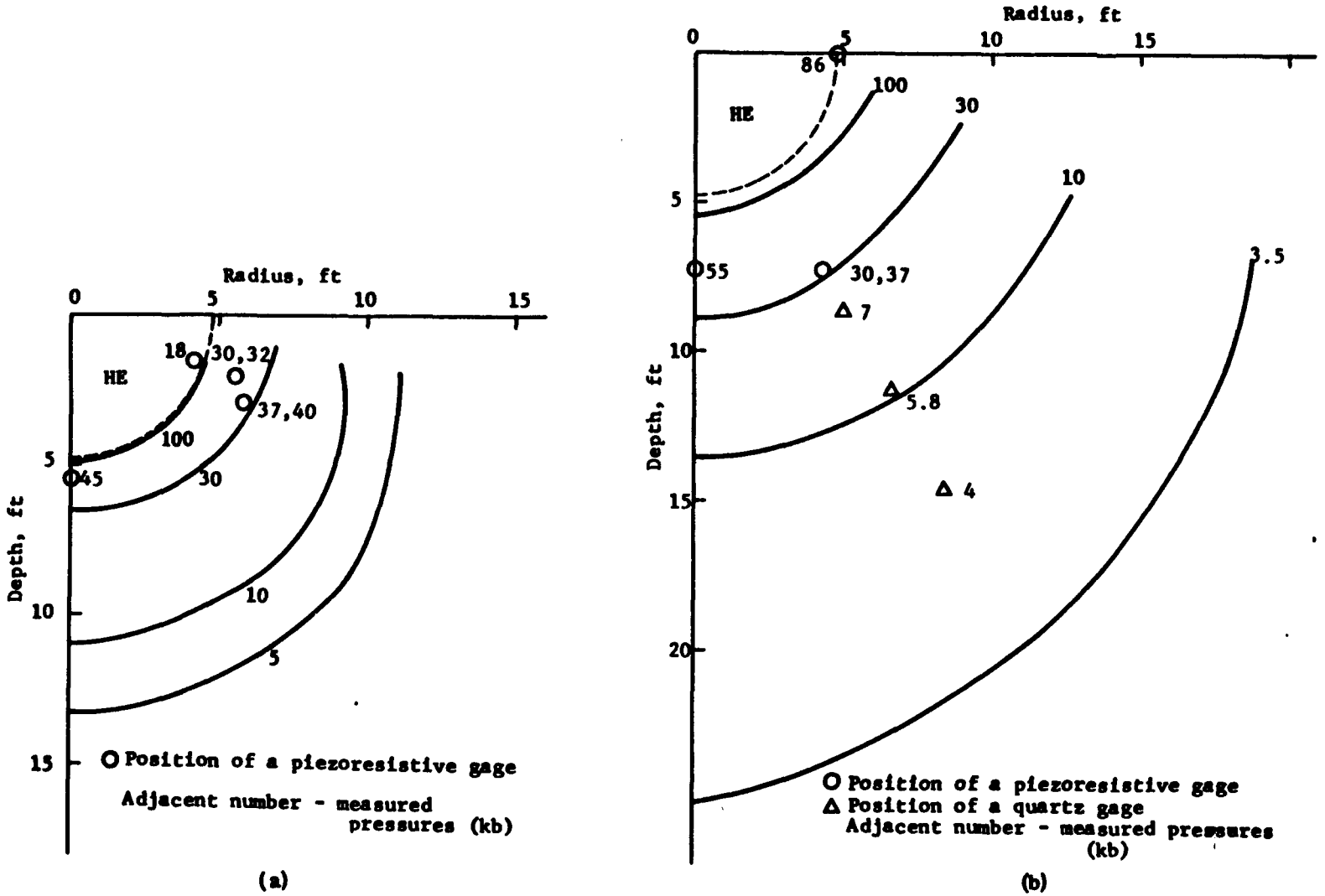

Figure 3.8 Nadir angle dependence of stress, calculated compared with measured, (a) Flat Tops II and III, (b) Flat Top I.

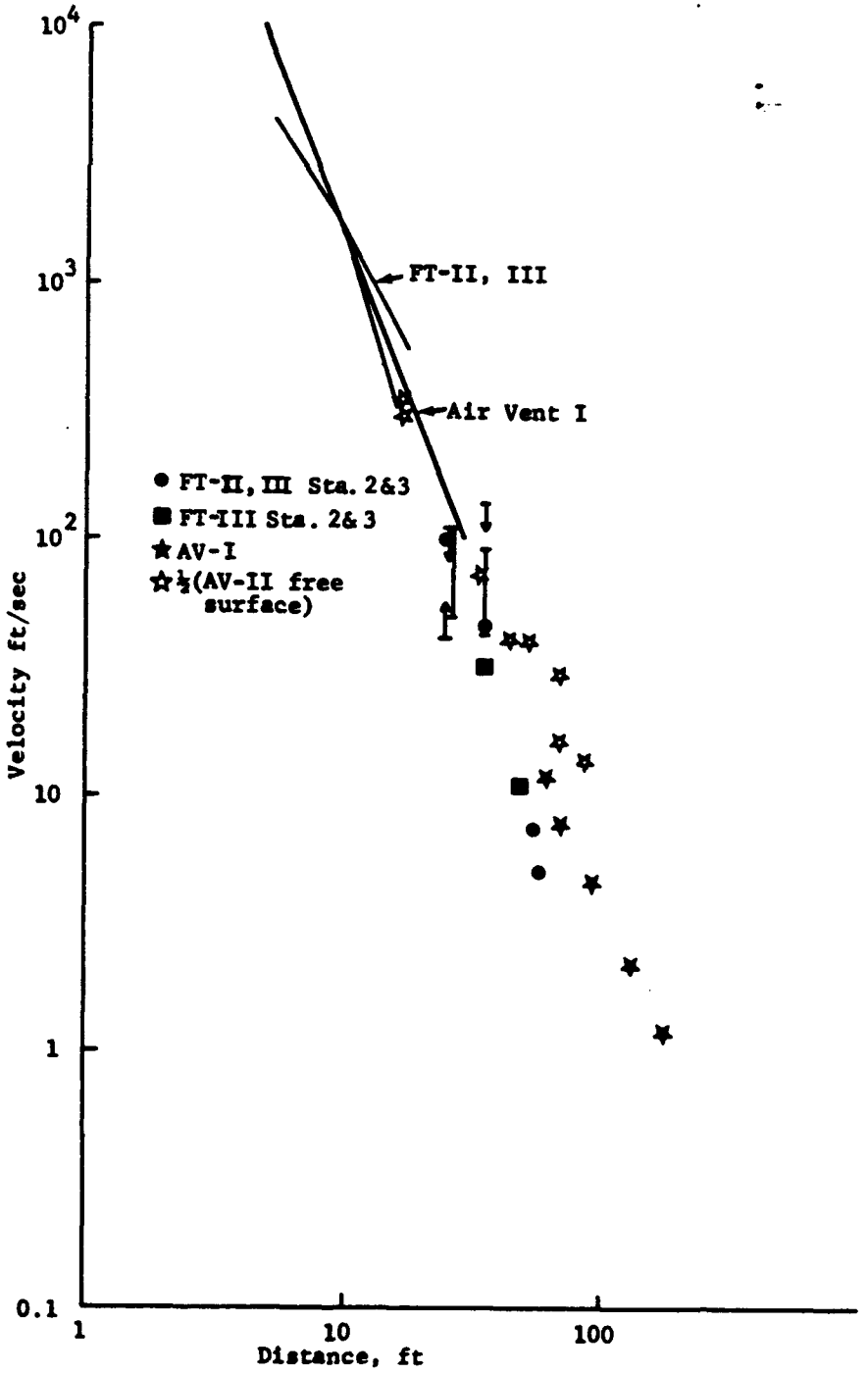

Figure 3.9 Measured velocities compared with calculations, body wave, Air Vent I and Flat Tops II and III.

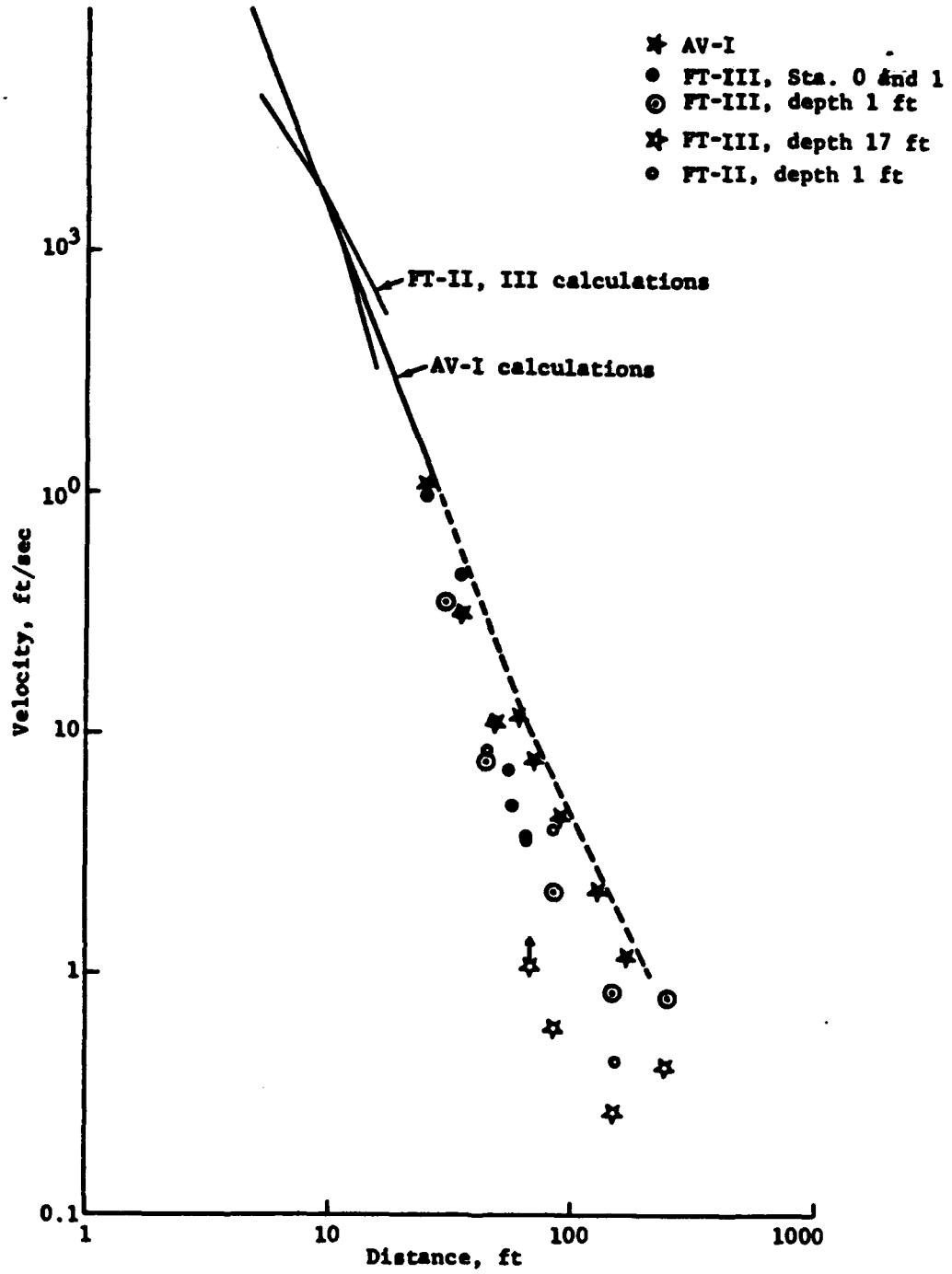

Figure 3.10 Measured velocities, body wave, and horizontal component of surface-influenced wave, Air Vent I and Flat Tops II and III.

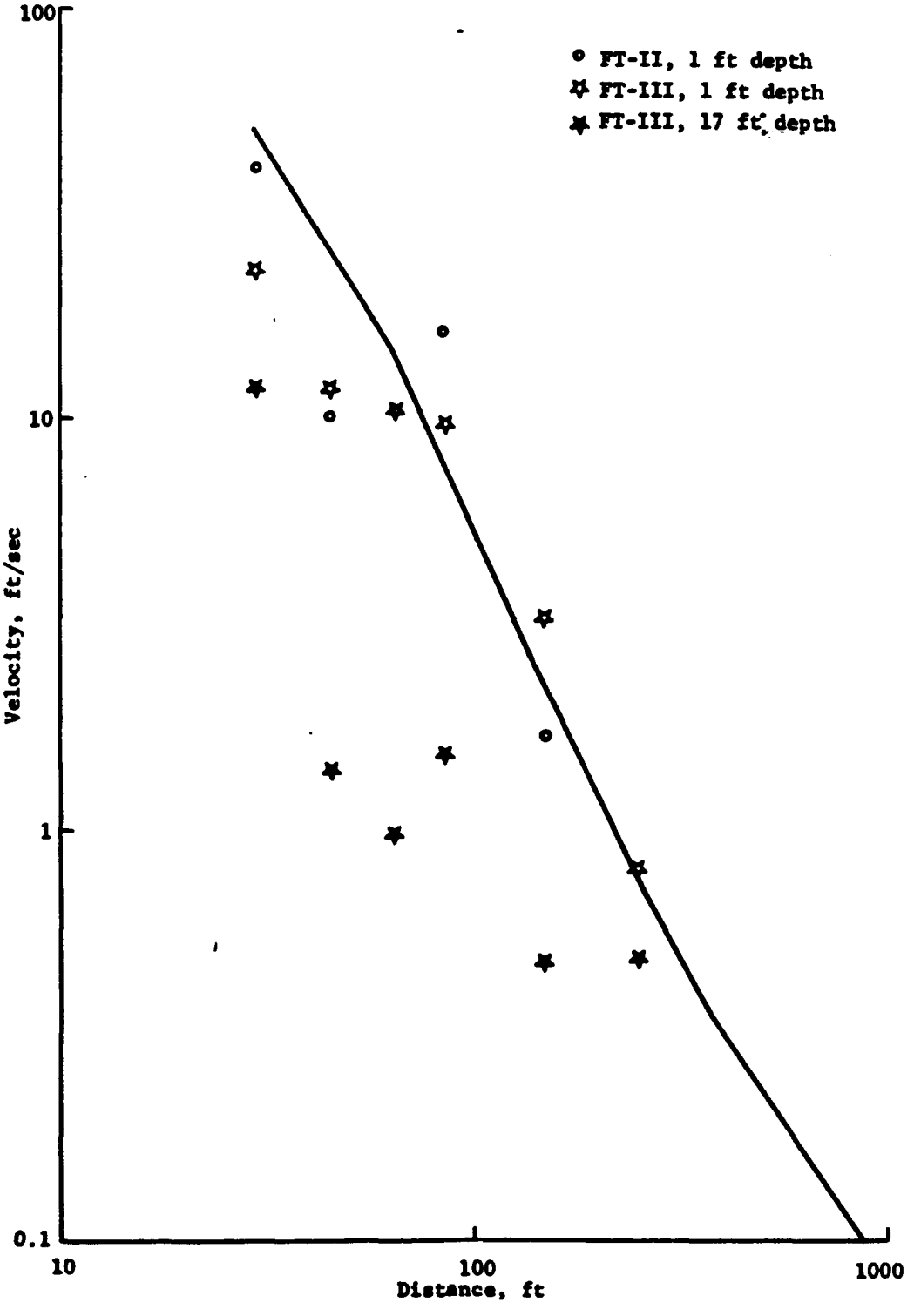

Figure 3.11 Measured vertical velocities compared with air pressure, Flat Tops II and III.

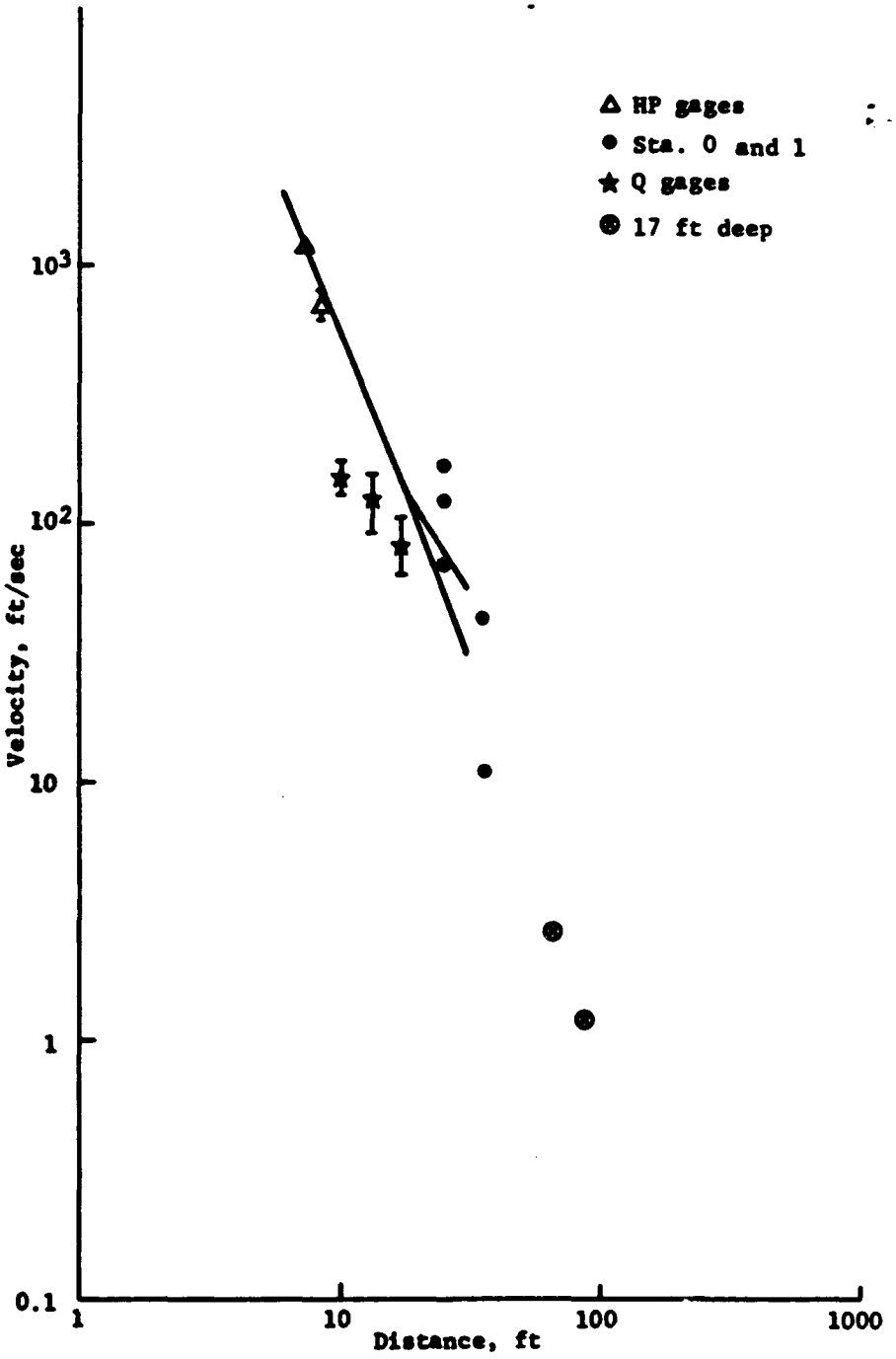

Figure 3.12 Measured velocities compared with predictions and body wave, Flat Top I.

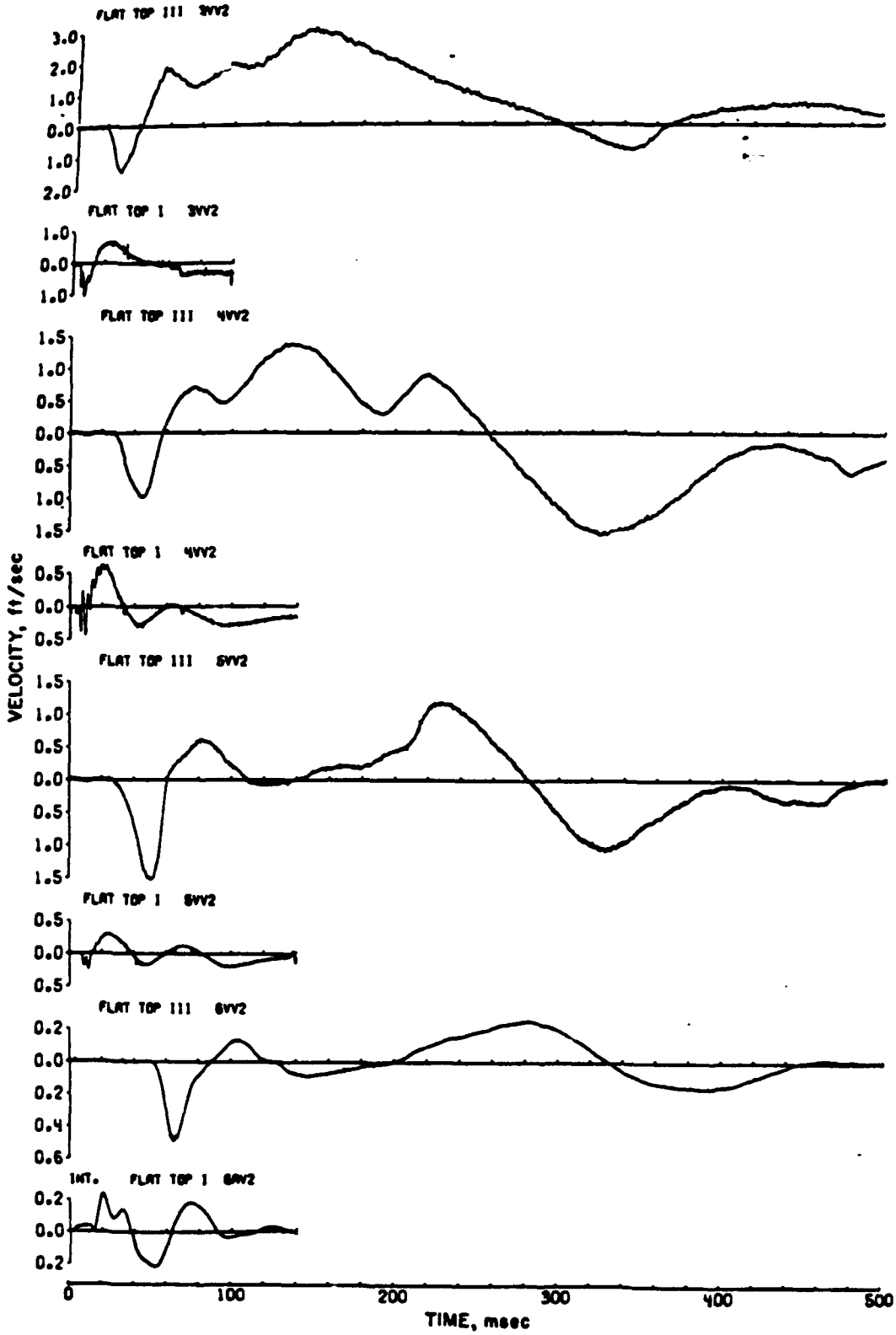

Figure 3.13 Vertical particle velocity versus time. Comparison of Flat Top III and Flat Top I, 17-foot nominal depth.

CHAPTER 4

CRATERING

4.1 INTRODUCTION—EXPERIMENTAL METHODS

Because the theoretical study of cratering is still in its infancy, almost all cratering experiments are carried out with empirical goals, using not active instrumentation but before-and-after comparisons. The Air Vent/Flat Top experiments were no exception.

The apparent crater dimensions were measured using aerial photogrammetry and, where applicable, surveys by rod, chain, and transit. To determine residual subsurface motions, sand columns were used. Sand columns are made by drilling down to the depth expected to be cratered or disrupted and then filling the holes with like material, marked by the addition of contrasting dye and with metal discs or tags placed as indicators of original depth. The columns are excavated after the shot and their new positions determed by survey. Finally, the original surface was marked by various means, of which red paint was both the simplest and most effective.

For Flat Top I in limestone, these methods had to be modified. Grout columns were used instead of sand, and the metal discs were replaced by under-reamed rings in the walls of the holes.

4.2 BACKGROUND OF PURPOSES

The empirical purposes of the Air Vent/Flat Top cratering measurements were these:

To Compare Chemical with Nuclear Explosions (HE vs NE). Attempts to set up equivalence factors date back to the earliest nuclear cratering events (Reference 41) but have been frustrated by the lack of completely comparable tests. It has long been evident that NE is less effective in cratering than HE, but neither the effectiveness nor the proper scaling is clear. Indeed, it may be asked whether one should even expect one HE-NE equivalence since the theoretical considerations, as far as they have advanced, imply that such an equivalence changes with depth of burst, energy level, and with design of the energy source. Under these circumstances and because of the ban on atmospheric tests, Air Vent/Flat Top could not speak directly to the question of HE-NE equivalence.

To Compare Playa with Alluvium as a Cratering Medium. Almost all previous nuclear cratering shots had been carried out in the alluvium of Area 10, but that area was no longer available to the DOD. It was hoped the results of Air Vent would provide a bridge to make that previous experience applicable and comparable to the Ferris Wheel B-series. For this purpose, the series of 256-pound charges was fired at various depths of burst for direct comparison with similar shots previously fired in Area 10.

To Determine Proper Scaling of HE Surface Bursts. Numerous experiments in the past had implied other than cube-root scaling. For buried charges, the Plowshare Program uses the $W^{1/3.4}$ scaling originally suggested by Vaile (References 42, 43). Dimensional analysis suggests cube-root scaling for surface bursts, tending

toward quarter-root for larger, buried bursts (References 44, 45). Data from hemispherical charges fired on the surface at Suffield and one man's analysis of Pacific craters suggest radius scaling distinctly larger than cube root, $W^{0.4}$ or so (References 46; 47, Appendix I). The Suffield data were the only data spanning a large range of yields, but a scaling larger than cube root had tended to be rejected because of the seeming inapplicability of hemispheres, and a high water table, and because there was no evident way to explain such a departure from the results of dimensional analysis. As to the Pacific craters, another man's analysis suggested just the opposite, scaling less than cube root, which is some indication of how poor the data really are (Reference 48). It seemed in order, therefore, that one purpose for Air Vent be to pin down surface-burst scaling in playa, a nearly ideally homogeneous medium.

To Investigate Differences Due to Change in Medium. Flat Top I was added to the program primarily because of a pressing need for information on ground shock from surface bursts on rock, but it also gave crater information. It is well known that crater sizes vary greatly with medium; they are smaller in rock than in alluvium, greater in wet soil than in dry, etc. Few large shots had ever been fired on hard rock; the most nearly comparable shots were the buried shots in basalt fired in Buckboard and Pre-Schooner.

4.3 THEORY

As mentioned above, the theory of cratering is in its infancy. Only the dimensional analysis of craters

has been exhaustive (References 44, 45). Ground-shock calculations, as described in Chapter 3, do treat the beginning of the process that will eventually lead to a crater, but no calculation of a surface burst has been carried to the point where it gives an unequivocable indication of crater radius. Brode did note in his original ground-shock calculation (Reference 33) that late-stage velocities divided up and down at the eventual crater depth (Figure 5.15), but these calculations were only carried to 105 msec real time. The latest ground shock calculations do little better.

Craters from bursts at near-optimum depths, on the other hand, have yielded quite well to theoretical analysis. Such calculations treat the burst as contained up to the time a signal returns reflected from the free surface. At that point, a cavity has been formed still under high pressure. It is presumed thereafter only to grow upward, pushing up the skin of soil over it until that skin ruptures (Reference 49, pp 75-98). These calculations are quite useful in the Plowshare program but in that form are inherently not applicable to surface bursts.

4.4 MEDIA

Flat Tops II and III were located on the flat playa of the large lacustrine silt deposit known as Frenchman Flat in Area 5 of the Nevada Test Site. The soil supports hardly any vegetation and is extremely homogeneous. Chemically, it is about 50-percent SiO_2, about 17-percent each $MgCO_3$ and $CaCO_3$, 8-percent $Al_2)_3$, and 4-percent Fe_2O_3 (Reference 17). Normally its density is 90 to 100 lb/ft^3, and its water content is 12 to 15

percent. However, as stated in Chapter 3, the Flat Top III area sat under water for several weeks during the winter of 1963-64, so at the time of the test the soil density there was 100 lb/ft^3 and the moisture content 23 percent, probably with a fair amount of local variation.

Flat Top I was fired in a fairly competent limestone outcrop in Area 9 of NTS. The material was almost pure $CaCO_3$ at near crystalline density of 2.60 gm/cm^3. A thin overburden of alluvium and broken rock was removed before placing the charge (Figure 4.1). The natural material was heavily bedded, with a strike of N27°W (333°) and a dip of about 40 degrees to the SW.*

4.5 CRATER DIMENSIONS

Dimensions of apparent and true craters are given in Table 4.1. Pictures and contour maps of the four larger shots are shown in Figures 4.2 through 4.10. The phrase "apparent crater " means just that: the hole as it appears immediately after the shot, with dimensions measured relative to the preshot ground surface. The apparent crater includes a layer of material that has fallen back from above, hiding the dimensions of the "true crater." The profile of the true crater is determined (in playa) by observing the points on the

*The strike may be defined as the azimuth of the line of intersection of the strata with the ground surface, unless the surface deviates significantly from the horizontal. The dip is the angle which the beds make with the horizontal, measured perpendicular to the strike.

sand columns above which the column material has been carried away by the blast; these ends, of course, are generally sheared to the side from where they started. In rock the true crater is determined by removing any loose rock. The Air Vent data listed show the range of uncertainty; the Flat Top data are best estimates.

Air Vent data for shots fired deeper than a scaled depth of 1.5 ft/lb$^{1/3}$ are not dimensions of a crater or hole, but of a "negative crater" or mound.

4.5.1 Results of Surface-Burst Scaling. The surface shots in Air Vent/Flat Top shows a clear departure from cube-root scaling for radius. Over the range of explosive charges, 64 to 40,000 pounds, regression analyses give the apparent and true crater dimensions listed in Table 4.2. The uncertainty of the exponents in this table corresponds to plus or minus one standard deviation.

The same apparent crater results are shown graphically in Figure 4.11. Also on these curves are shown three points from the Toboggan series, apparent craters from 8-pound charges fired in the playa of Yucca Flat. These points are plotted because they were in ostensibly the same material, even though they were not used in the regression analyses for Table 4.2.

The scatter in these data is small enough to make us reasonably sure that the departure upwards from cube root for radius scaling is real and significant, at least over this range of charge sizes. It is an interesting historical note that investigation of this very range to 20 tons

was sufficient to convince those working in Plowshare that they should use a scaling less than cube root for buried charges (References 50, 51). Data at larger scales have since confirmed the choice, one usually explained by pointing to gravity effects.

Clearly the Air Vent/Flat Top data do not explain noncube-root scaling; they do substantiate that it is real, for reasons unknown, thus making other observations or claims for greater-than-cube-root scaling more tenable.

Two possible explanations have been put forth. The dimensional analysis that points to gravity as causing the departure downwards from cube root in scaling buried shots implies that gravity should play little or no role in surface shots but that medium viscosity contributes to violate similarity. The qualitative effect of this violation is to yield larger scaled crater dimensions for larger explosions (Reference 52). Also, if the strength properties of the soil are rate-dependent, the soil should yield at lower stress levels to the longer pulses of larger explosive sources (Reference 58, paper by Vortman). Whether this would explain the Air Vent/Flat Top data depends on what the time constants and residual strengths are for playa, and these are not known.

4.5.2 Playa-Alluvium Comparison. The data from Air Vent which relate apparent crater dimensions to depth of burst are illustrated in Figures 4.12 and 4.13 with comparable data from 256-pound charges fired in Area 10 alluvium. Several differences are apparent.

In playa, bursts at a depth greater than 9.5 feet (1.5 $ft/lb^{1/3}$) resulted in mounds, but charges at similar

depths in alluvium resulted in real craters. The formation of these mounds may be related to the observed fact that the playa, unlike Area 10 alluvium, bulked up significantly and decreased in density from 95 to 75 lb/ft^3.

Where craters were formed in playa, the apparent-crater radii averaged about 20 percent smaller than in alluvium at the same depths. In other words, the Area 5 playa behaves more like rock where cratering is concerned.

Air Vent I may be compared, by scaling, with the 256-pound data of Air Vent II. It is plotted in Figures 4.2 and 4.3, scaling both by cube root and by the 1/3.4 power. Cube root is the closer match, in contrast with the experience of Area 10, where the 1/3.4 power is better.

Air Vent I may also be compared directly with Stagecoach 2, a nominally identical shot except that it was fired in Area 10. Table 4.3 compares their crater dimensions. True-crater dimensions were not obtained on Stagecoach 2, but comparison of apparent-crater dimensions shows Air Vent I to be only 5 percent smaller than Stagecoach 2, not 20 percent smaller as the 256-pound charges were.

These comparisons with Air Vent II and Stagecoach 2 might be explained several ways. The Air Vent I area had a slightly higher moisture content than the Air Vent II area; this tends to increase crater sizes. It might be that the transition from the 0.369 scaling for surface bursts to the 1/3.4 scaling for buried bursts occurs at a greater depth in Area 5 playa than in Area

10 alluvium. It might mean that the differences between playa and alluvium become less at higher yields. There is no way to choose among these hypotheses from the data now available.

4.5.3 Results, Flat Tops II and III. There were several variations between the two shots which might explain the fact that Flat Top III quite obviously made a bigger crater than Flat Top II. The moisture content of the soil was greater for Flat Top III by a factor of 1.6. In the same test the layer of backfill around the half-buried charge was tamped; this had not been done for Flat Top II. The grouted instrument column of Flat Top II, though it had been in place nearly a year, was found to be quite hard and intact. Finally, in stacking Flat Top III, what had been the first four-block layer in Flat Top II was redistributed elsewhere in the charge.

It is probable that most of these differences, even if they should be mentioned, were trivial. The difference in backfill density was slight. The grout column was only 8 inches in diameter. Relocating the four blocks raised the center of gravity of the stack but this would, if anything, have made the Flat Top III crater smaller.

The most important difference was probably the moisture content. This is suggested by the different appearance of Flat Top III and particularly of its ejecta, damp clods that hung together even after impact with the surface; clods thrown out of Flat Top II broke up on impact (Figure 4.14).

4.5.4 Results—The Flat Top I Crater. A stereo picture of Flat Top I crater is shown in Figure 4.8, and an isopach map showing the differences in ground level before and after the shot in Figures 4.9, the lip region, and 4.10, the interior of the crater. Measurements were made of the Flat Top I crater as they had been for the shots in playa, but no attempt was made to refine them to the same degree because of the irregularity of the rock surfaces.

The Flat Top I crater was asymmetrical, being roughly elliptical in shape with the major axis falling along the strike and the minor axis along the dip. For this reason, the 27-foot radius quoted in Table 4.1 is the average radius, computed from the zero isopach as

$$R_a = \sqrt{\frac{A}{\pi}} .$$

The actual diameter up-and-down-strike was about 60 feet, and across the dip, 50 feet. A most significant asymmetry was the overall tilt of the crater bottom in the down-dip direction: the maximum depth of the crater lay 7 feet down-dip from ground zero, and the crater slope on that side was noticeably steeper than on the other three radii. The crater lip, too, was quite irregular, being over 6 feet high S65°W of ground zero but almost missing just north of that point, or due west of ground zero. Indeed, the effect of the bedding planes was everywhere evident in the crater, the figures shown here being very poorly descriptive of that point.

To compare the Flat Top I crater with Flat Top II (which was a more typical crater and better documented by sand columns than Flat Top III), Flat Top I was considerably smaller. The radius was 76 percent that of Flat Top II, the depth 84 percent, and the volume 42 percent. These fractions are comfortably close to the handbook values of 0.8, 0.8, and 0.5, respectively (Reference 53).

At the time the Project 1.9 report was written, Rooke had no other hard-rock surface bursts, except very small ones, to compare with the Flat Top I crater. Since then, there have been a number of surface shots reported in basalt in the so-called MTCE series (Reference 54), which were stacked spheres weighing 4,000 and 16,000 pounds. Together with 64-pound data, these imply scaling for radius and depth of

$$R_a = 1.30W^{0.27} \text{ , and}$$

$$D_a = 0.085W^{0.28} \text{ .}$$

However these slopes are greatly influenced by the data from the small charges; without them, the best fit is

$$R_a' = 0.47W^{0.38} \text{ , and}$$

$$D_a' = 0.085W^{0.46} \text{ .}$$

It would appear these are not self-consistent and truly intercomparable data; but Flat Top I does agree with them generally.

4.5.5 Residual Displacements. The sand column array for Flat Top II was much broader and deeper than that for Flat Top III because the former had been designed for an HE shot and the latter for the NE Ferris Wheel B-1 shot. Thus Flat Top II had a sand column 50 feet deep just next to ground zero, but the same column for Flat Top III was only 30 feet deep. The ground zero grout column on Flat Top I was adequately deep, 100 feet, but postshot drilling along it had to be abandoned at a depth of 35 feet because the bit tended to wander, probably because of bedding discontinuities. The ground zero column on Air Vent I went 43 feet below the charge center.

The postshot tops of the ground zero sand columns in all shots define the true crater depth, which for Flat Top II was at about 15 feet. The first identified vertical marker was the one placed originally at the 20-foot depth; it had been displaced downward 2.7 feet. Vertical displacements decreased linearly with depth to zero at about 50 feet or at a little over three true crater depths. On Flat Top III, the maximum vertical displacements were 2.5 times as great but, extrapolated, they appear to decrease to zero at about the same depth. On Flat Top I, vertical displacements were smaller. The highest ring measured, originally at a depth of 11 feet, was displaced downward about 1 foot. The lowest ring measured, originally at a depth of 29 feet, was displaced downward about 0.8 foot. If this

trend were to continue downward linearly, residual displacements would not disappear until a depth of 100 feet. That seems unlikely, however; what can be said with certainty is that there were appreciable permanent vertical displacements beyond a depth of 30 feet, roughly three true crater depths from the surface.

In Air Vent I the highest marker recovered, originally at 7.8 feet from charge center, was found displaced an additional 8.1 feet or a little more than 100 percent farther! In several of the smaller Air Vent shots, marker tabs that had originally been within a foot of the edge of the charge were recovered.

The remarkable fact about these displacements is that they are detectable at large distances even in rock and even when the rock in the floor of the true crater still appears sound. In thinking about cratering shots in a fine-grained and relatively noncohesive material such as playa, it is easy to imagine a continuously distributed shearing action which, directly under the shot, looks like compression and causes a ground-zero sand column to shorten and become fatter at the same time. In rock, however, the idea of such a motion is hard to believe; yet the rock must move. The rock mass must move along cracks and joints to accommodate such displacements.

Similarly, the lip is thrust up and for the most part out, under its postshot burden of fallback material. On Flat Tops II and III, the average upthrust of the lip, discounting fallback, was 1.5 and 2.0 feet, respectively; the net outward motion of the lip could

not be determined, though at 50 feet it was 0.7 and 1.6 feet. The plastic upthrust zone reached out 200 feet in these two shots, or 6 radii. At the very crater edges there was clear evidence of the ground surface having folded over. In Flat Top I, the average lip upthrust was about 1.5 feet. Horizontal displacements were generally outward but, at the larger distances to the southwest (down-dip), net horizontal displacements were back toward the shot. Only two radii were sufficiently well surveyed before the shot to make such measurements, so any generalization based on these observations is questionable.

4.6 SUMMARY OF MAIN POINTS

Radii of high-explosive surface bursts in playa scale by a factor significantly larger than the cube root of the yield, in contrast to underground and near-optimum-depth bursts where the opposite is true. In rock, the data are not definitive.

The playa of Area 5 yields craters appreciably smaller than the alluvium of Area 10. The deepest bursts form a mound rather than a crater.

Permanent displacements under the charge extend for about three true crater depths even in rock. Radially, upthrusts extend for about five crater radii in playa, three in rock. Craters in rock do show finite permanent displacements.

Soil moisture content is an important factor influencing crater dimensions, more moisture yielding larger craters.

TABLE 4.1 CRATER DATA

Shot	Charge Weight	DOB		Apparent Dimensions			True Crater Dimensions		
		Actual	Scaled	R	D	V	R	D	V
	lb	ft	$ft/lb^{1/3}$	ft	ft	ft^3	ft	ft	ft^3
Air Vent I	40,000	17.2	0.5	47.61	22.5	7.25×10^4	49.7-52.1	31.6-32.1	$11.7\text{-}13.5 \times 10^4$
II-1	256	-0.865	-0.136	3.20	0.82	13.3	4.0-4.2	2.28-2.67	57.9-87.1
-2A	256	0	0	5.54	2.39	95.46	5.8-6.8	4.27-4.40	202.0-259.4
-2B	256	0	0	5.40	2.43	93.22	-	-	-
-3	256	+0.865	+0.136	6.72	3.38	235.4	7.9-8.7	5.03-5.40	325.3-449.3
-4	256	1.59	0.25	7.62	3.72	247.0	8.25-8.7	5.42-5.70	450.1-529.5
-5A	256	3.175	0.5	8.84	4.13	426.0	9.2-10.8	6.94-7.36	689.2-963.1
-5B	256	3.175	0.5	8.50	4.35	381.0	-	-	-
-6	256	4.76	0.75	9.58	4.64	517.0	11.05-12.0	9.11-9.56	1150-1583
-7A	256	6.35	1.0	9.82	4.36	505.7	10.8-11.6	10.42-1073	1572-1903
-7B	256	6.35	1.0	9.94	4.49	544.0	-	-	-
-8	256	7.94	1.25	10.32	3.98	483.0	12.0-14.75	12.46-12.8	2059-3007
-9A	256	9.53	1.5	10.98	3.63	486.0	13.8-15.4	13.71-13.97	2712-3380
-9B	256	9.53	1.5	11.02	2.34	332.0	-	-	-
-10A	256	12.7	2.0	22.9[a]	-3.81[a]	-1178[a]	13.05-15.0	-	-
-10B	256	12.7	2.0	26.4[a]	-4.13[a]	-2500[a]	-	-	-
-11A	256	15.9	2.5	22.6[a]	-4.11[a]	-2678[a]	-	-	-
-11B	256	15.9	2.5	22.3[a]	-4.41[a]	-2722[a]	-	-	-
-12	256	19.05	3.0	22.0[a]	-2.67[a]	-1878[a]	-	-	-
-13	256	22.2	3.5	23.4[a]	-1.35[a]	-1003[a]	-	-	-
-14	256	25.4	4.0	24.7[a]	-0.63[a]	-900[a]	-	-	-
III-1A	64	0	0	3.41	1.57	24.02	3.8-4.5	2.6-2.71	51.0-68.1
-1B	64	0	0	3.41	1.82	26.10	3.4-4.2	2.6-2.7	41.6-60.4
-1C	64	0	0	3.26	1.81	22.79	3.6-4.2	2.69-2.89	48.4-62.7
-1D	64	0	0	3.52	1.87	28.33	3.6-4.2	2.52-2.72	44.1-58.7
-2A	1,000	0	0	9.36	4.27	442.0	9.8-11.5	6.56-6.76	873-1141
-2B	1,000	0	0	10.12	4.55	517.0	10.2-12.0	6.18-6.38	873-1182
-2C	1,000	0	0	8.92	4.27	440.0	10.4-11.8	5.96-6.26	901-1113
-3A	6,000	0	0	16.44	6.57	2520	18.5-21.5	8.27-9.47	3944-5554
-3B	6,000	0	0	17.52	6.91	2703			
Flat Top II	40,000	0	0	35.8	11.3 (12.9)	24,000	38	15.3 (16.0)	43,000
III	40,000	0	0	38.8	18.0 (18.6)	38,000	44	23.0	62,000
I	40,000	0	0	27	9.5 (12.7)	10,000	38	10.8 (14.5)	- 24,000
Toboggan (Ref.61)	8	0	0	1.55 1.47 1.31	0.91 0.67 0.65	2.33 1.76 1.54			

[a]Not a crater; dimension of resulting mound

TABLE 4.2 REGRESSION FITS TO DATA FROM SURFACE BURST CRATERS

R_a (ft) = $0.727\ W^{0.369 \pm 0.006}$

D_a (ft) = $0.426\ W^{0.331 \pm 0.04}$

V_a (ft^3) = $0.261\ W^{1.082 \pm 0.021}$

R_t (ft) = $0.868\ W^{0.364 \pm 0.006}$

D_t (ft) = $0.795\ W^{0.296 \pm 0.014}$

V_t (ft^3) = $0.667\ W^{1.056 \pm 0.017}$

R = radius
D = depth
V = volume
a = apparent crater
t = true crater
W = charge weight in pounds

TABLE 4.3 COMPARISON OF CRATERS

		Stagecoach 2	Air Vent I
Charge Weight	lbs	40,000	40,000
DOB	ft	17.1	17.2
R_a	ft	50.5	47.6
D_a	ft	23.6	22.5
V_a	ft^3	83,600	72,500

Figure 4.1 Limestone surface after removal of alluvial overburden. Ground zero is approximately centered in the white (unpainted) area. (39-01-NTS-64)

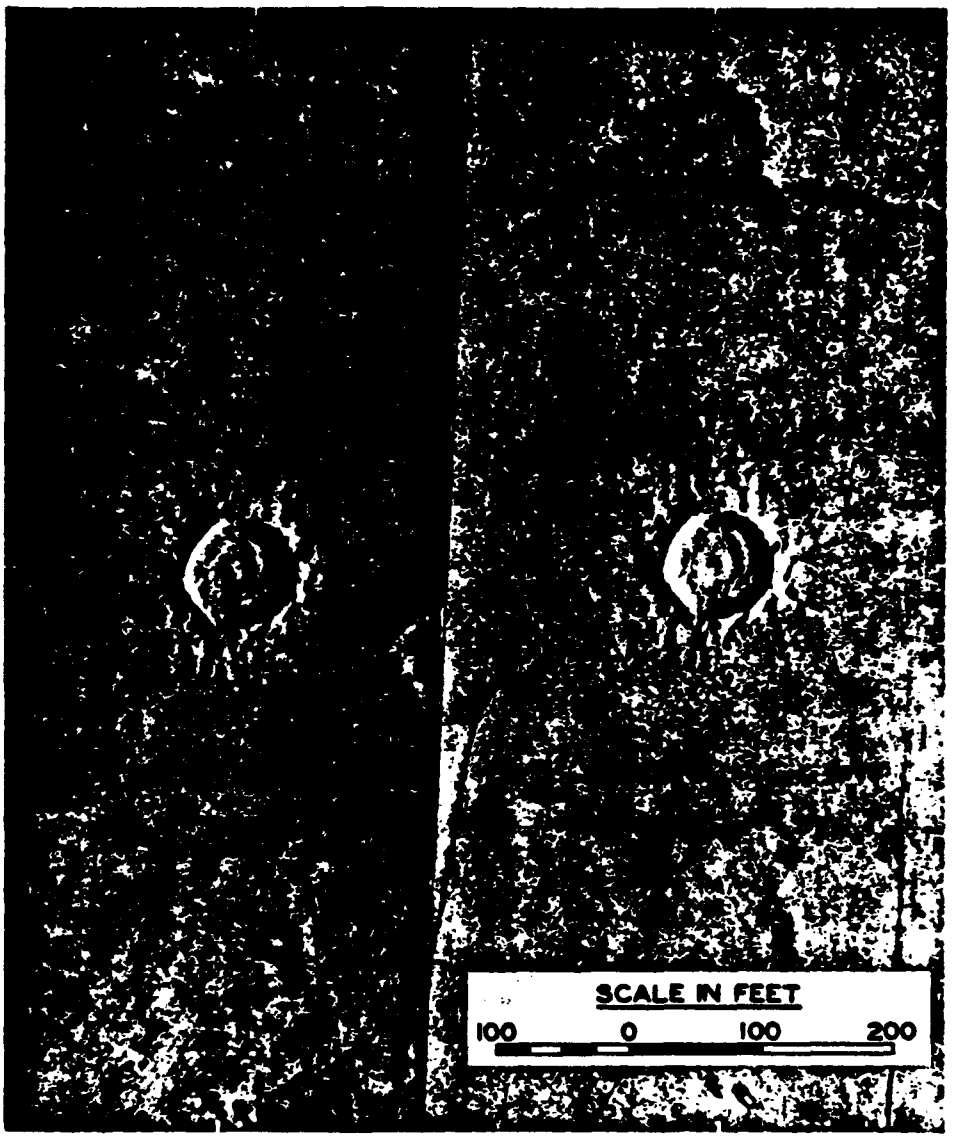

Figure 4.2 Aerial stereopair of Flat Top II crater. For three-dimensional effect, view through stereoscope. Ground zero is located at intersection of tic marks.

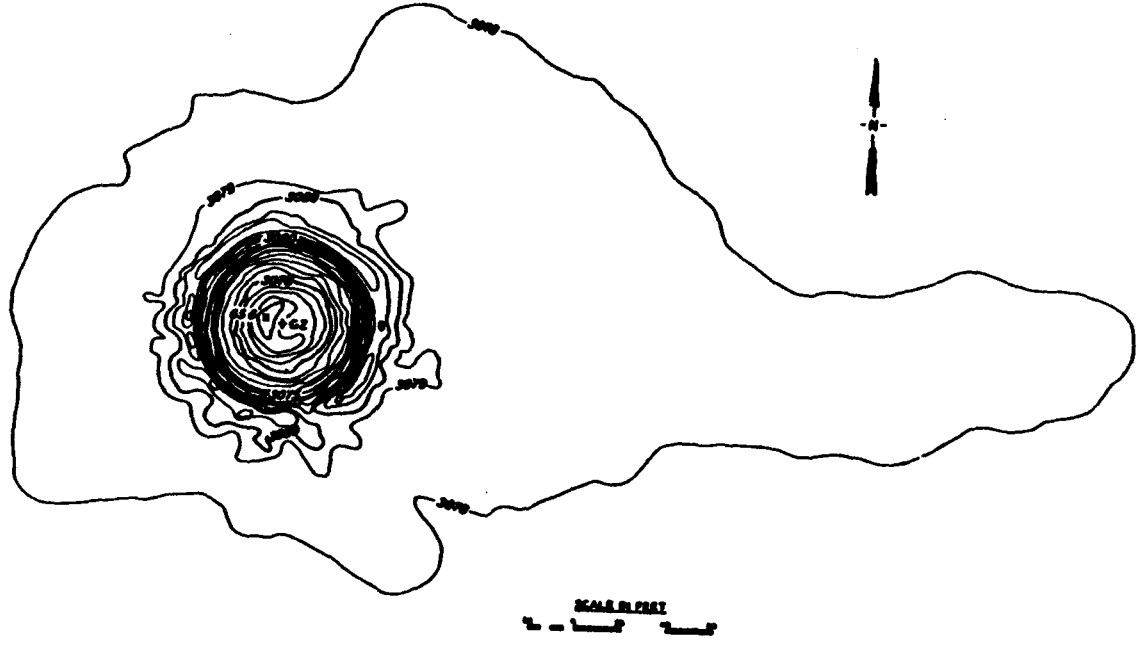

Figure 4.3 Postshot contours prepared from aerial photographs, Flat Top II crater. Contour interval is 1 foot.

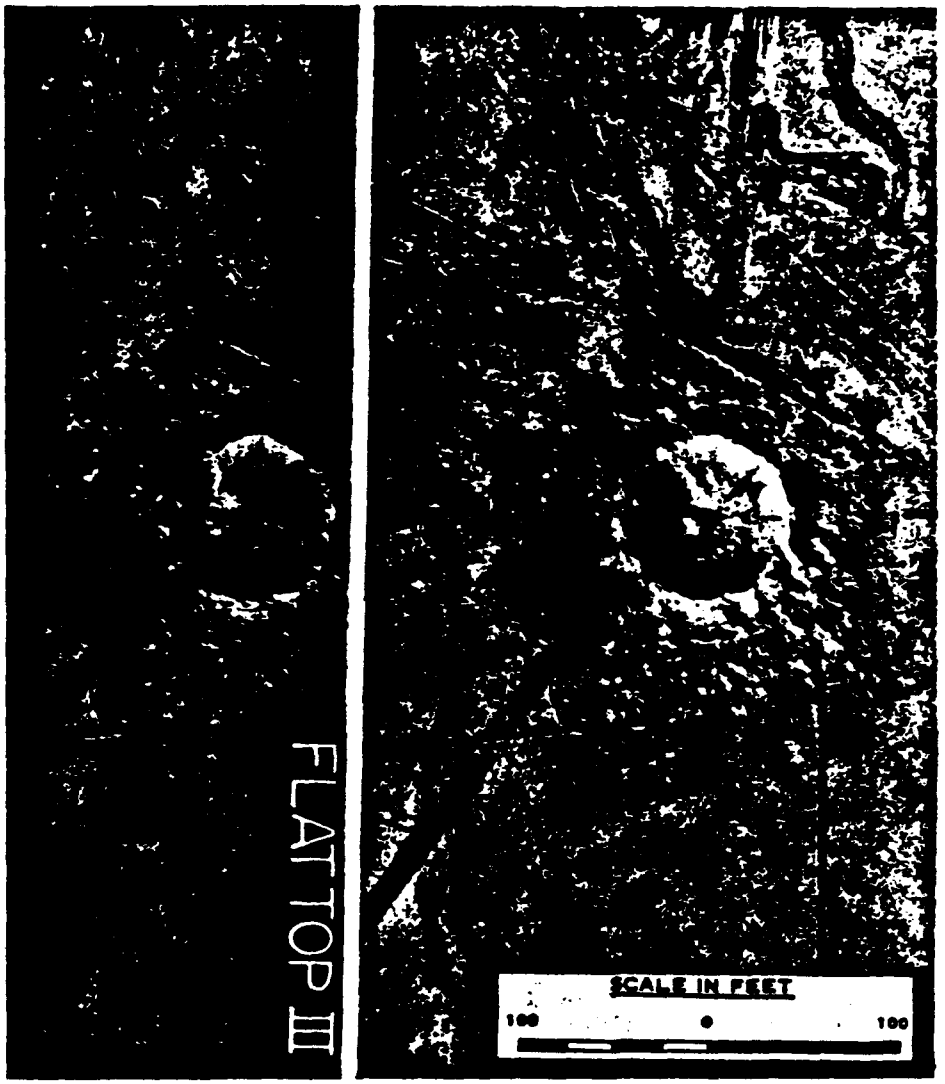

Figure 4.4 Aerial stereopair of Flat Top III crater.

Figure 4.5 Postshot contours prepared from aerial photographs, Flat Top III crater. Contour interval is 1 foot.

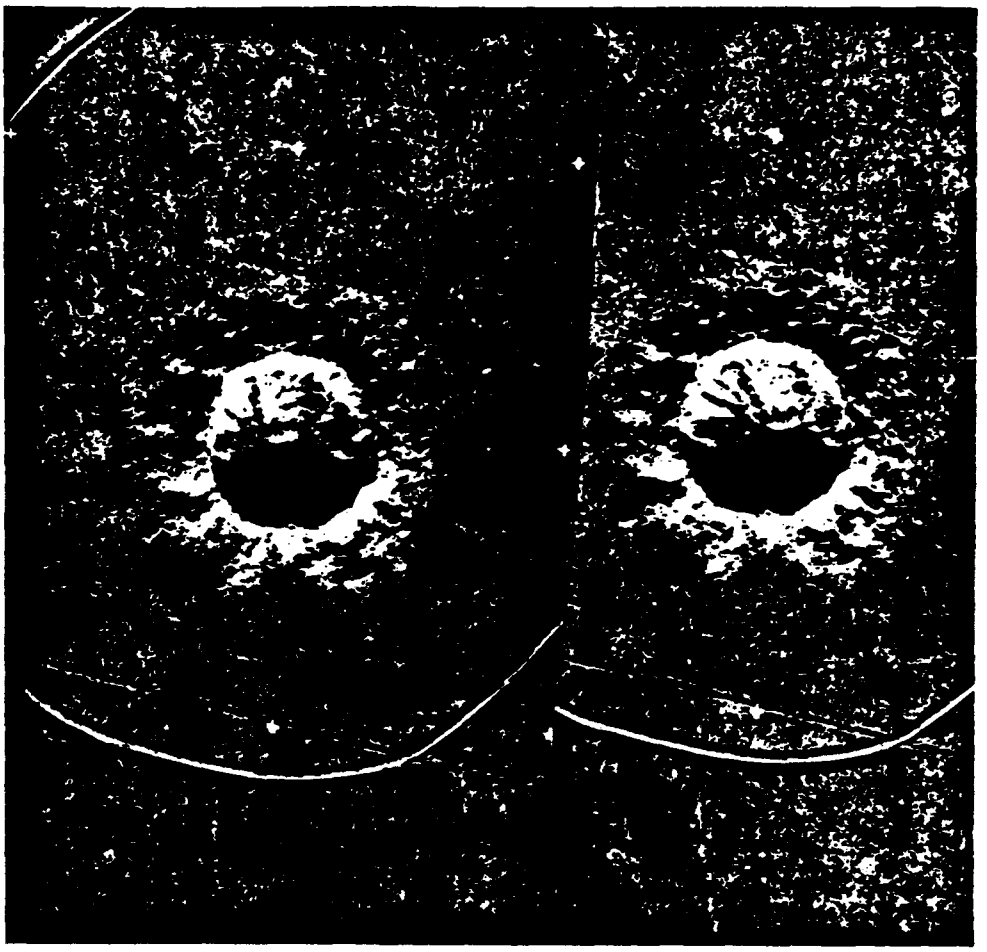

Figure 4.6 Aerial stereopair of Air Vent I crater.

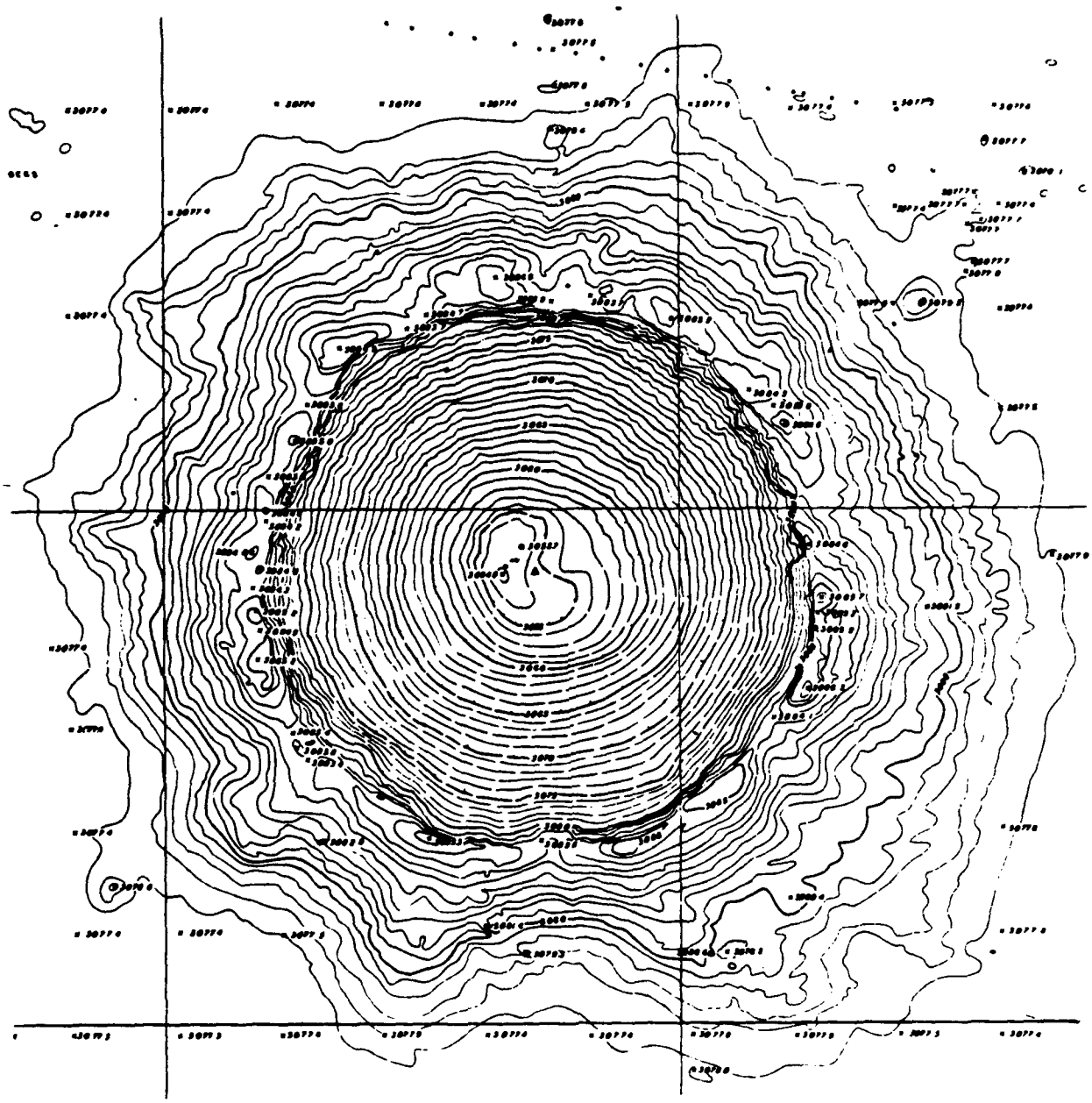

Figure 4.7 Postshot contours prepared from aerial photographs, Air Vent I crater.

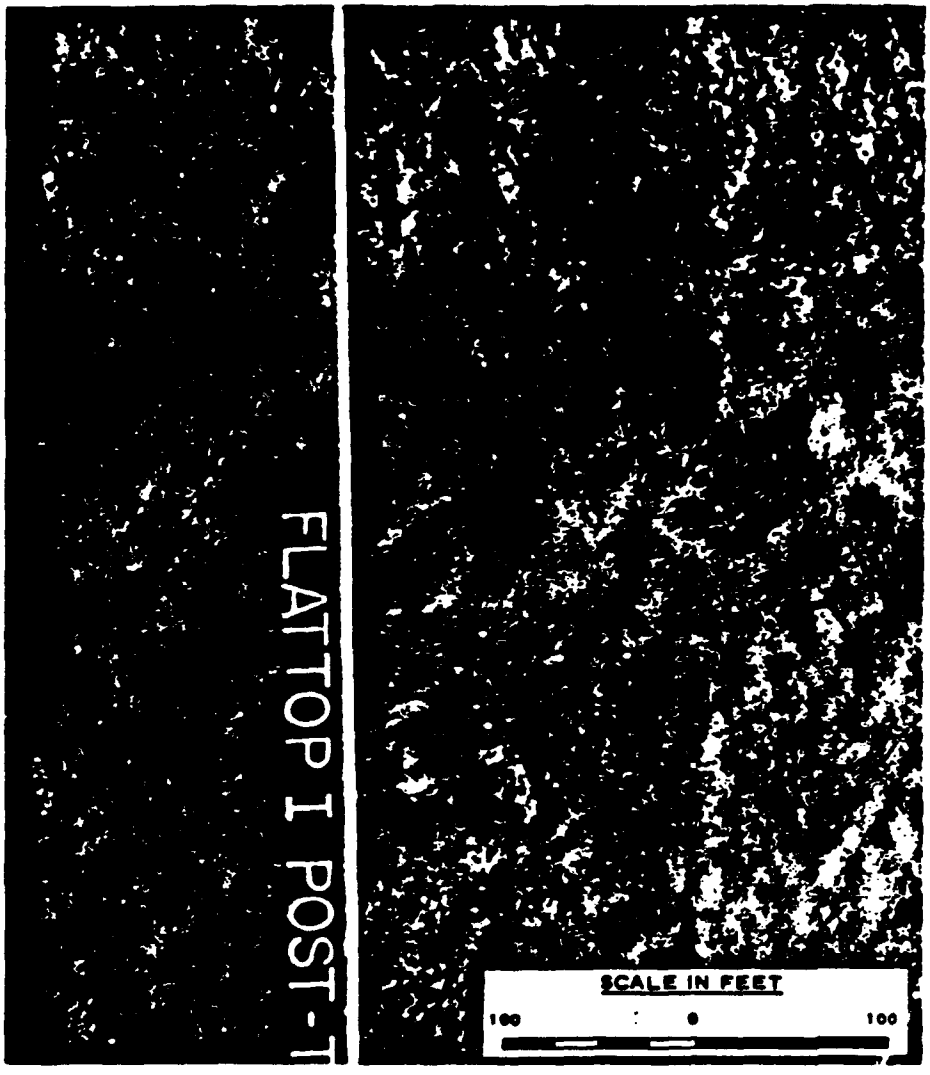

Figure 4.8 Aerial stereopair of Flat Top I crater.

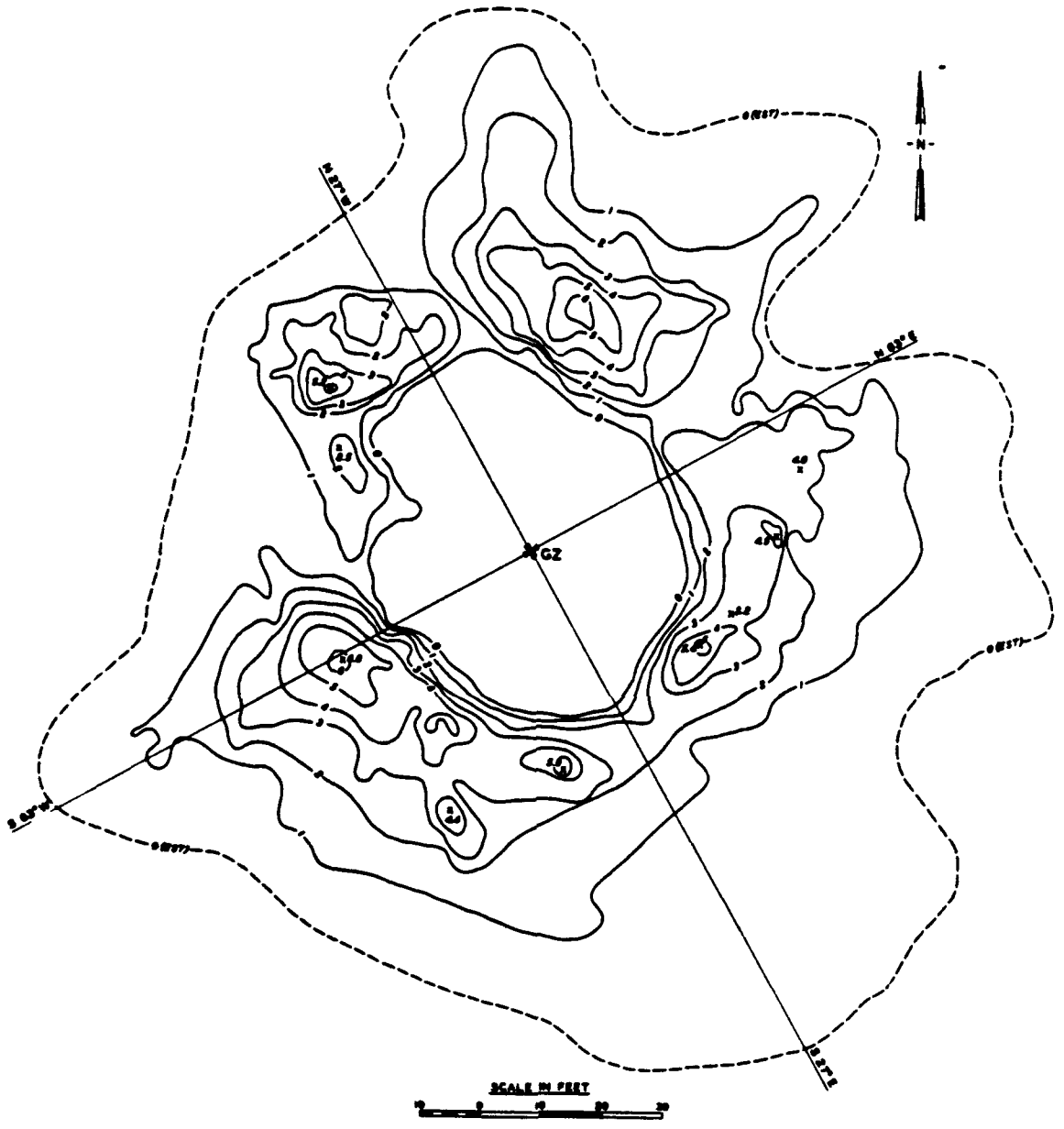

Figure 4.9 Isopach map of crater lip, Flat Top I. Contour interval is 1 foot.

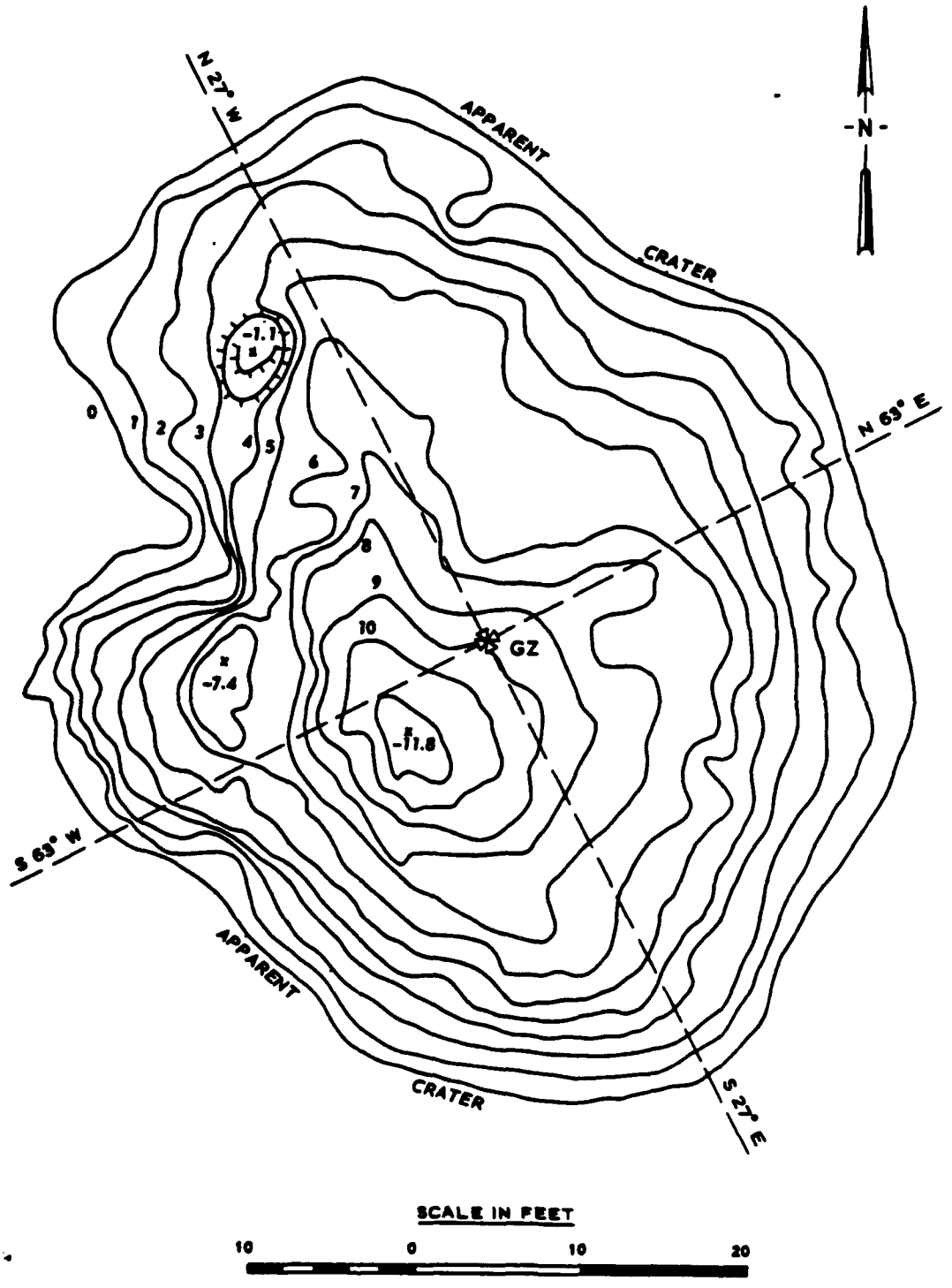

Figure 4.10 Isopach map of apparent crater, Flat Top I. Contour interval is 1 foot.

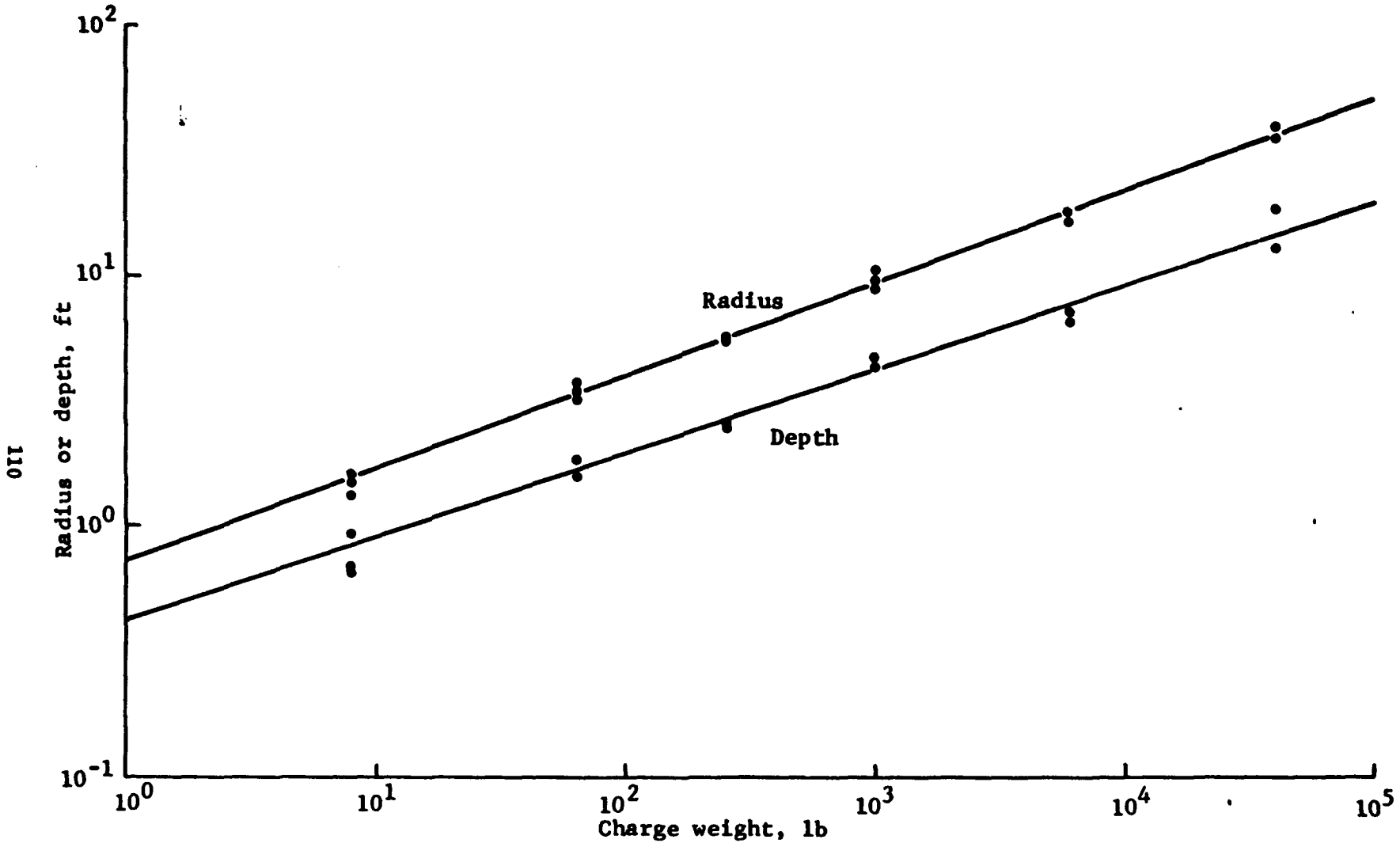

Figure 4.11 Radius and depth of apparent crater versus charge size, all Air Vent/Flat Top surface bursts.

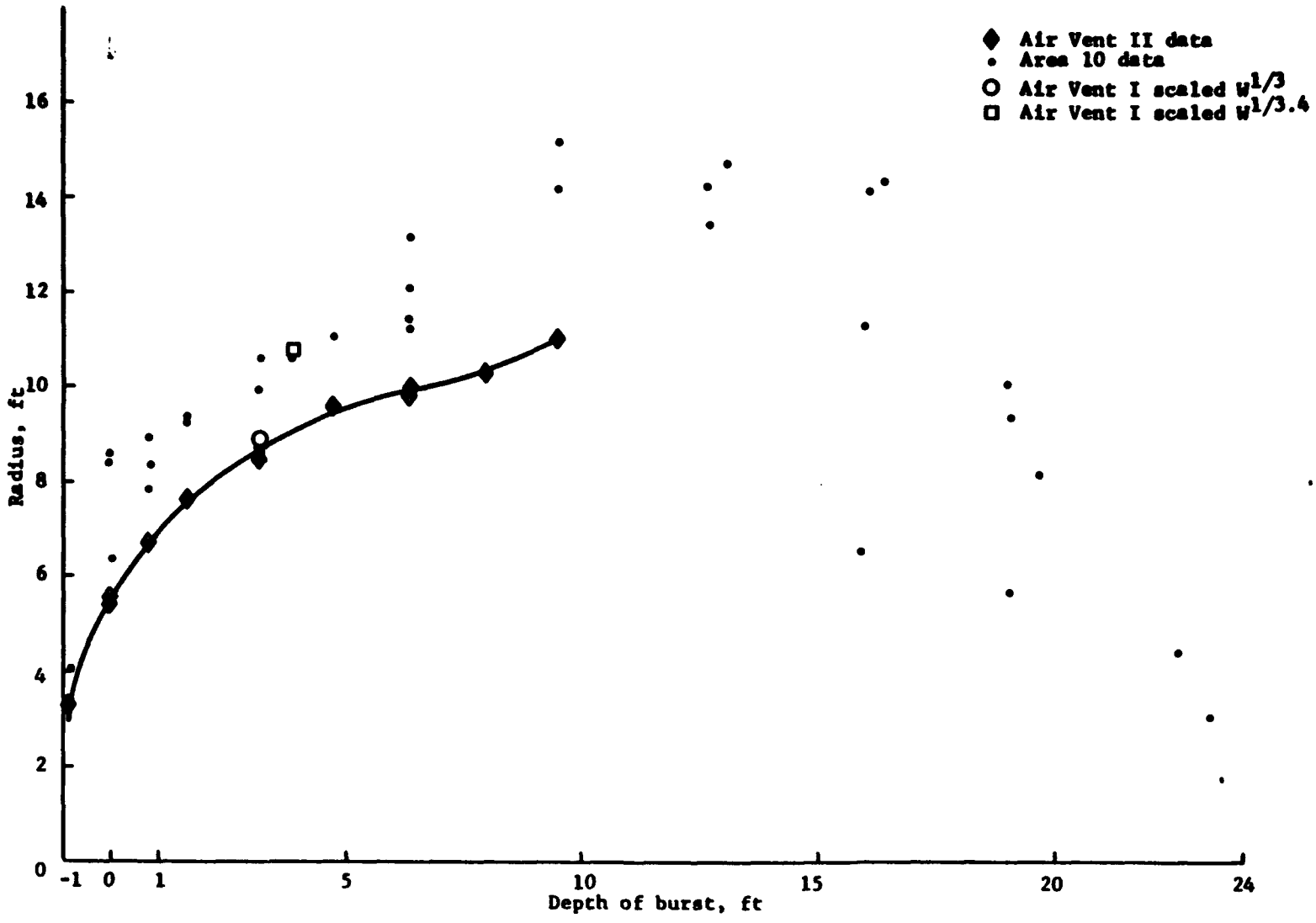

Figure 4.12 Radius of apparent crater versus depth of burst, comparison of Air Vent II with Area 10 data.

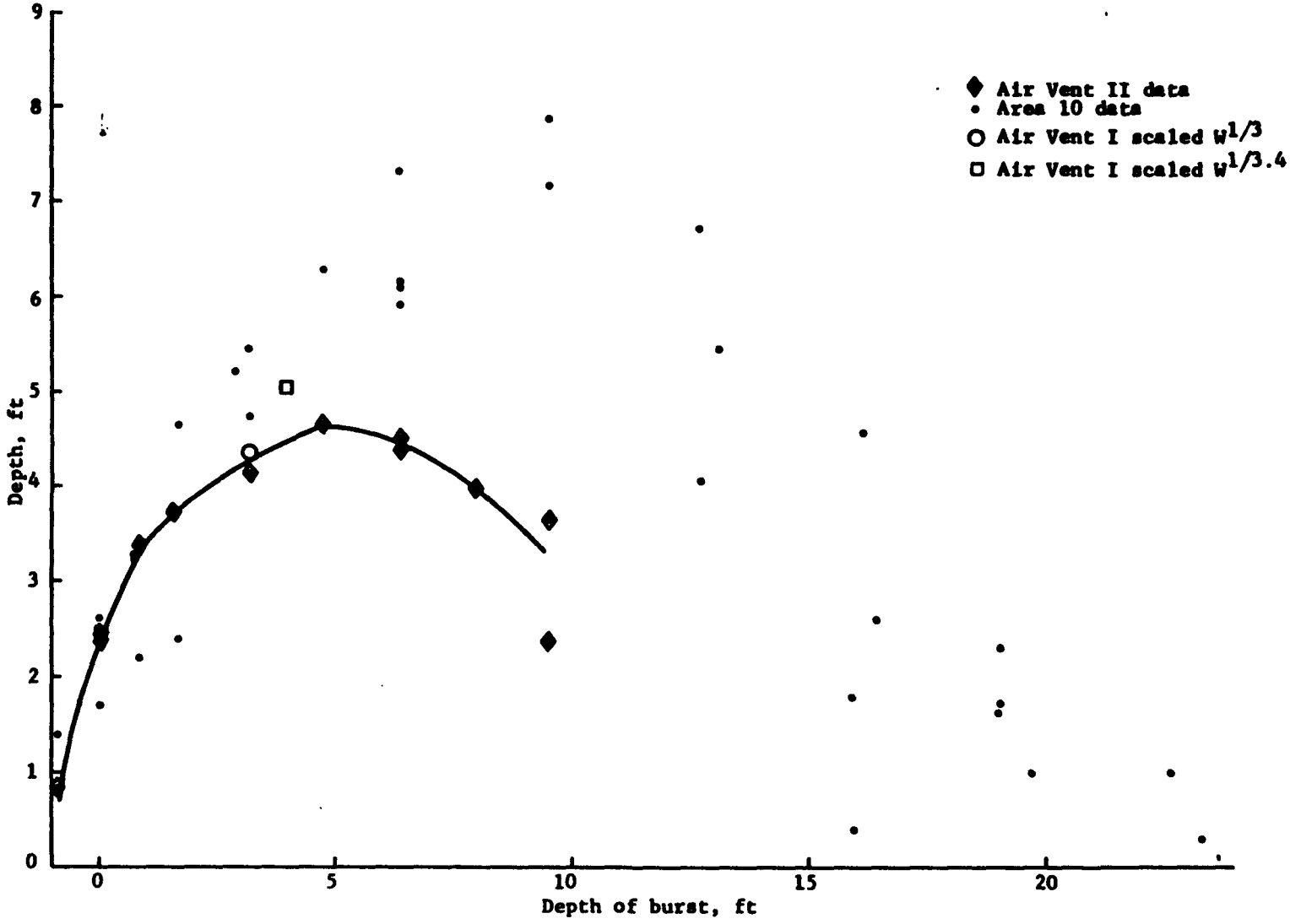

Figure 4.13 Diameter of apparent crater versus depth of burst, comparison of Air Vent II with Area 10 data.

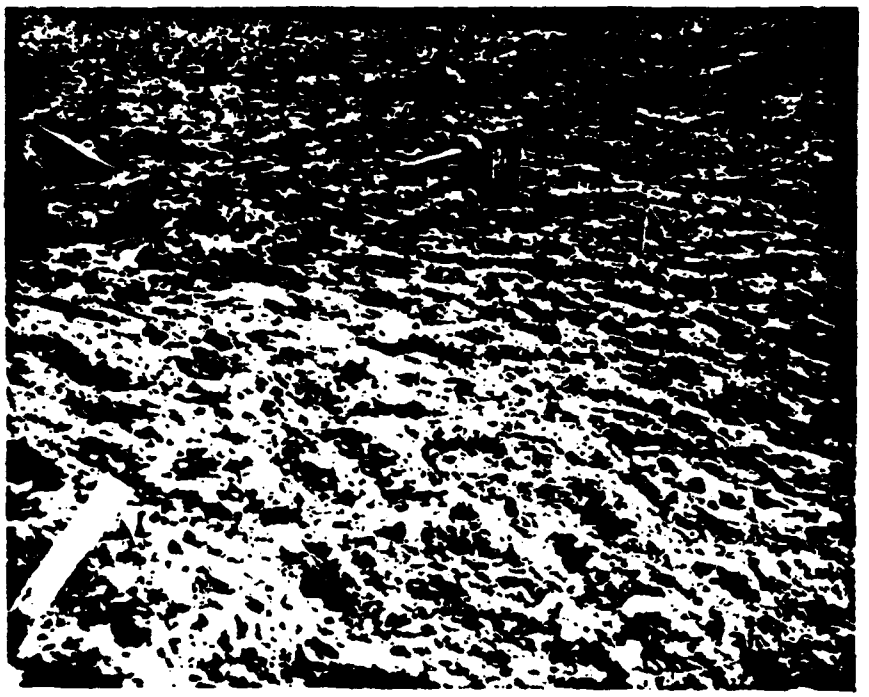

Figure 4.14 Flat Top III lip area showing the many wet clods produced. (33-15-NTS-64)

CHAPTER 5

EJECTA

5.1 BACKGROUND AND METHODS

Interest in ejecta stems from the military need to predict such things as the amount of soil that might cover a silo door or the number of explosive-propelled missiles that might hit an antenna. As recently as 1952, Vaile concluded a study of missiles from the Jangle underground shot, saying that "on large, shallow underground explosions damage by the mechanism of air blast will extend further than damage by the mechanism of missiles. This conclusion is sufficiently firm that no further missile experiments appear necessary" (Reference 55). Times have changed, and there is now concern with higher overpressure regions where missiles do matter.

Nevertheless, Vaile's was the pioneer work in the study of ejecta, together with dust collection studies on the UET series done at about the same time (Reference 27, Ch. 4). The experimental methods used in Air Vent/Flat Top were developed from the ones they used. The areas over which ejecta spreads are so vast and the cover at the outer edges so thin and spotty that one must sample by putting out plates, pans, or tarps to catch the ejected material. Each was laid out like polar coordinate paper, with catchers on numerous radii, at logarithmically increased spacing from near the crater to as far as ejecta is expected (Table 5.1). Very

near the crater, ejecta thickness was measured by direct survey of the surface of the ejecta and of the upthrust ground surface below.

Another basic measurement used on the larger shots was putting objects in the region to be cratered to see where they went. These objects were spherical pellets of several sizes and densities, and a few cubes, as enumerated in Table 5.2. In Flat Top I, the traceable objects were pieces of the grout cylinders, coded by dye and inclusion of glass beads. Also in Flat Top I, the more distant ejecta were easily identifiable fragments, so that in a few areas it was practicable to find each individual particle and survey its resting point.

5.2 THEORY

The theory of ejecta also is in its infancy, and prevailing prediction schemes show it; they are basically devices for extrapolating the results of HE and NE measurements to much larger yields. One scheme takes note of actual depths of ejecta at various distances for a small prototype and increases the scale of depth and range to correspond to the larger crater resulting from a larger explosion. The other presumes to know or guess the velocities with which ejecta are sent out and then calculates their trajectories. The two experimental methods above reflect these two general schemes.

As with cratering, successful calculations have been made in the Plowshare program for buried charges, basically by carrying calculations beyond the point

described in Section 4.3 (Reference 56). Again, Plowshare methods are inherently not applicable to surface bursts.

The first predictive scheme, the scaling of ejecta thickness versus range, is based on these ideas: the material that appears outside the crater must come from within it; therefore, the mass missing from the crater must be expressible as

$$M_m = \int_{R_a}^{\infty} 2\pi\delta \; r \; dr \; . \qquad (5.1)$$

Assuming a nearly constant fraction of the crater becomes ejecta, this missing mass must scale as the crater volume does. In its simplest form, then, this predictive method is just a cube-root scaling. A more advanced form sets

$$M_m \sim V_a \sim R_a^2 \, D_a \; ,$$

or in effect,

$$\frac{M_m}{M_a} = k \int_{R_a}^{\infty} 2\pi \; \frac{\delta}{D_a} \; \frac{r}{R_a} \; \frac{dr}{R_a} \; . \qquad (5.2)$$

The benefit of the latter form is that it appears to be effective in relating ejecta data from bursts at various depths to each other. This predictive scheme, then, starts with a prototype, requires the user to

estimate crater dimensions for the size of explosion he is concerned with, then tells him to scale the radial dimensions of the prototype as the apparent crater radius and depths as the apparent crater depth (Reference 47). This scheme contains the implicit assumption that crater and ejecta scale alike.

A very much simplified (and misused) version of this is the formula

$$\delta = \frac{D_a}{2}\left(\frac{R_a}{R}\right)^{3.85} \qquad \text{(Reference 47, p 103).}$$

Carlson, who developed this first predictive method to its present form, was among the first to point out, as in his Air Vent report (Reference 3), that in practice larger charges do not put their ejecta as far out scalewise as do small charges. Since each individual piece of ejecta presumably must travel at least part of its path ballistically, this scheme implicitly assumes there is some mechanism for making particles from larger charges go faster than those from small charges. Ordinary cube-root scaling would have particles at geometrically similar positions starting with the same velocity. The mechanism producing different velocities might be acceleration by the blast wave, initial turbulence or updraft, changes in energy deposition in the ground or, conceivably, interaction of particles with each other. At the other extreme, ejection at the same velocity, the scaling would be:

$$\frac{M_m}{M_a} = \int_{R_a}^{\infty} 2\pi\left(\frac{\delta}{M_a}\right) r\, dr \ . \qquad (5.3)$$

The second predictive method has never been codified as succinctly as the first, though it has been used several times (References 57, 58). The initial velocity field can be presumed from calculations such as Brode's or PI's (References 33, 36) or it can be inferred from pellet recovery data and scaled up to the charge size of interest. This method requires that the initial particle size distribution be known or estimated, if anything more elaborate than vacuum trajectories is accounted for. A decision must be made whether or not to include air drag and the effect of blast wind.

5.3 RESULTS

The raw data are extremely detailed and may be found in the project reports (References 3, 4, 10, and 11) or in the records of the project agencies.

5.3.1 Areal Density—Playa Shots. The variation, with range, of areal densities of ejecta from some of the Air Vent II charges is shown in Figure 5.1. The lines shown represent the best fit to the data by the method of least squares; the scatter about the lines of points representing the mean of all observations on a ring is not shown but is on the order of 25 percent. These were all 256-pound charges but varied in depth of burst. The figure illustrates a systematic tendency for deeper shots to spread more ejecta over larger ranges than shots of lesser burst depth. Decay exponents are nearly the same except for the surface shot.

Curves not included for the deeper bursts would tend to lie along the right edge of the curves shown.

If the same curves are plotted after scaling by Equation 5.2, they lie nearly on top of each other as shown by Figure 5.2. This is the empirical justification of Equation 5.2.

On the other hand, if such curves are plotted for a series of charge sizes, the result is Figure 5.3. We note now a tendency for ejecta thicknesses to fall off more quickly with distance on the larger shots than on the smaller. The point is more obvious if we plot some of these curves scaled as in Equation 5.2 (Figure 5.4). It becomes very obvious that the scaling of Equation 5.2 breaks down if pushed over too large an extrapolation of yield. Larger shots do not put their ejecta out as far, relatively, as do small charges.

Yet the fact that the scaling of Equation 5.2 is as good as it is would indicate that one of several factors—airblast, turbulence, updraft, interaction, or others—must be at work to make ejecta from large shots leave the vicinity of the crater faster than ejecta from small shots. The other extreme, ejection at the same velocity, is tried in Figure 5.5 and is surprisingly good, though not as good as Figure 5.4. The fact that Equation 5.3 works as well as it does is because the ejecta thickness/distance curves decrease nearly as the inverse cube.

5.3.2 Areal Density—Flat Top I. Ejecta densities on the limestone shot were much less evenly distributed than on the playa shots (Figure 5.6). One rock landing on a pad in a ring could make quite a change. Nevertheless, such rocks are part of the ejecta and must be averaged in, even if scatter results. Flat Top I was in limestone, but most of the ejecta was collected on alluvium. Limestone is so different in appearance from alluvium that it was immediately obvious that some of the material found on the pads must have been material blown on them by the air blast. This added material ran 10 to 40 percent of the sample. Eliminating it, the variation of ejecta areal density with range was that shown in Figure 5.6. When this curve is superimposed on Figure 5.3, it is found that, barring more scatter and more irregularity, it is much like similar curves for Flat Tops II and III.

5.3.3 Pellet Chasing. About 3000 pellets each were installed in Air Vent I and Flat Tops II and III. Coded grout cylinders were installed in Flat Top I. In each shot, of the coded material placed within the eventual true crater, 42 to 48 percent was recovered (Table 5.3). Sand column evidence is an aid in distinguishing the region above the true crater which we call fallback, also a region of permanent distortion underneath the true crater boundary (Chapter 4 and References 5, 12). The pellets are useful in delineating two more zones, one of ballistically ejected fragments and one of material scoured or pushed into the ejecta lip. The vertical transition between the latter two zones is abrupt, "as if the transition had

taken place across a shear plane " (Reference 11, p. 84). The operational distinction between these zones is that material in the ballistic zone is found at large distances, material in the scoured zone close by in the lip, and there is that distinct break. Figures 5.7 through 5.10 show how the crater volume is divided up and the final ground ranges of coded material starting at various positions within this volume.

It is of interest to see how ejecta distribution as estimated by pellet data compares with that determined by collector pans. The comparison has been made for the three playa shots (Reference 58, paper by Ahlers). Figure 5.11 shows that the ejecta distribution as inferred from the pellets is, in general, farther out.

As Chabai did before him (Reference 30, p. 74), Ahlers uses pellet information to try to deduce something about initial velocities. There is an inherent difficulty, of course, in that one thing is measured, a displacement, and two components are to be inferred of a vector velocity. An organizing principle is necessary. On Scooter, an underground burst, Chabai assumed that initial velocities were all radial from the charge. In the Air Vent/Flat Top shots, Ahlers assumed that for each horizontal layer of pellets there was one epicenter. He also assumed a parametric form for the magnitude of initial velocities, approximately a power-low decrease with distance from the epicenter, and using the ensemble of data from pellets, originally all at one level below the surface, he determined the necessary parameters by iteration of the method of least squares. He took into account air drag but not air

blast. Begging the details, Ahlers found the velocity patterns shown in Figures 5.12 through 5.14. For comparison, Figure 5.15 shows a late-time velocity field computed by Brode (Reference 33).

5.3.4 Mass Balances. By whatever theory or prediction method, the ejecta has to come out of the crater. Both kinds of prediction schemes explicitly conserve mass or try to.

To untangle the mass balance, some terms must be defined. Carlson and Ahlers use apparently similar terms that are different in detail. Both men's terms are defined in Table 5.4—which may also serve as a guide for References 4 and 10, where these terms are not defined. Carlson's terms are simpler and will be used here.

For the smaller Air Vent shots, Carlson lists the necessary volumes and masses in Tables 4.1 and 4.2 of Reference 3. For the four larger shots, the necessary volumes and masses are extracted from the sources and given here in Table 5.5. (No attempt has been made to resolve discrepancies in volumes between Tables 4.1 and 5.5.)

Some of the more interesting ratios are the ratios of ejecta mass to true crater mass (M_e/M_t), fallback mass to true crater mass (M_f/M_t), and mass deficit to true crater mass (M_β/M_t), the last being how much the sum of the first two falls short of unity. These and the ratio of mass upthrust to true crater mass are listed in Table 5.6. Flat Tops II and III agree with

the smaller playa shots by straddling their averages. For instance, previous playa surface bursts had an ejecta-true crater ratio (M_e/M_t) of 0.35 ±0.05; Flat Top II has 0.46 and Flat Top III 0.26. Since the ejecta level for Flat Top III was only slightly higher (Figure 5.3), the difference in the two comes principally from the 50-percent difference in true crater volumes (Table 4.1). The mass deficit in most of these shots is about 25 percent, Flat Top III being high at 40 percent and Flat Top I low at near zero. Carlson attributes this mass deficit to compaction and distortion.

5.3.5 Comminution. There is no evidence that the particle size of the playa was changed by any of these shots, except in an inverse sense. In its normal state there is enough cohesion in playa that with careful handling the stuff can be cut and carried about in large blocks. When particle sizes are quoted for it, it has been agitated enough to break up this loose cohesion and it then appears to be very fine material indeed. However, the ejecta from playa craters seemed, much of it, to have flown through the air as abrading clods. This is testified to by pictures showing the tracks of such clods and by finding clods among the ejecta. They were particularly noticeable in Air Vent I; Ahlers notes that some went as far as 1800 feet from ground zero, and hundreds were found in the apparent lip (Reference 4, p. 101). Clods show up clearly in Figures 4.2, 4.4, 4.6, and 4.14.

For shots in rock the study of comminution, or the degree of size reduction, is essential. In Flat Top I,

core from drill holes showed from one to four fractures per vertical foot, some of which were due to the drilling. This puts a lower limit on the preshot block size of the medium.

The bedding of the limestone caused differences in the size of lip ejecta up and down dip from ground zero. Up-dip, large blocks of limestone parted along bedding planes, sliding up and away from ground zero. One such block measured 5 by 3-1/2 by 2 feet. Nothing that big was in the ejecta along the western (down-dip) sides of the crater. Some 160 yd^3 of material was removed from a 30-degree sector to the southwest out to three apparent crater radii from ground zero. When sized, this material had a mass mean diameter of about 100 mm (4 inches) (Reference 11, p. 103). The distribution was broad, however, and many larger and many smaller pieces were found.

5.3.6 Missiles. Among the most spectacular phenomena on Flat Top I were the missiles. They were strikingly obvious to observers—almost literally so, since a manned camera station about 3000 feet southwest of the shot reported a rock struck within 30 feet of them.

The increase in scatter, with distance, of data on ejecta areal density (Figure 5.5) was in part because of an increasing concentration with distance of ejecta mass in a relatively few, large fragments. At the 270-foot sampling ring, over 80 percent of the mass collected from 10 pads was in a single fragment. A particularly large splash crater was seen 1250 feet

southwest of ground zero. The crater diameter was about 5 feet and its depth about 1.5 feet. Secondary particles of the limestone fragment which struck there were found as far as 75 feet beyond the impact point.

A helicopter ride over the area gave the impression that the greatest concentration of missiles and maximum ranges from ground zero occurred in a poorly defined lobe to the northwest—along the strike. There was a lesser lobe to the southeast and still smaller ones to the northeast and southwest.

An effort was made to look for missiles beyond 2500 feet. The safety criteria for missiles from fly rock—which, among other things, permitted that camera station to be at 3000 feet—had been based on data which indicated that there would be essentially no ejecta thrown beyond 2550 feet from ground zero (Reference 59, Table 1736); however, it is obvious that this range was far exceeded.

Virtually all the ejecta found beyond 2500 feet from ground zero were in the form of comminuted but coherent masses of dust-size limestone particles. The massive fragments had considerable cohesive strength but were friable and could be powdered between the fingers. They were white and showed grooves or slickensides on surfaces not broken by the shock of landing (Figure 5.16). Such pieces of ejecta are referred to as shatter cones.

The point of impact of the more distant missiles was marked by a splash of white limestone dust. Fig-

ure 5.17 shows the impact point of a shatter cone about 3300 feet southwest of ground zero, on the east side of Balloon Hill. At least one missile landed on the back side of Balloon Hill, about 4000 feet to the southwest. The most distant missile found in the southeast sector was about 4060 feet horizontally from, and 325 feet vertically above, ground zero. The terrain to the northwest is mountainous and was not explored on foot.

A 60-degree sector to the southeast of ground zero was explored in detail, mapping the final resting point of every missile found. The maximum concentration beyond 2500 feet was of 3 to 4 impact points per 10,000 ft^2 (Reference 11, pp. 80-81, 91).

5.3.7 Rays. An aerial photograph of all Air Vent II shots is found in Figure 5.18. The tendency to form a rayed ejector pattern appears to depend on depth of burst. The most distinctive rays occurred on Air Vent II shots 8, 9A, and 9B which were slightly below the depth that gives maximum crater volume. On surface bursts, there is a less obvious tendency for rays to form.

In Flat Top I there were definitely rays. They were formed in both directions of the strike, up and down dip, to the north and to the N40°E. Several of these may be seen in Figure 4.9. In alluvium and playa there is no evident reason for the particular directions rays take. In Flat Top I, the rays tended to correlate with joint patterns in the rock.

Because of rays and missiles, the azimuthal variation of ejecta areal density is irregular, with a non-Gaussian distribution of amounts of material found on collector pads.

5.3.8 Range and Azimuth Dispersion. The use of pellets and coded grout makes it possible to speak of the dispersion of material that started at the same place in the crater. There is clear evidence of much dispersion both in range and azimuth (References 4, p. 72; 10, p. 147; 11, pp. 118, 119). On Flat Top I the dispersion was 25 percent in range and 12 percent in azimuth.

In Air Vent I and Flat Tops II and III, except for this dispersion, ejection was substantially radial. On Flat Top I there was a definite clockwise shift from radial.

TABLE 5.1 SAMPLER ARRAYS

	Air Vent I	Air Vent II & III	Flat Top II & III	Flat Top I
Number of radii	12	16	16	24
Number of rings	18	11	12	3-9
Inner radius, ft	50	6-19	60	100
Outer radius, ft	3450	75-240	500	520
Number of stations	216	162	180[a]	111

[a]Plus distant stations in rectangular array.

TABLE 5.2 PELLETS USED IN EJECTA EXPERIMENTS

Shape	Diameter	Density	Air Vent I	Flat Top II	Flat Top III
	in.	lb/ft^3			
Sphere	1-1/2	82	2530	1859	2626
Sphere	3	84	96	194	222
Sphere	3/4	83	96	194	222
Sphere	1-1/2	486	96	194	222
Sphere	1-1/2	43	96	194	222
Cube	1-1/4	83	96	-	-
		Total	3010	2635	3514

TABLE 5.3 FRACTION OF PELLET RECOVERY

		Air Vent I	Flat Top II	Flat Top III
Ballistic Zone				
Ground range (ft)	>1400		0.39	0.54
	1200-1400		0.30	0.38
	1000-1200	0.54	0.51	0.47
	800-1000	0.72	0.70	0.17
	600-800	0.91	0.58	0.82
	400-600	0.76	0.68	0.65
	200-400	0.73	0.81	0.65
	100-200	0.57	0.68	0.61
	<100	0.41		0.39
	T	0.65	0.68	0.58
Scoured Zones		0.37	0.13	0.38
Subtotal:		0.47 (701/1500)	0.42 (806/1917)	0.48 (1487/3094)
Deformation Zone		0.12	0.04	None placed
Beyond True Crater		0	0	None placed
Overall Total		0.27 (811/3010)	0.35 (821/2355)	0.48

TABLE 5.4 DEFINITION OF TERMS FOR MASS BALANCE

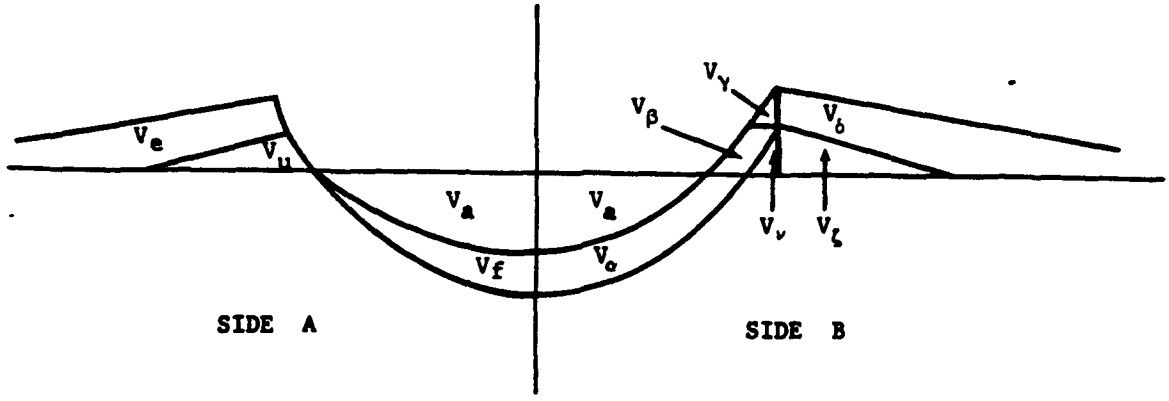

Carlson (Side A):

V_a = volume of apparent crater
$V_t = V_a + V_f$ = volume of true crater
V_f = volume of fallback
V_u = volume of upthrust
V_e = volume of ejecta
$M_m = M_t - M_f$ = missing mass (no longer in crater)
$M_\beta = M_m - M_e$ = mass deficit

Ahlers (Side B):

	Entries below relate to the appropriate Tables in References 4 and 10:
V_a = volume of apparent crater	(line 1)
$V_t = V_a + V_\alpha$ = true crater	(line 2)
V_ν = precrest true lip	(line 11)
V_ζ = postcrest true lip	(line 12)
$V_\nu + V_\zeta$ = total true lip	(line 13)
V_α = below-grade fallback	(line 15)
V_β = above-grade fallback	(line 16)
$V_\alpha + V_\beta$ = total fallback	(line 17)
$V_\beta + V_\gamma$ = precrest above-grade ejecta	(line 18)
V_δ = postcrest ejecta	(line 19)
$V_\beta + V_\gamma + V_\delta$ = total above-grade ejecta	(line 20)
V_γ = precrest ejecta above true lip	(line 21)
$V_\gamma + V_\delta$ = total ejecta	(line 22)
$V_\alpha + V_\beta + V_\gamma + V_\delta$ = total fallback + ejecta	(line 25)

TABLE 5.5 VOLUME AND MASS QUANTITIES NEEDED IN MASS BALANCE

Volume[a]	Air Vent I	Flat Top II	Flat Top III	Flat Top I
V_t	126,000	37,200	67,000	24,300
V_a	54,100	23,050	38,600	10,000
V_f	59,000	14,500	30,000	14,000
V_u	16,600	6,200	6,100	-
V_e	59,100	20,800	23,500	22-26,000
Mass[b]				
M_t	12.07×10^6	3.37×10^6	6.73×10^6	4.0×10^6
M_a	5.19×10^6	2.09×10^6	3.87×10^6	1.65×10^6
M_f	4.37×10^6	1.10×10^6	2.28×10^6	1.4×10^6
M_u	1.56×10^6	0.57×10^6	0.61×10^6	-
M_e	4.37×10^6	1.54×10^6	1.73×10^6	$2.7\text{-}3.1 \times 10^6$
M_m	7.70×10^6	2.27×10^6	4.45×10^6	2.6×10^6
M_β	3.33×10^6	0.73×10^6	2.72×10^6	$-(0.1\text{-}0.5 \times 10^6)$

[a]Volumes in ft^3.
[b]Masses in lbs.

Sources:
Air Vent I — Ref. 4, p. 42 (Table 3.2)
Flat Top II — Ref. 10, p. 107 (Table 3.2)
Flat Top III — Ref. 10, p. 108 (Table 3.3)
Flat Top I — Ref. 11, p. 70-71, 78

TABLE 5.6 MASS RATIOS

Shot	M_e/M_t	M_u/M_t	M_f/M_t	M_β/M_t
Air Vent I	0.36	0.13	0.36	0.28
Flat Top II	0.46	0.17	0.33	0.22
Flat Top III	0.26	0.09	0.34	0.40
Flat Top I	0.67-0.77	Not determined	0.35	-(0.02-0.12)
All Air Vent Surface Bursts	0.35 ±0.05	0.10 ±0.03	0.40 ±0.03	0.26 ±0.06
All Air Vent Nonsurface Bursts Except Air Vent I	0.49 ±0.08	0.12 ±0.05	0.44 ±0.10	0.08 ±0.05

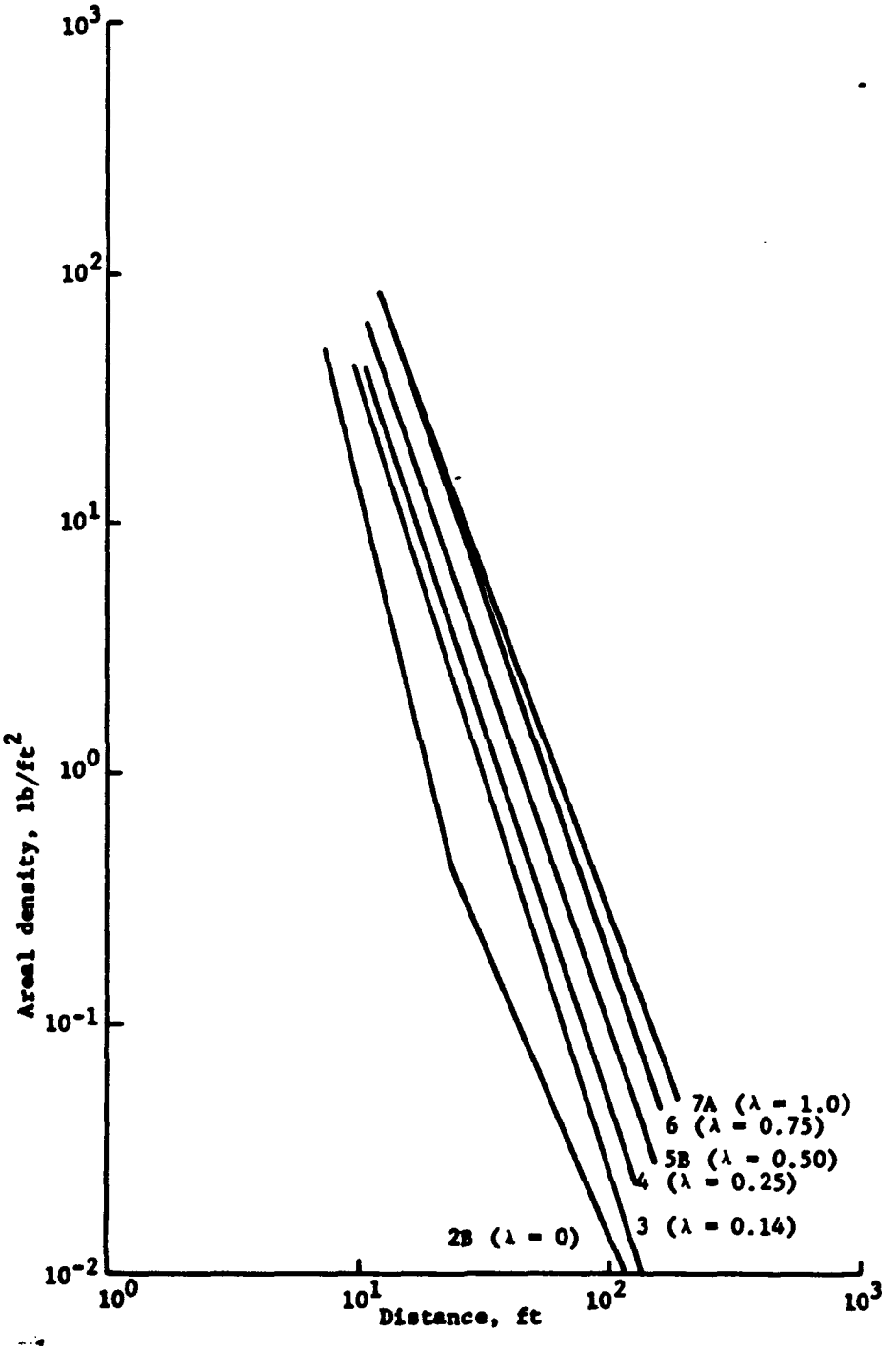

Figure 5.1 Areal density of ejecta versus distance, comparison of various depths of burst, Air Vent II.

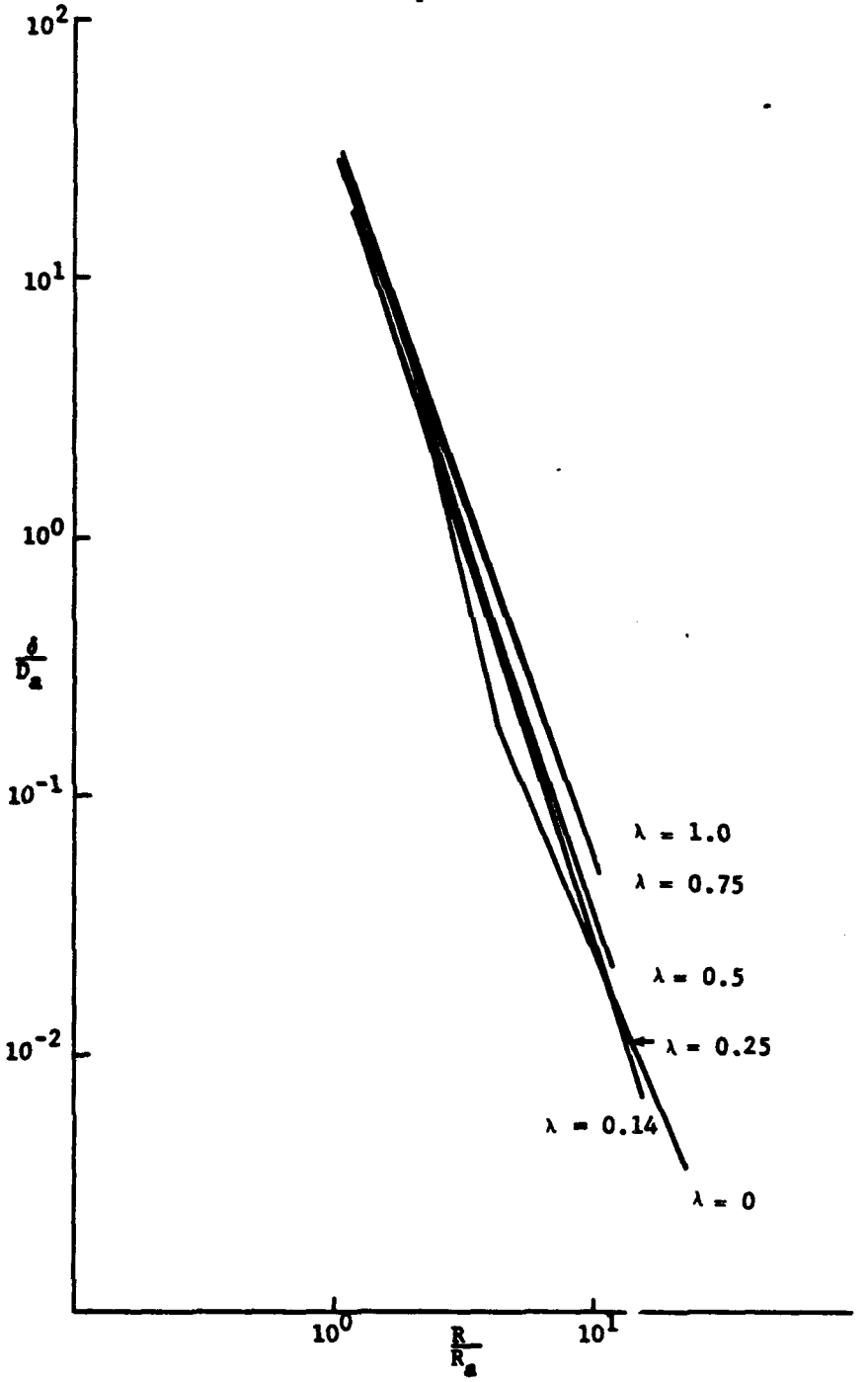

Figure 5.2 Areal density of ejecta scaled by crater dimensions, comparisons of various depths of burst, Air Vent II.

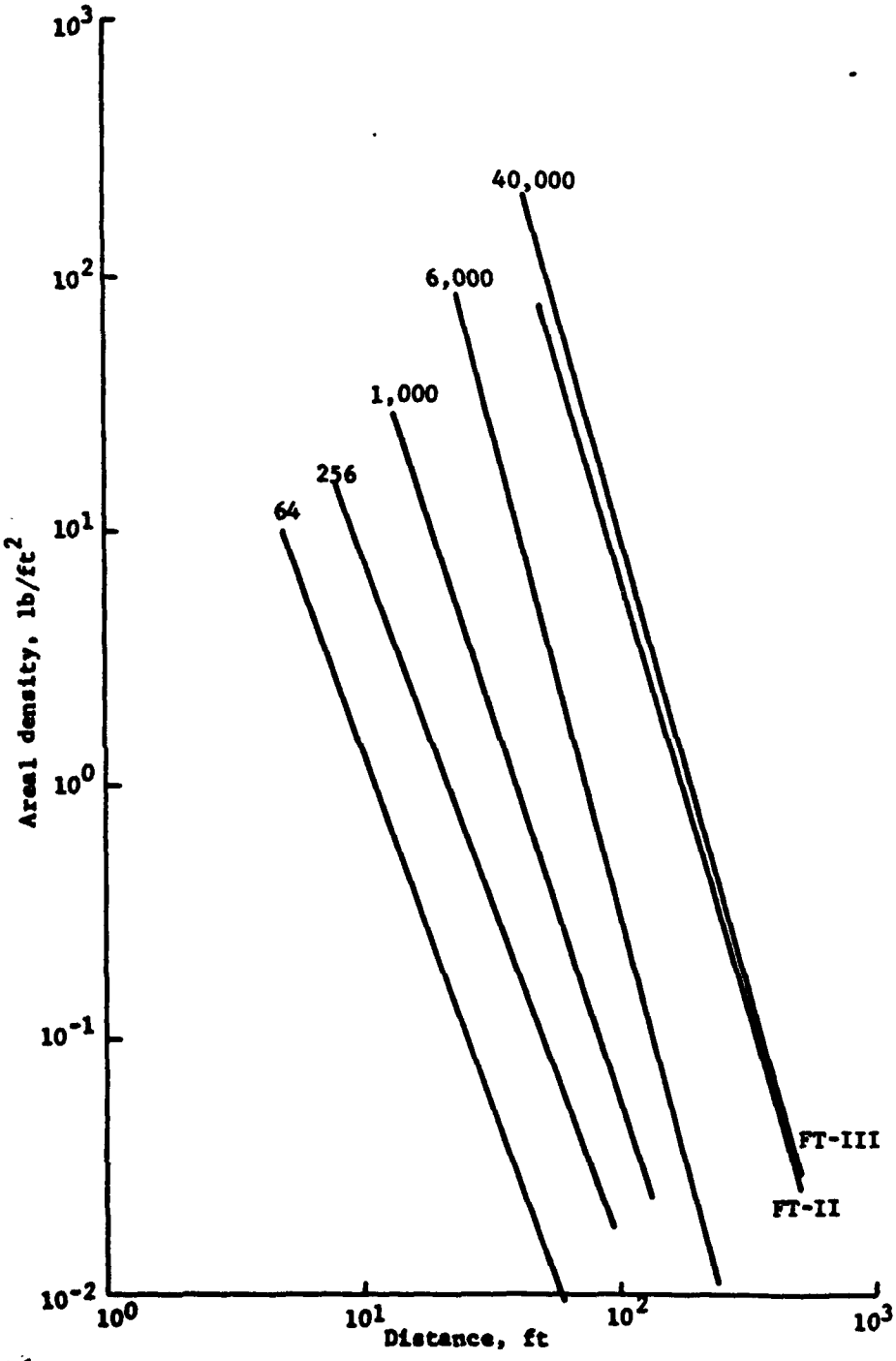

Figure 5.3 Areal density of ejecta versus distance, comparison of various sizes of surface bursts.

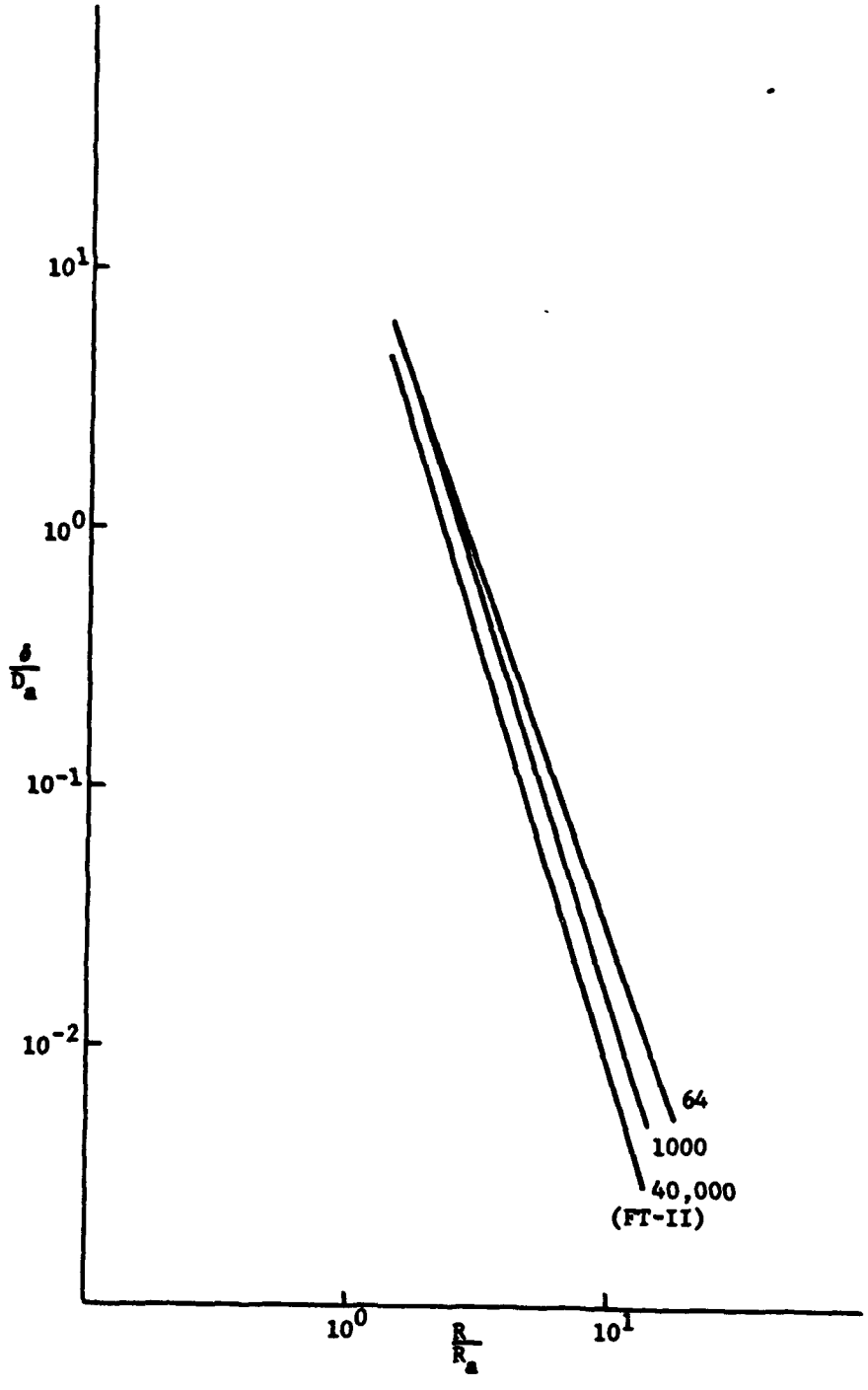

Figure 5.4 Areal density of ejecta scaled by crater dimensions, comparison of various sizes of surface bursts.

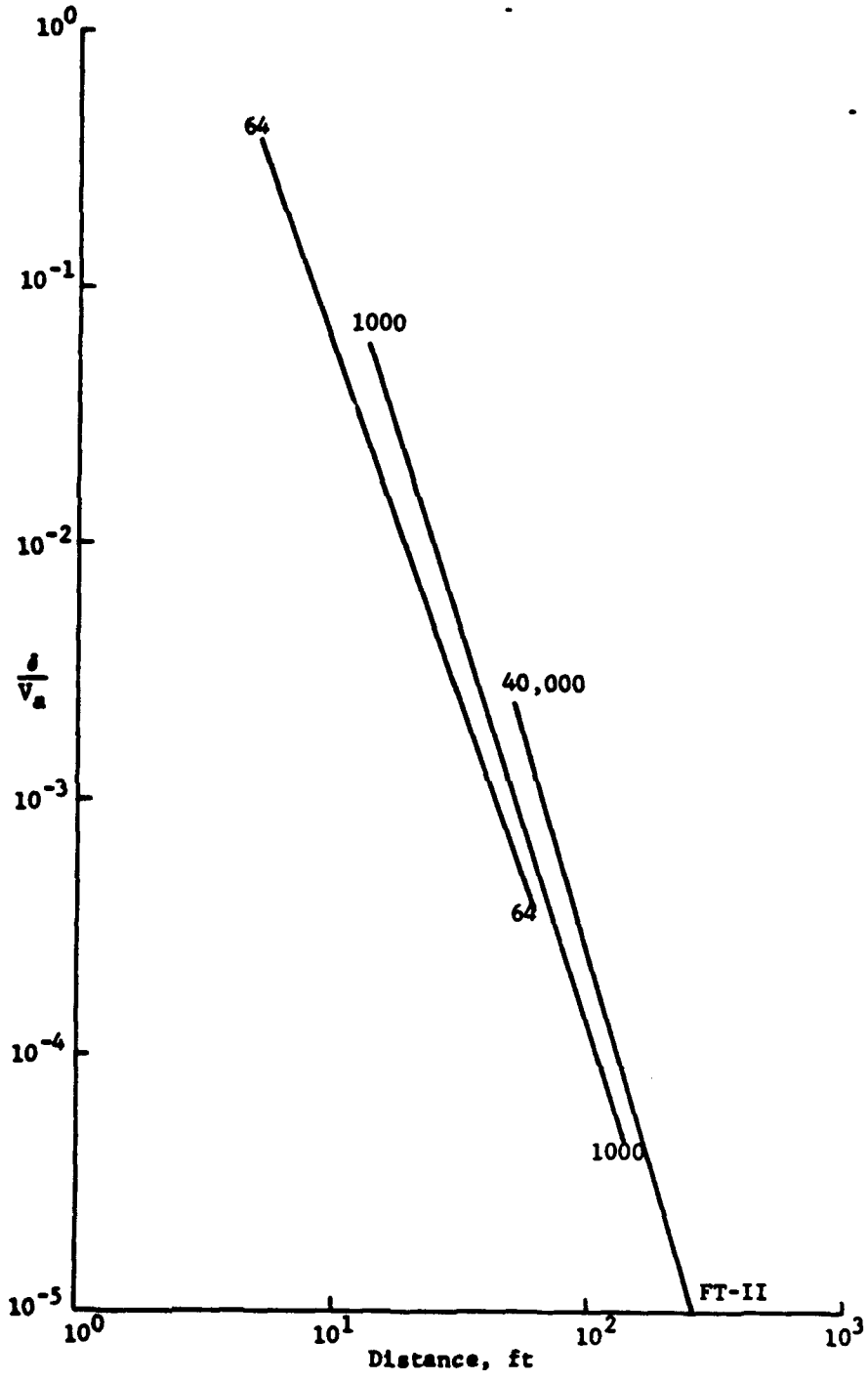

Figure 5.5 Areal density of ejecta scaled ballistically, comparison of various sizes of surface bursts.

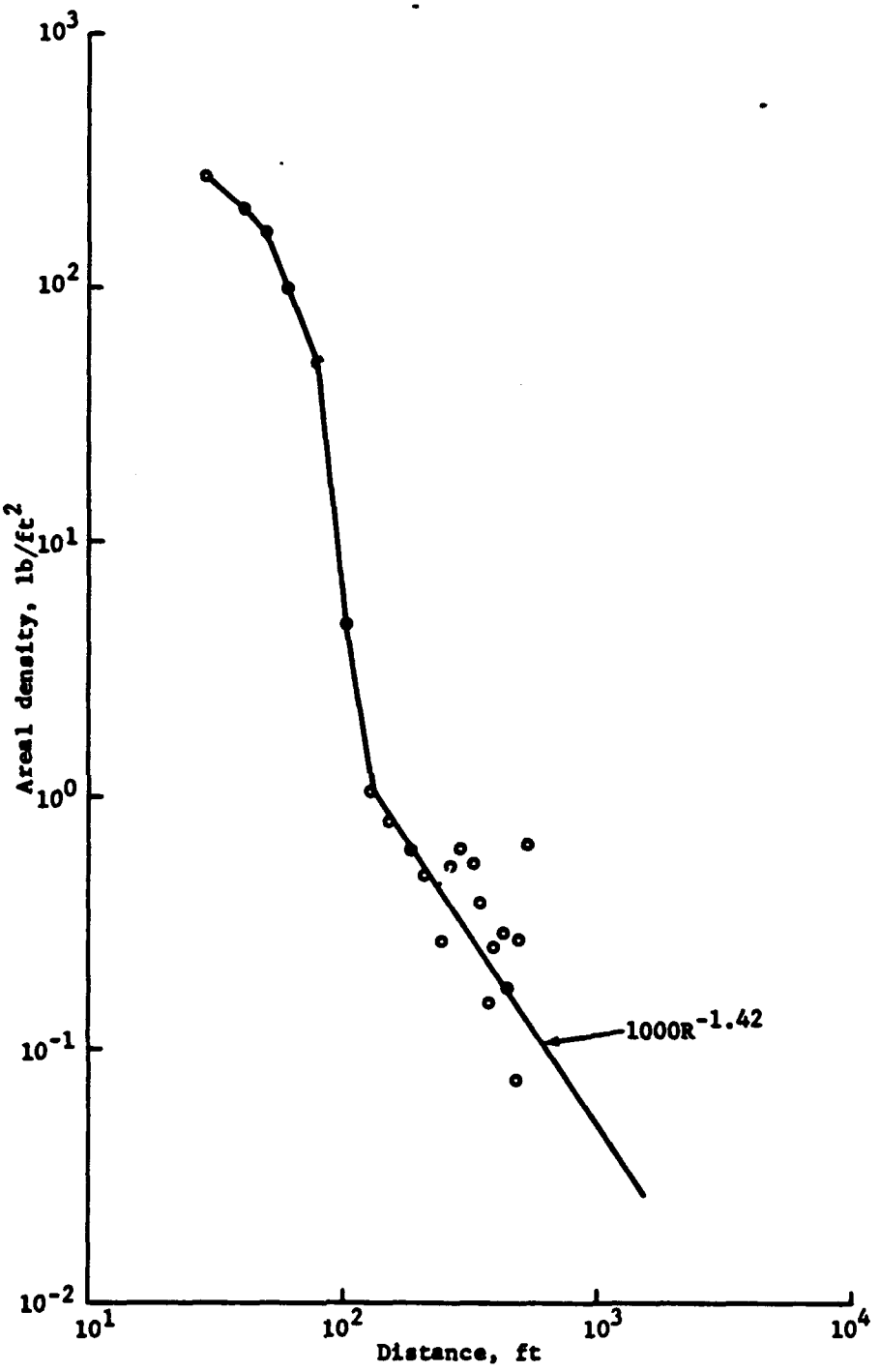

Figure 5.6 Areal density of ejecta versus distance, Flat Top I.

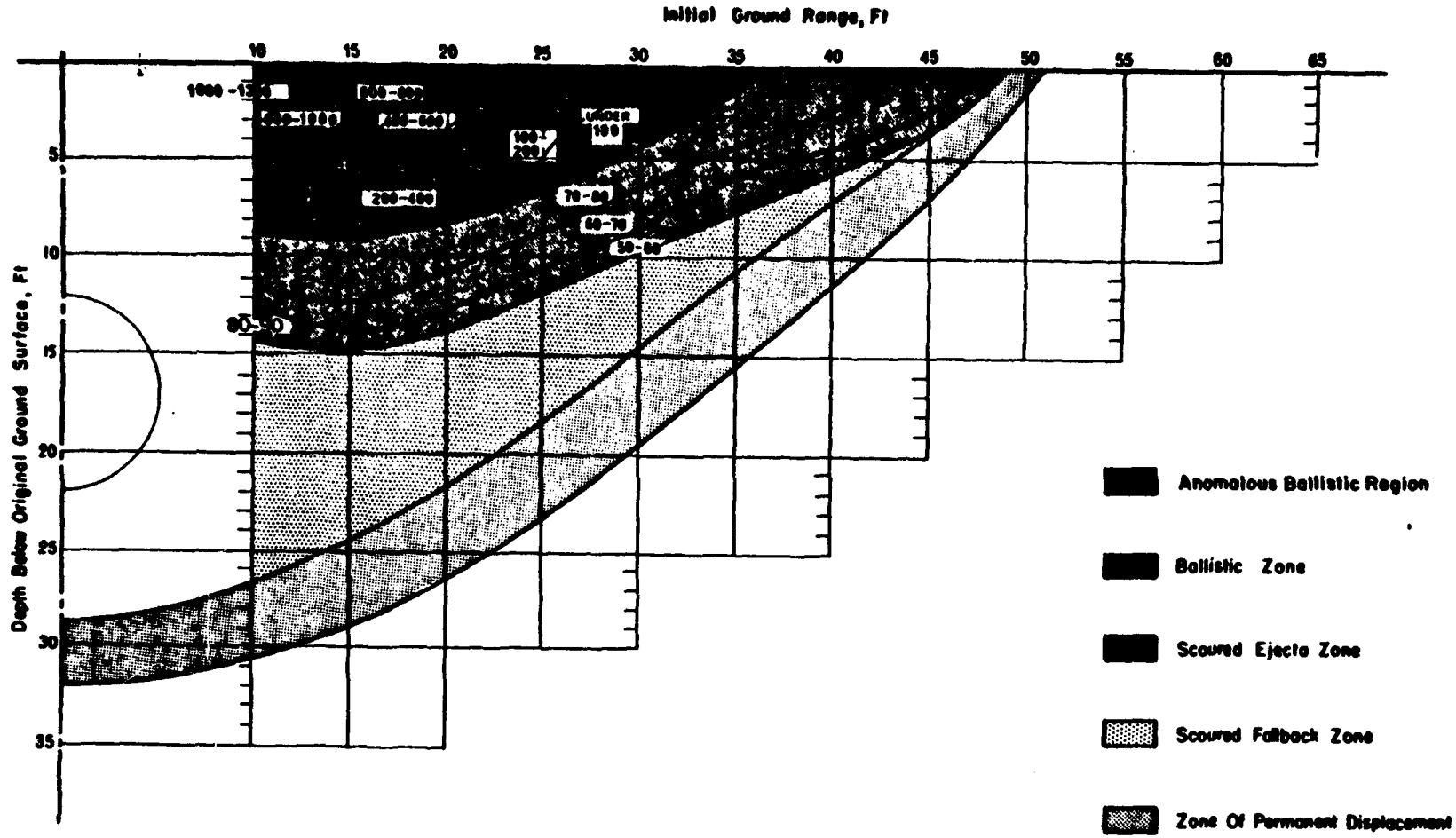

Figure 5.7 Crater zones, Air Vent I.

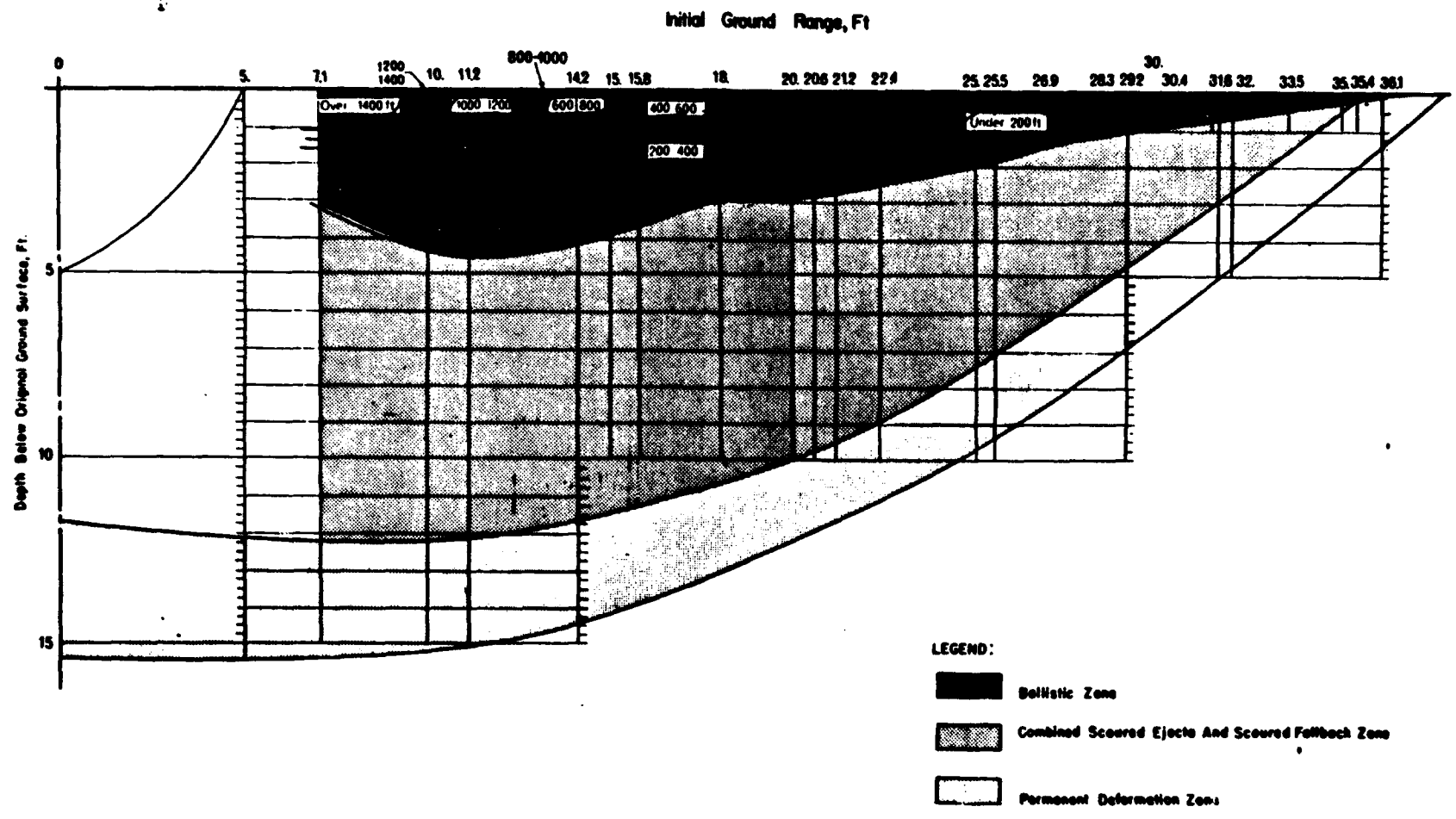

Figure 5.8 Crater zones, Flat Top II.

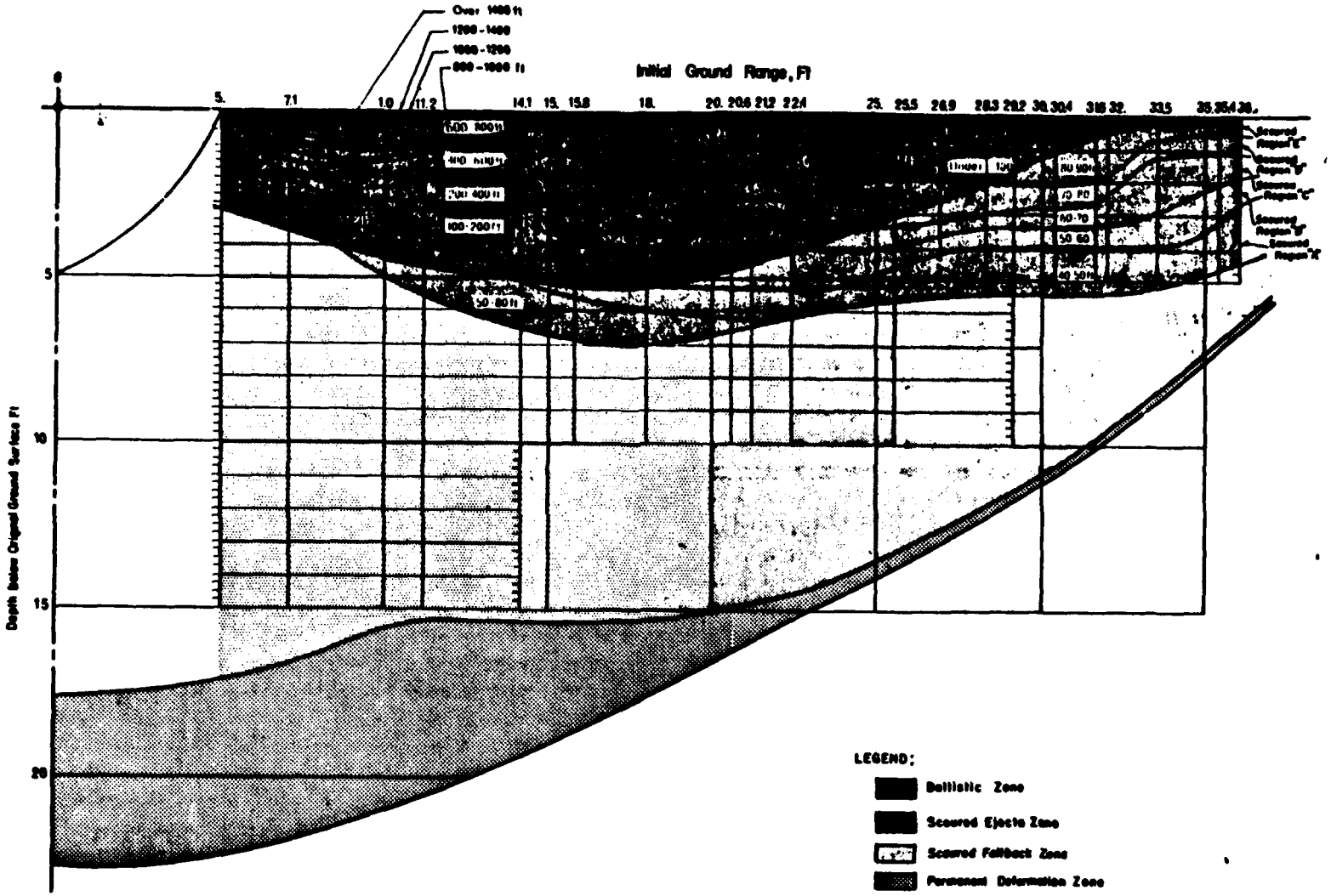

Figure 5.9 Crater zones, Flat Top III.

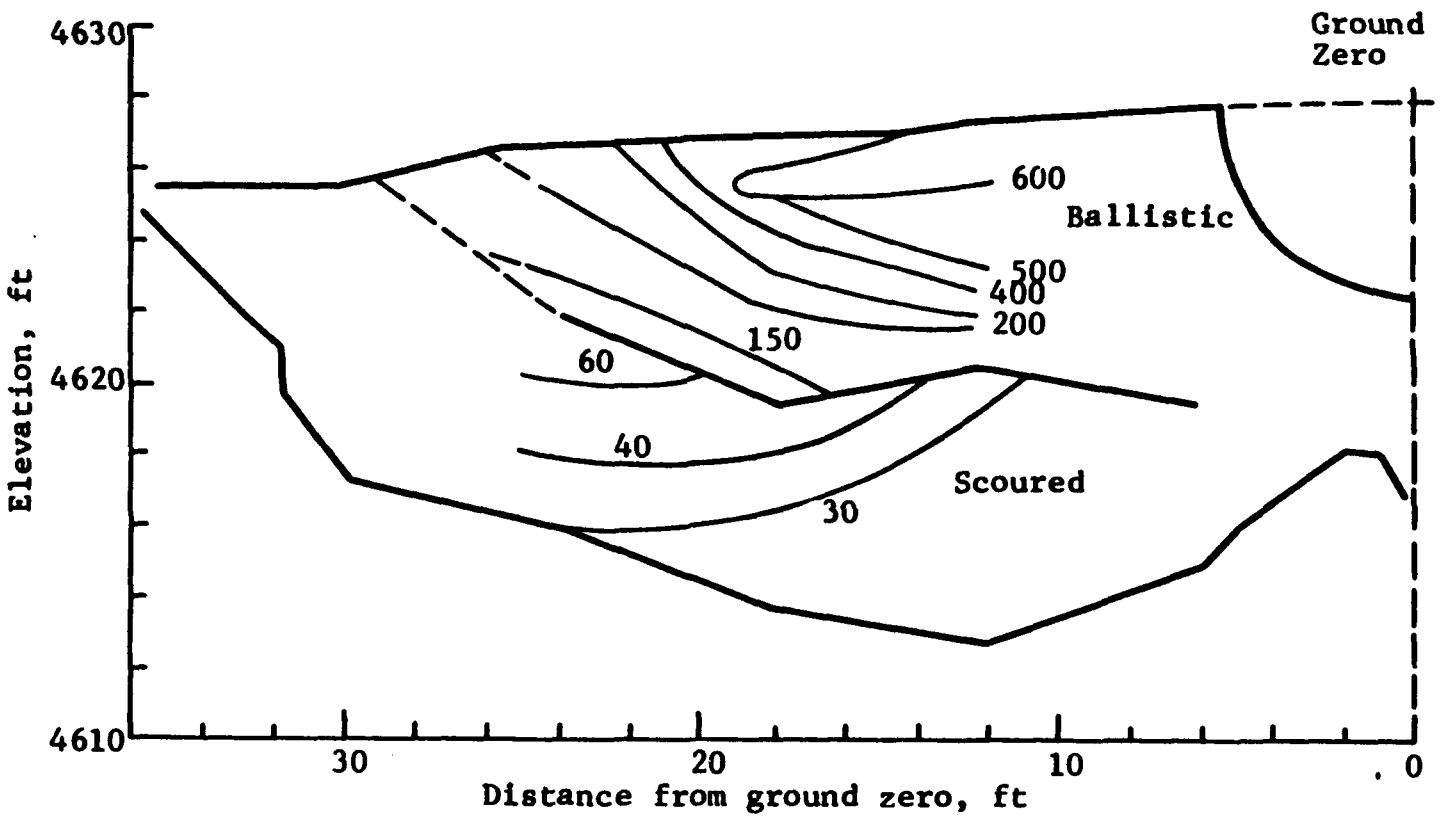

Figure 5.10 Crater zones, Flat Top I.

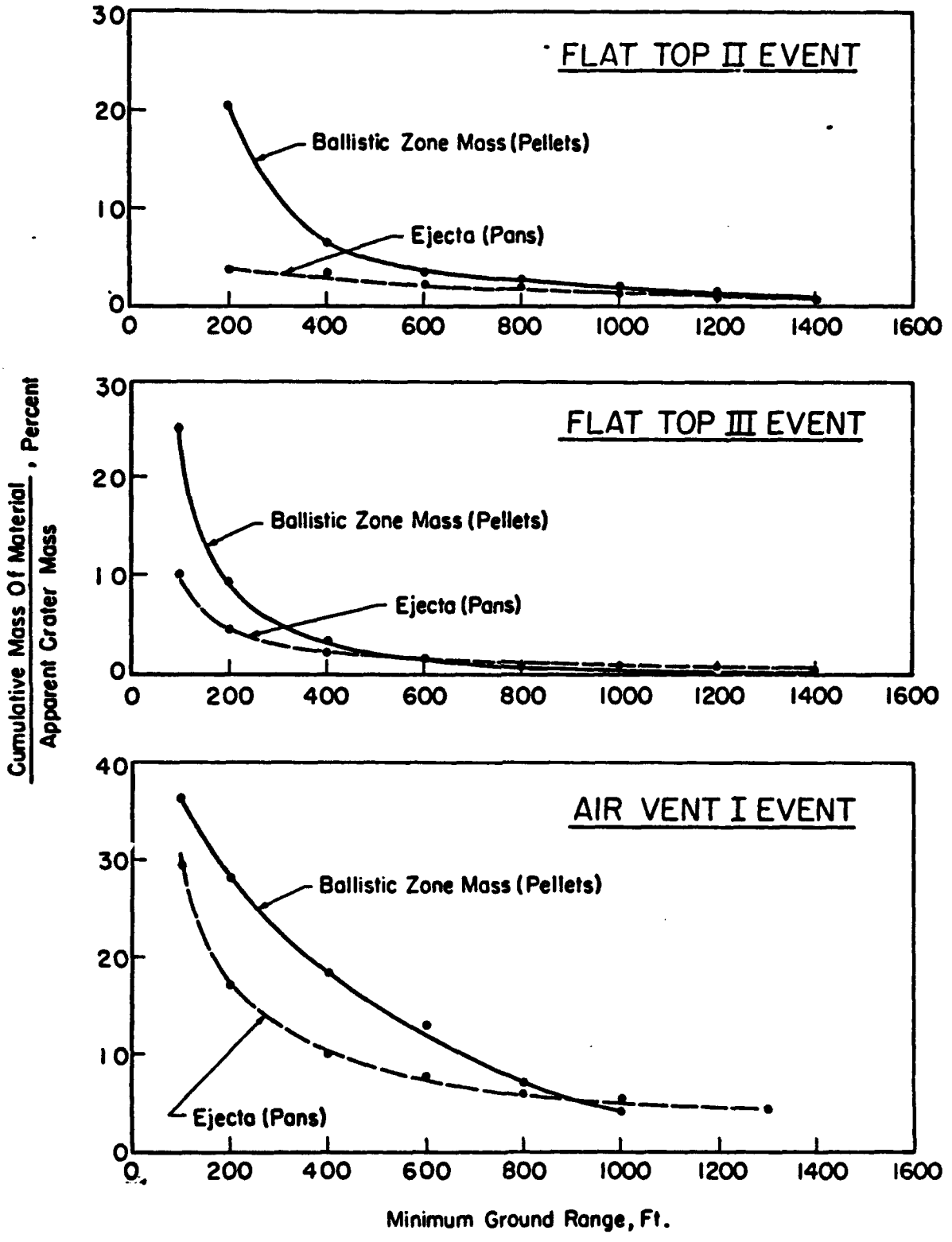

Figure 5.11 Comparison between measured ejecta and ballistic zone mass.

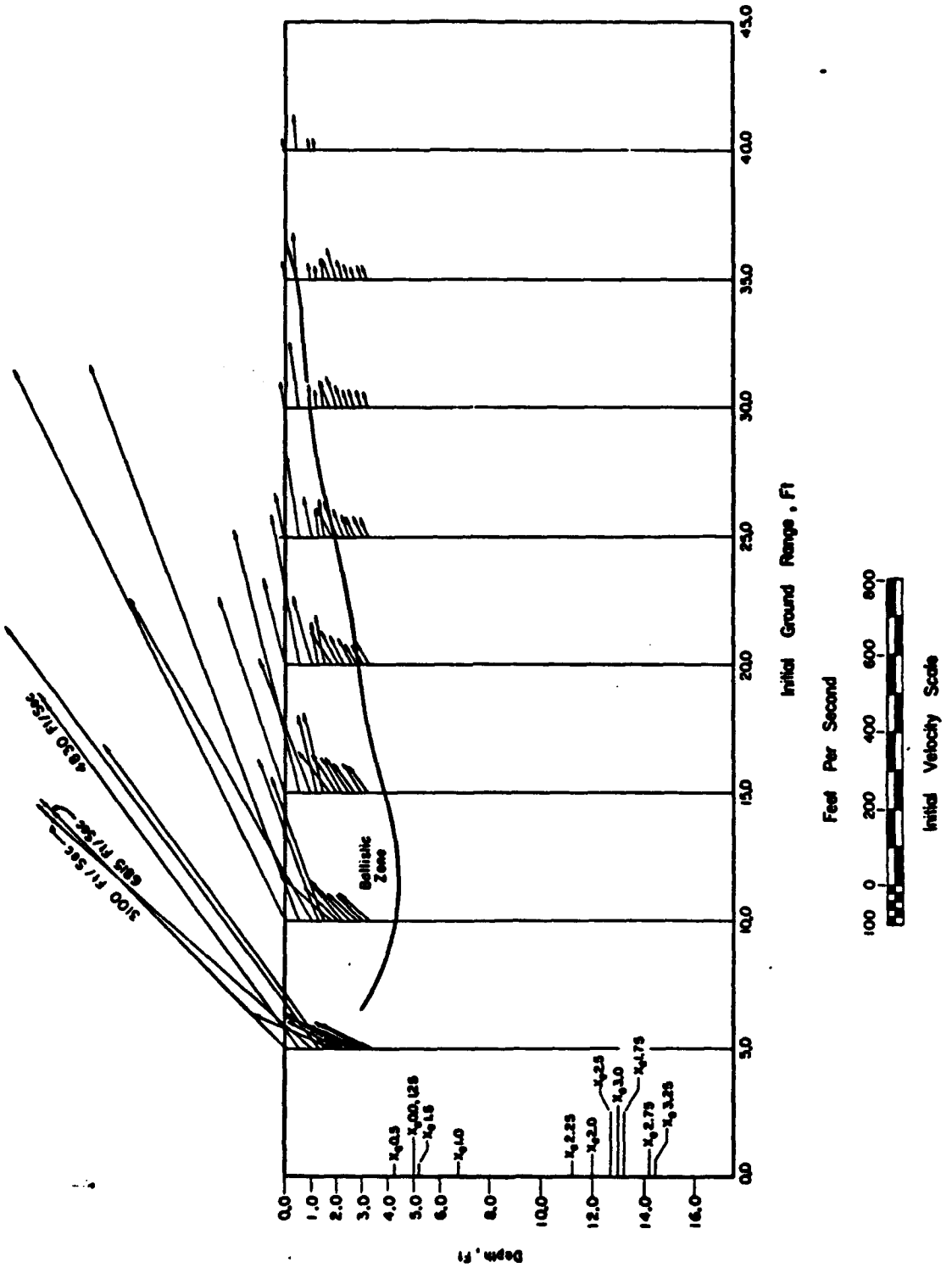

Figure 5.12 Initial velocity field, Flat Top II.

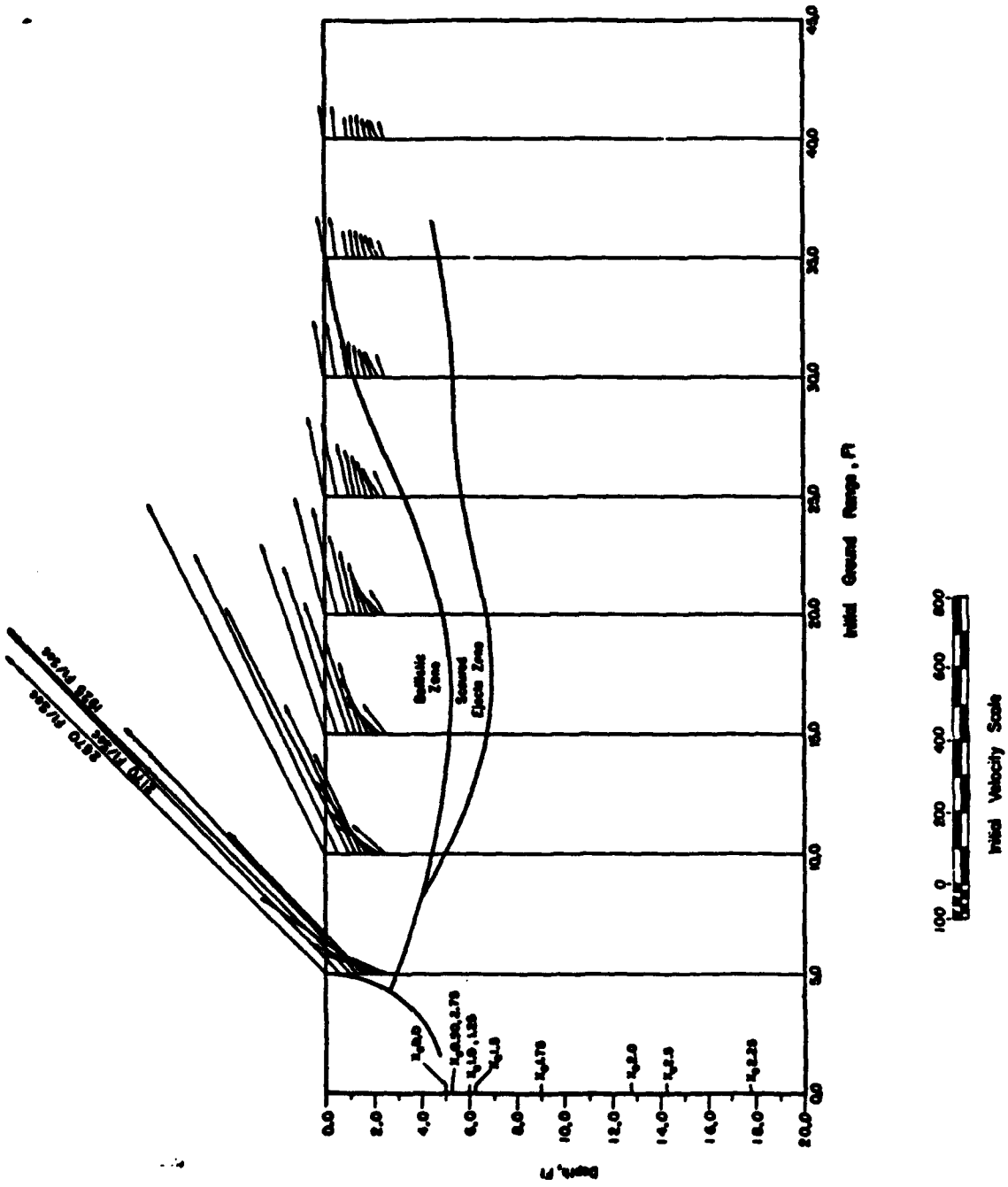

Figure 5.13 Initial velocity field, Flat Top III.

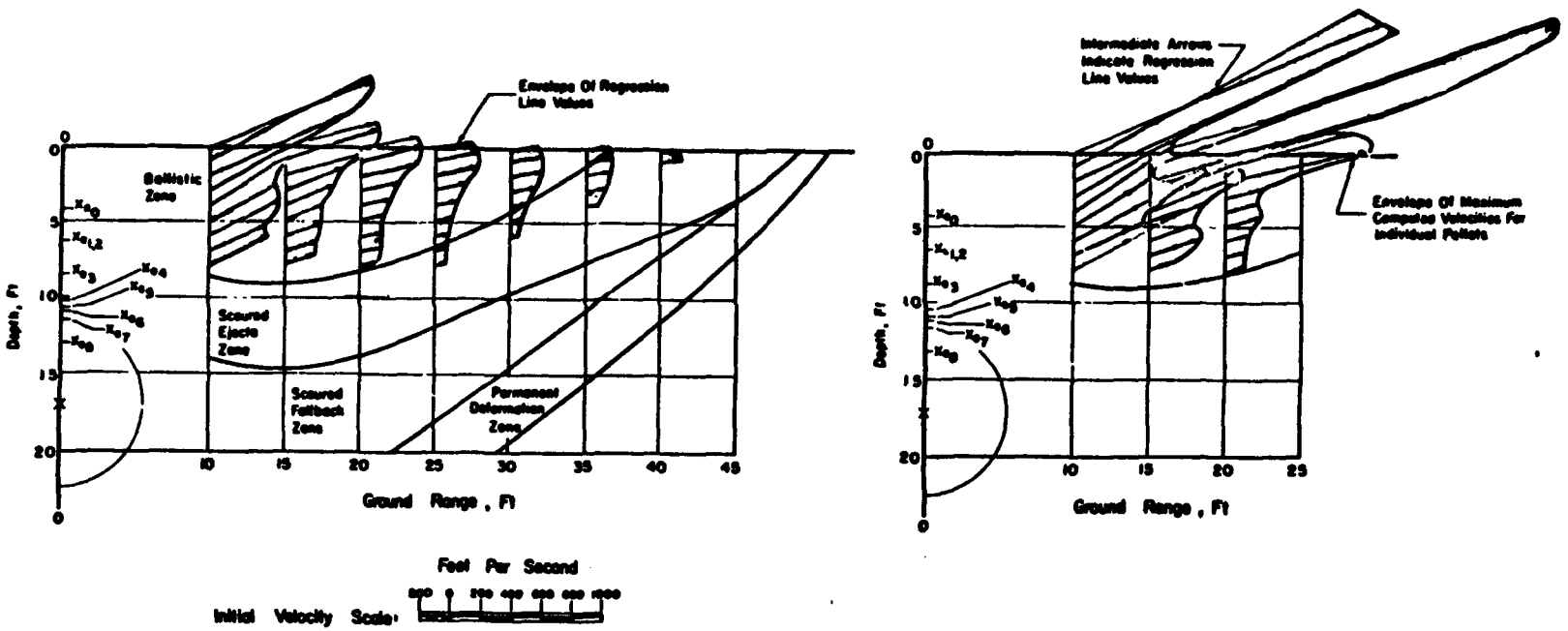

Figure 5.14 Initial velocity field. Air Vent I.

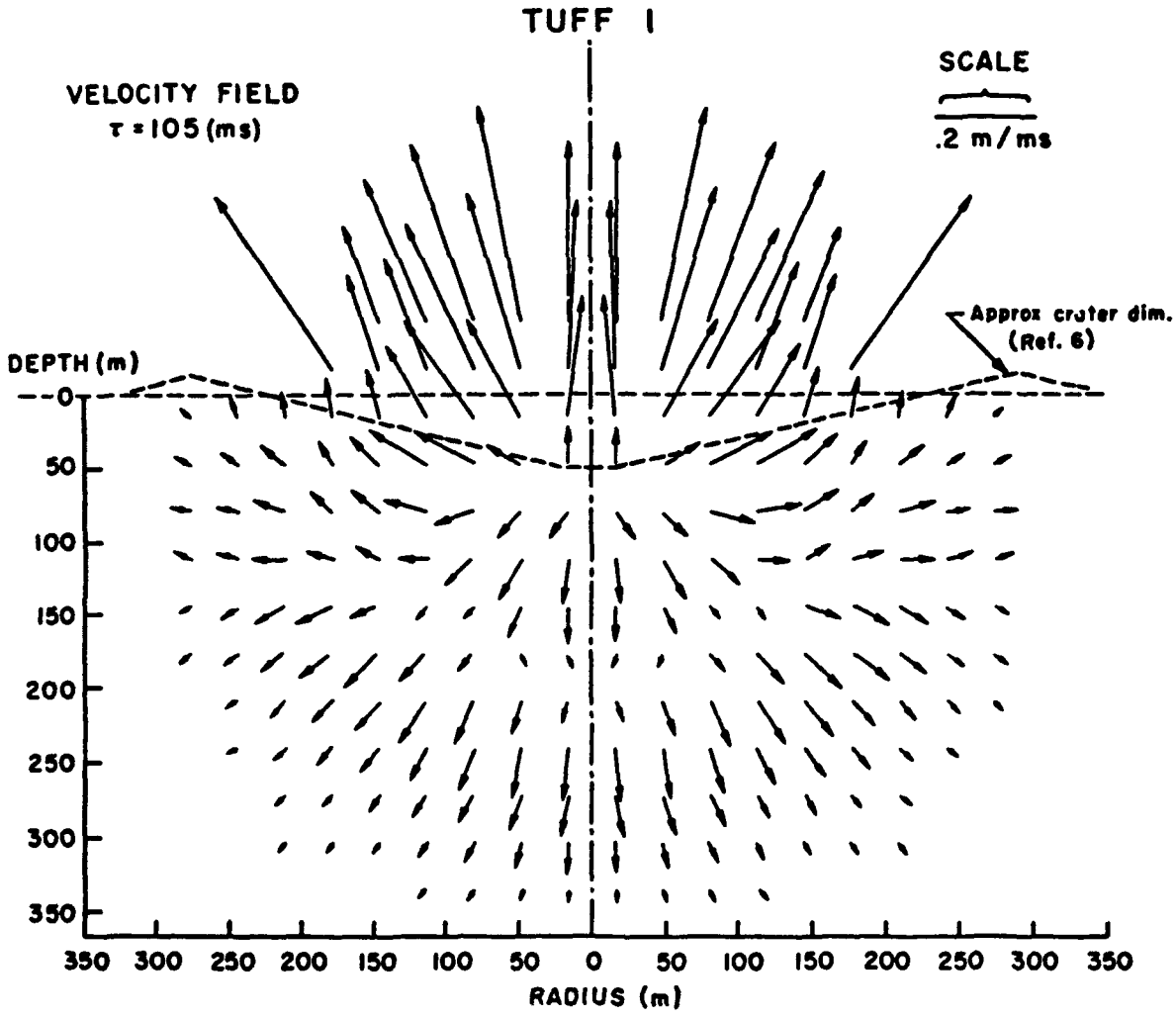

Figure 5.15 Computed velocity field, megaton surface burst at 105 msec.

Figure 5.16 A typical shatter cone, Flat Top I (69-09-NTS-64)

Figure 5.17 Splash formed by impact of a shatter cone at a distance of 3300 feet from Flat Top I. (69-10-NTS-64)

Figure 5.18 Aerial view of Air Vent II craters.

CHAPTER 6

MISCELLANEOUS

6.1 CLOUD RISE

The Weather Bureau Research Station at Las Vegas, Nevada, has a continuing responsibility for predicting fallout from nuclear shots at NTS and, therefore, for predicting the rate and height of clouds. For this reason they helped support Project 9.8 (Technical Photography) to get late-time photography of the larger Air Vent/Flat Top shots and obtained data on all shots of 1000 pounds or more.

The cloud heights recorded are given in Table 6.1. These depend on charge size, as the table shows. They also depend critically on atmospheric stability and on the winds. When a meteorologist uses the phrase, atmospheric stability, he implies a comparison of the actual lapse rate (temperature decrease with height) with an adiabatic lapse rate; the latter is the lapse rate to be expected in an atmosphere in adiabatic pressure equilibrium. A lapse rate less than adiabatic is termed stable since a parcel of gas rising in it is decelerated. The wind affects cloud rise because its associated turbulence tends to destroy the integrity of the cloud.

The Weather Bureau report on the Air Vent/Flat Top clouds (Reference 16) was a short study of how these clouds, as additional data, met the basic theoretical

ideas and how they fitted the empirical formulae being used. These were modified to the form

$$H_T = 750\ W^{1/4}\ t^{1/2} + 32.7\ (t - 10)\ W^{1/7}\ ,$$

the addition of the second term being the change.

6.2 SEISMIC SIGNALS

The picture of seismic signals from surface and near-surface bursts is a decoupling by a factor of 2 to 4 in amplitude compared with contained shots, but the pattern is not completely consistent in that there are some outstanding exceptions. As with close-in shock, HE gives stronger signals than NE.

The Tonopah and Darwin stations of the Sandia seismic network were operated on Air Vent I and on Flat Tops I and II (Reference 60). Signals from Flat Top I were 0.32 ±0.11 times those from Flat Top II (12 data). This ratio is not considered significant since the seismic signals traveled entirely different paths from the various sites. Signals from Air Vent I were 1.2 ±0.3 times as big as those from Flat Top II. This ratio is meaningful. No comparison with a contained burst is possible because we have no data from a contained HE burst in Area 5.

TABLE 6.1 CLOUD RISE DATA

Shot	Size	DOB	Height	Time	Notes
	lb	ft	ft	sec	
Air Vent III-2A	1,000	0	1700	200	Rise about done
Air Vent III-2B	1,000	0	1600	200	Rise about done
Air Vent III-2C	1,000	0	1900	200	Rise almost done
Air Vent III-3A	6,000	0	2700	200	Rise almost done
Air Vent III-3B	6,000	0	2000	200	Rise done
Flat Top I	40,000	0	5300	200	Still rising 6 ft/sec
Flat Top II	40,000	0	7000	200	Still rising 20 ft/sec
Flat top III	40,000	0	5400	200	Still rising 15 ft/sec
Air Vent I	40,000	17	400	200	Rise complete at 10 sec

REFERENCES

1. Kintzinger, P.R.; "Earth Particle Motion"; Air Vent Final Report, SC-RR-64-549, October 1964; Sandia Corporation; For Official Use Only.

2. Vortman, L.J.; "Surface Motion Photography"; Air Vent Final Report, SC-RR-64-1703, March 1965; Sandia Corporation.

3. Carlson, R.H. and Jones, G.D.; "Ejecta Distribution Studies"; D2-90575, November 1965; The Boeing Company.

4. Ahlers, E.; "Crater Ejecta Studies/Phase I"; IITR-Project M6072, May 1965; IIT Research Institute.

5. Flanagan, T.J.; "Crater Studies"; SC-RR-64-1704, April 1966; Sandia Corporation.

6. Keefer, J.H., et al; "Air Blast Phenomena"; Project 1.1, Ferris Wheel Series, Flat Top Event, POR-3001, April 1966; Army Ballistic Research Laboratories, Aberdeen Proving Ground, Maryland.

7. Sauer, F.M., et al; "Earth Motion and Pressure Histories—Flat Tops I, II, and III"; Flat Top Projects 1.2 and 1.3a, Ferris Wheel Series, Flat Top Event, POR-3002, November 1965; Stanford Research Institute, Menlo Park, California.

8. Lieberman, Paul; "Close-in Pressure-time Histories for the Flat Top Experiments"; Project 1.3b, Ferris Wheel Series, Flat Top Event, POR-3004, October 1966; IIT Research Institute, Chicago, Illinois.

9. Bass, R.C. and Hawk, H.L.; "Close-in Shock Studies"; Project 1.4, Ferris Wheel Series, Flat Top Event, POR-3005, October 19, 1965, Sandia Corporation, Albuquerque, New Mexico

10. Ahlers, E.B.; "Crater Ejecta Studies—Flat Tops II and III"; Project 1.5a, Ferris Wheel Series, Flat Top Event, POR-3006, May 1965; IIT Research Institute, Chicago, Illinois.

11. Anthony, M.V., et al; "Ejecta Distribution from the Flat Top I Event"; Project 1.5b, Ferris Wheel Series, Flat Top Event, POR-3007, October 18, 1965; The Boeing Company, Seattle, Washington.

12. Rooke, A.D. and Davis, L.K.; "Crater Measurements"; Project 1.9, Ferris Wheel Series, Flat Top Event, POR-3008, August 9, 1966; Waterways Experiment Station, Vicksburg, Mississippi.

13. Bulin, G.V. and Seknicka, J.E.; "Permanent Horizontal and Vertical Earth Displacement"; Project 1.11, Ferris Wheel Series, Flat Top Event, POR-3009, May 20, 1966; AF Weapons Laboratory, Kirtland AFB, New Mexico.

14. Polatty, J.M., et al; "Grouting Support"; Project 9.1, Ferris Wheel Series, Flat Top Events, POR-3010, November 15, 1965; Waterways Experiment Station, Vicksburg, Mississippi.

15. Donovan, L.P., et al; "Technical Photography of Flat Tops I, II, and III"; Project 9.8, Ferris Wheel Series, Flat Top Event, POR-3011, November 1, 1965; EG&G, Las Vegas, Nevada.

16. Armstrong, R.H.; "Early-Time Cloud Rise from Chemical High Explosive Detonations"; U.S. Weather Bureau Research Station, Las Vegas, Nevada, UC-53, Meteorology, August 1965.

17. Flanagan, T.J.; "Hugoniot Equation of State of Materials for the Ferris Wheel Program"; SC-M-66-451, Sandia Corporation, September 1966.

18. Vortman, L.J. and Shreve, J.D.; "The Effect of Height of Explosion on Blast Parameters"; SC-3858, Sandia Corporation, June 1956.

19. (a) "Scientific Observations on the Explosion of a 20-ton TNT Charge, Vol. 2, Tripartite Blast Measurements"; Suffield Report No. 203, September 1961.

(b) Kingery, C.N. and Panilla, B.F.; "Peak Overpressure vs Sealed Distance for TNT Surface Bursts (Hemispherical Charges)"; Ballistic Research Laboratory Memo Report 1518, April 1964.

20. Kirkwood, J.G. and Brinkley, S.B.; "Theoretical Blast-Wave Curves for TNT"; OSRD-5481, August 1945.

21. Broyles, C.D.; "IBM Problem M Curves"; SCTM 268-56-51, December 1, 1956.

22. Moulton; "Nuclear Weapons Blast Phenomena"; DASA-1200, Vol. 1, March 1960; Secret Restricted Data.

23. Brode, H.L.; Physics of Fluids 2, 217, "Blast Wave from a Spherical Charge"; 1959.

24. Sauer, F.M.; "Ground Motion Produced by Aboveground Nuclear Explosions"; AFSWC-TR-59-71, April 1959; Secret Restricted Data.

25. Lampson, C.W.; "Final Report on Effects of Underground Explosions"; OSRD-6645, March 1946.

26. Doll, E.B. and Salmon, V.; "Scaled HE Tests"; Operation Jangle, WT-377, April 1952; Stanford Research Institute, Menlo Park, California.

27. Engineering Research Associates, Inc.; "Underground Explosion Test Program, Vol. I, Soil"; August 1952; also, "Vol. II, Rock," 1953.

28. Sachs, D.C. and Swift, L.M.; "Small Explosion Tests, Project Mole"; AFSWP-291, December 1955.

29. Vortman, L.J., et al; "Project Stagecoach, 20-ton HE Cratering Experiments in Desert Alluvium, Final Report"; SC-4596 (RR), May 1962.

30. Perret, W.R., et al; "Project Scooter, Final Report"; SC-4602 (RR), October 1963.

31. Newmark, N.M. and Haltiwanger, J.D.; "Air Force Design Manual -- Principals and Practice for Design of Hardened Structures"; AFSWC-TDR-62-138, December 1962.

32. Sachs, R.G.; "The Dependence of Blast on Ambient Pressure and Temperature"; BRL-466, May 1944.

33. Brode, H.L. and Bjork, R.L.; "Cratering from a Megaton Surface Burst"; RM-2600, June 30, 1960.

34. Hamada, H.B.; "Predictions for Ferris Wheel Events B1 and B2"; AFWL Memo SWRS 63-26, May 1963; Secret Restricted Data.

35. Godfrey, C.S., et al; "Prediction Calculations for Free-Field Ground Motion"; AFWL-TDR-64-27, May 1964.

36. Godfrey, C.S., et al; "Calculation of Underground and Surface Explosions"; AFWL-TR-65-211, June 1966.

37. Swift, L.M. and Eisler, J.E.; "Close-in Earth Motion"; Project 1.2, Operation Sun Beam, Shot Small Boy, POR-2201, March 1965; Stanford Research Institute, Menlo Park, California; Confidential Formerly Restricted Data.

38. Godfrey, C.S.; Physics International; Letter to: Sauer, et al; March 2, 1964.

39. Perret, W.R.; "Ground Motion Studies at High Incident Overpressure"; Project 1.5, Operation Plumbbob, WT-1405, June 1960; Sandia Corporation, Albuquerque, New Mexico.

40. Godfrey, C.S.; Physics International, Letter to: Sauer, et al; Subject: "Flat Top I Calculations"; September 9, 1964; also, letter dated June 8, 1965.

41. Lewis, J.G.; "Crater Measurements"; Project 1.6, Operation Teapot, WT-1105, July 1955; Army Ballistic Research Laboratories, Aberdeen Proving Ground, Maryland.

42. Vaile, R.B.; "Crater Survey"; Project 3.2, Operation Castle, WT-920, June 1955; Stanford Research Institute, Menlo Park, California; Secret Restricted Data.

43. Vaile, R.B.; "Pacific Craters and Scaling Laws"; Journal of Geophysical Research 66, pp 3414-3438, October 1961.

44. Chabai, A.J.; "Crater Scaling Laws for Desert Alluvium"; SC-4391 (RR), December 1959.

45. Chabai, A.J.; "Scaling Dimensions of Craters from Nuclear Explosions"; SC-RR-65-70, February 1965.

46. Jones, G.H.S., et al; "Surface Burst of 100-ton Hemispherical Charge, Ground Displacement, Suffield Technical Paper 250," May 1962.

47. Carlson, R.H., et al; "Ejecta Distribution from Cratering Events in Soil and Rock"; WL-TR-64-111, February 1965; Secret Restricted Data.

48. Laupa, Armas; "On the Scaling of Pacific Nuclear Craters"; RM-4308-PR, October 1964; Secret Formerly Restricted Data.

49. "Engineering with Nuclear Explosions: Proceedings of the Third Plowshare Symposium"; TID-7965, April 1964.

50. Violet, C.E.; "A Generalized Empirical Analysis of Cratering"; Journal of Geophysical Research 66, pp 3461-3470, October 1961.

51. Nordyke, M.D.; "An Analysis of Cratering Data from Desert Alluvium"; Journal of Geophysical Research 67, pp 1965-1975, May 1962.

52. Chabai, A.J.; "On Scaling Dimensions of Craters Produced by Buried Explosives"; Journal of Geophysical Research 70, pp 5075-5098, October 1965.

53. "Capabilities of Nuclear Weapons"; TM 23-200, 1964; Confidential.

54. O'Brien, T.E., et al; "Multiple Threat Cratering Experiment"; AFWL-TR-67-8. Vol. I, April 1967.

55. Vaile, R.B. and Salmon, V.; "Evaluation of Missile Hazard, Underground Shot"; Project 4.5, Operation Jangle, WT-338, May 1952; Stanford Research Institute, Menlo Park, California.

56. Cherry, J.T.; "Computer Calculations of Explosion-Produced Craters"; UCRL-14998, July 1966.

57. Hess, W.N. and Nordyke, M.D.; "Throwout Calculations for Explosion Craters"; Journal of Geophysical Research 66, p 3405, October 1961.

58. Finlayson, F.C., et al, (ed.); "Proceedings of the Symposium on Nuclear Craters and Ejecta"; Aerospace Corporation, to be published; Secret Restricted Data.

59. AMC Safety Manual, AMCR-385-224 (formerly ORD M7-224), June 1964.

60. Hankins, D.M., Sandia Corporation, unpublished data.

61. Carlson, R.H.; "Project Toboggan, High-Explosive Ditching from Linear Charges"; SC-4483 (RR), July 1961.

Pages 158-161 deleted

UNCLASSIFIED

Security Classification

DOCUMENT CONTROL DATA - R & D

(Security classification of title, body of abstract and indexing annotation must be entered when the overall report is classified)

1. ORIGINATING ACTIVITY (Corporate author) Defense Atomic Support Agency Washington, D.C. 20305	2a. REPORT SECURITY CLASSIFICATION UNCLASSIFIED 2b. GROUP N/A

3. REPORT TITLE

Scientific Directors Summary

4. DESCRIPTIVE NOTES (Type of report and inclusive dates)

Final report of Air Vent/Flat Top Events accomplished on Ferris Wheel Series

5. AUTHOR(S) (First name, middle initial, last name)

M. L. Merritt, Scientific Director, Sandia Corporation, Box 5800, Albuquerque, New Mexico 87115

6. REPORT DATE	7a. TOTAL NO. OF PAGES	7b. NO. OF REFS
	163	61

8a. CONTRACT OR GRANT NO. b. PROJECT NO. c. d.	9a. ORIGINATOR'S REPORT NUMBER(S) POR-3000 (WT-3000) 9b. OTHER REPORT NO(S) (Any other numbers that may be assigned this report)

10. DISTRIBUTION STATEMENT

Each transmittal of this document outside the agencies of the U.S. Government must have prior approval of Director, Defense Atomic Support Agency, Washington, D.C. 20305.

11. SUPPLEMENTARY NOTES	12. SPONSORING MILITARY ACTIVITY
	DOD/DASA

13. ABSTRACT

Air Vent and Flat Top were HE experiments studying ground shock and cratering. There were 33 shots varying in size from 64 pounds to 20 tons, all spheres and all but one in the playa of NTS Area 5. The 20-ton shots comprised one at 17-foot depth (Air Vent I) and two half-buried in playa (Flat Tops II and III), and one half-buried in limestone (Flat Top I).

Air blast measurements were made on the three Flat Top shots. Results are much as predicted preshot.

Ground motion measurements were made on the Flat Top shots and on Air Vent I. Associated calculations were made postshot; their results are in general agreement with the data but do not go out to distances where most of the data were taken. Air-blast-induced ground motions on Flat Tops II and III in playa were superseismic through the whole range of measurement. Acceleration and vertical component of velocity were dominated by air-blast-induced shock; displacements and horizontal components of velocity by direct ground shock. Flat Top I in limestone was subseismic through most of the range of measurement. Gages at similar positions had similar wave forms, but the time scale of records in limestone was much faster than of records in playa. Horizontal velocities were larger in limestone than in playa; vertical velocities higher in playa than in limestone.

DD FORM 1 NOV 65 1473 REPLACES DD FORM 1473, 1 JAN 64, WHICH IS OBSOLETE FOR ARMY USE.

UNCLASSIFIED

Security Classification

UNCLASSIFIED
Security Classification

14. KEY WORDS	LINK A		LINK B		LINK C	
	ROLE	WT	ROLE	WT	ROLE	WT
Ferris Wheel Series						
Air Vent/Flat Top Events						
Air Pressure Measurements						
Ground Shock						
Cratering						

UNCLASSIFIED
Security Classification